UNIVERSITÉ CATHOLIQUE DE LOUVAIN

DOCTORAL THESIS

# Performance Analysis of SWIPT Networks

*Author:*
Ayse Ipek AKIN ATALAY

*Supervisor:*
Prof. Dr. Luc VANDENDORPE

*A thesis submitted in fulfillment of the requirements for the degree of Doctor of Philosophy*

*in the*

Louvain School of Engineering

July, 2022

# Declaration of Authorship

I, Ayse Ipek AKIN ATALAY, declare that this thesis titled, "Performance Analysis of SWIPT Networks" and the work presented in it are my own. I confirm that:

- This work was done wholly or mainly while in candidature for a research degree at this University.
- Where any part of this thesis has previously been submitted for a degree or any other qualification at this University or any other institution, this has been clearly stated.
- Where I have consulted the published work of others, this is always clearly attributed.
- Where I have quoted from the work of others, the source is always given. With the exception of such quotations, this thesis is entirely my own work.
- I have acknowledged all main sources of help.
- Where the thesis is based on work done by myself jointly with others, I have made clear exactly what was done by others and what I have contributed myself.

Signed:

---

Date:

---

UNIVERSITÉ CATHOLIQUE DE LOUVAIN

# *Abstract*


Louvain School of Engineering

Doctor of Philosophy

**Performance Analysis of SWIPT Networks**

by Ayse Ipek AKIN ATALAY

In the recent years, the saturation of the smartphone market penetration fostered the development of new applications to connect human beings with smart objects. However, the explosive growth in the number of connected devices brings some concerns about the highly growing traffic and the environmental effect of batteries production and disposal. Simultaneous wireless information and power transfer (SWIPT) technique has been emerged as a solution to mitigate with these concerns. However, SWIPT also comes with some obstacles such as the limitations on the energy transfer efficiency due to the propagation losses and the constraints on the minimum received power imposed by the current radio frequency (RF) harvesting technologies. This restricts the range of application of wirelessly powered devices by limiting them to the execution of very simple computational tasks. Following this line of thought, the integration of SWIPT with mobile edge computing (MEC) has appeared as an enticing emerging research direction to increase the computational capabilities of SWIPT enabled systems.

This dissertation focuses on studying the performance of SWIPT enabled MEC system in the presence of spatially correlated shadowing. The first step taken towards this objective is the analysis of the performance of SWIPT enabled systems with special emphasis on the impact of spatially correlated shadowing on the achievable rate-energy trade-off. Stochastic geometry is used to model the random location of the network nodes and the geometry of the propagation environment. For indoor environments, the shadowing effect of the walls is modelled by using Manhattan Poisson Line Process (MPLP) where the locations of the RF energy sources, also referred to as power heads (PHs), and the end-user devices are modelled as instances of a homogeneous Poisson Point Process (PPP). The impact of multi user interference (MUI) is also addressed in relation with both the topology of the network and the characteristics of the venue in which the system is deployed. The numerical results show that the ambivalent role of MUI is the most important factor in shaping the achievable trade-offs and, consequently, how the level of network densification must be wisely chosen in accordance with the topological characteristics of the propagation environment.

Capitalizing on the analytical tool developed in the first part of the dissertation, the analysis of the achievable performance trade-offs has been extended to SWIPT-enabled computing systems. Energy depleted by the CPU to execute the computational tasks in a mobile computing system has been put in relation with multidimensional performance region showing that the most efficient use of the CPU is obtained when the number of logical operation per bit is chosen in accordance with the level of MUI. In other words, when the offloading of the tasks is not available, the rate at

which the task can be performed is essentially limited by the interference due to the high density of PHs required to enable RF energy harvesting.

The last part of the dissertation addresses the study of SWIPT-MEC systems and provides an analytical tool to compute the probability of successfully execute a task as a function of the network parameters. Numerical results shows the dependence of the optimal task offloading rate to both the PHs density and the complexity of the task. The last chapter is devoted to a comprehensive study of SWIPT-enabled MEC systems in the presence of spatially correlated shadowing at a network level. The proposed results show that the performance can be improved by choosing either local computation or offloading based on an adaptive energy minimization strategy.

# *Acknowledgements*

I would like to thank to my supervisor Prof. Luc Vandendorpe who gave me this opportunity and offered me continuous support, encouragement and mentorship. Thank you as for guiding me and thank you for your patience and flexibility when I had major changes in my life.

I greatly appreciate and acknowledge the support of Dr. Ivan Stupia, a true friend and co-researcher, who stood by me when things were discouraging and boosted my confidence. His guidance from the initial step in research enabled me to develop an understanding of the subject.

I would like to thank my committee members: Prof. Claude Oestges, Prof. Jérôme Louveaux, Prof. Marco Di Renzo and Prof. Björn Ottersten for their time, their useful comments and feedback that helped me to improve my dissertation.

I would like to thank to my friends, Nafiseh, Hamed, Amir, Maxime and Antoine for the fun kicker and ping pong matches which were the best times of my Ph.D. My special thanks are for Dr. Nafiseh Janatian who was a close friend since the first day I joined the team. Also I thank you to Dr. Hamed Mirghasemi for his friendship and being such an officemate who made the office a fun place.

I would like to express my deepest gratitude for my dear parents Yildirim Akin and Oya Akin who believed in me and offered me irreplaceable motivation and amazing chances over the years. Most importantly, thank you for your unconditional, unequivocal, and loving support.

I have to thank to a very special person, my husband Yasin, for constantly listening to me ranting during days and nights. Support and understanding of him helped me to complete this thesis while being a mum and a Ph.D student at the same time.

The last word goes for Atlas, my baby boy, who has been the light of my life for the last two years and who has given me the extra strength and motivation to manage things in parallel.

# Contents

# List of Figures

# List of Tables

# List of Abbreviations

| | |
|---|---|
| **AP** | **A**ccess **P**oint |
| **AS** | **A**ntenna **S**witching |
| **AWGN** | **A**dditive **W**hite **G**aussian **N**oise |
| **BS** | **B**ase **S**tation |
| **CDF** | **C**umulative **D**istribution **F**unction |
| **CPU** | **C**entral **P**rocessing **U**nit |
| **EH** | **E**nergy **H**arvesting |
| **ETSI** | **E**uropean **T**elecommunications **S**tandard **I**nstitute |
| **FD** | **F**ull **D**uplex |
| **HetNet** | **Het**erogeneous **Net**work |
| **ID** | **I**nformation **D**ecoding |
| **IoT** | **I**nternet-**o**f -**T**hings |
| **J-CDDF** | **J**oint- **C**omplementary **C**umulative **D**istribution **F**unction |
| **LOS** | **L**ine **o**f **S**ight |
| **LPD** | **L**ow **P**ower **D**evices |
| **MC** | **M**obile **C**omputing |
| **MEC** | **M**obile **E**dge **C**omputing |
| **MIMO** | **M**ulti-**I**nput **M**ulti-**O**utput |
| **MCC** | **M**obile **C**loud **C**omputing |
| **MPLP** | **M**anhattan **P**oisson **L**ine **P**rocess |
| **MRC** | **M**aximum **R**atio **C**ombining |
| **MRT** | **M**aximum **R**atio **T**ransmission |
| **MUI** | **M**ulti-**U**ser **I**nterference |
| **NLOS** | **N**on **L**ine **o**f **S**ight |
| **NOMA** | **N**on-**O**rthogonal **M**ultiple **A**ccess |
| **OCRM** | **O**nline **C**omputation **R**ate **M**aximization |
| **OFDM** | **O**rthogonal **F**requency **D**ivision **M**ultiplexing |
| **PAPR** | **P**eak-to-**A**verage **P**ower **R**atio |
| **PDF** | **P**robability **D**ensity **F**unction |
| **PH** | **P**ower **H**ead |
| **PLP** | **P**oisson **L**ine **P**rocess |
| **PP** | **P**oint **P**rocess |
| **PPP** | **P**oisson **P**oint **P**rocess |
| **PS** | **P**ower **S**plitting |
| **RAN** | **R**adio **A**ccess **N**etwork |
| **RF** | **R**adio **F**requency |
| **RFEH** | **R**adio **F**requency **E**nergy **H**arvester |
| **SG** | **S**tochastic **G**eometry |
| **SINR** | **S**ignal-to-**I**nterference plus **N**oise **R**atio |
| **SIR** | **S**ignal-to-**I**nterference **R**atio |
| **SISO** | **S**ingle-**I**nput **S**ingle-**O**utput |
| **SS** | **S**patial **S**plitting |
| **SVD** | **S**ingular **V**alue **D**ecomposition |

| | |
|---|---|
| **SWIPT** | **S**imutaneous **W**ireless **I**nformation and **P**ower **T**ransfer |
| **TS** | **T**ime **S**witching |
| **UE** | **U**ser **E**quipment |
| **WIT** | **W**ireless **I**nformation **T**ransfer |
| **WPT** | **W**ireless **P**ower **T**ransfer |

*To my beloved husband Yasin and dear sweet son Atlas.*

# Chapter 1

# Executive Summary

Development of the new applications that enable complex machine-to-machine and human-to-machine interactions (referred as the Internet of Things (IoT)) has caused an explosive growth in the number of connected devices. This trend brings with it some concerns about highly growing traffic and the support of a massive number of connected devices. Moreover, current IoT devices (e.g. smart wireless sensors) operate on battery, raising serious questions about the the cost and the environmental impact of battery replacement due to the ecotoxicity of batteries production and disposals.

To overcome this obstacle, recycling the ambient energy through energy harvesting (EH) represents a sustainable solution for the current and future wireless systems: solar, indoor lighting, vibrational, thermal and radio frequency (RF) signals being examples of potential ambient energy sources [4–6]. Among all these options, RF-EH is one of the most appealing techniques since RF signals can be generated by both dedicated or ambient RF sources, where the power density required to harvest the incident RF energy ranges from 0.1 to 1000 $\mu$W/cm$^2$ [7].

With the development of a new generation of mobile low power devices (LPDs) with RF-EH capabilities, wireless power transfer (WPT) has gained attention as a promising technique to provide reliable and on-demand power supply to smart sensors and devices. In WPT systems, the power to supply the LPDs is provided by energy-bearing RF signals that are transmitted through the air from a dedicated RF energy source [8]. Depending on the application, WPT can be performed either on short distance (near-field) or on long distance (far-field). More recently, the development of more efficient RF-EH technologies brought with it the idea of unifying WPT and data communications infrastructures by developing techniques to simultaneously transfer information and power. Simultaneous wireless information and power transfer (SWIPT) is the term used to encompass a broad range of techniques in which the same RF signal is used to jointly convey data and power to wireless devices [9]. In the past decade, SWIPT has been regarded as a revolutionary concept that could lead to new dimensions for connecting the global world in a seamless manner, and reshaping several aspects of everyday-life and business applications [10]. Surveys and overview articles about SWIPT can be found in [11–14].

In spite of the huge expectations on the potential advantages of SWIPT, the development of such techniques in real-life applications has been jeopardized by the unavoidable limitations to the energy transfer efficiency due to the the propagation of the electromagnetic waves in the air, restricting the range of application of SWIPT systems to very simple ones. Moreover, the constraints on the minimum received power imposed by the current RF harvesting technologies (tens of microwatts) and the limitations imposed on RF emissions for guaranteeing the public safety suggest that the deployment of dedicated RF energy sources, also referred to as power heads (PHs), must be much denser than that of traditional access points in wireless networks. In this context, the shadowing effect due to the obstacles such as buildings (outside environment) or walls (indoor environment) and the role of multi-user interference become crucial aspects to be considered. In particular, due to its detrimental effect on coverage probability and information rate, interference is known as an undesired factor for the wireless information transfer (WIT) [15, 16]. However, in terms of WPT, interference has a beneficial effect since it can be used as an another energy source to be harvested [17, 18]. This conflict clearly introduces a new and non-trivial performance trade-off between information rate and harvestable energy for SWIPT-enabled networks.

The scenario depicted so far motivates the development of new analytical tools that are able to capture the peculiar aspects of SWIPT. The scope of this dissertation is to propose a new methodology for the performance analysis of SWIPT-enabled networks that is built upon three pillars: i) it shall capture the multi-dimensional nature of SWIPT (the so called rate-energy trade-off), ii) it shall provide a system-level perspective (i.e. beyond link performance), iii) it shall account for the specific topology of the network (i.e. density and distribution of PHs) as well as the geometry of the propagation environment (e.g. buildings, walls, etc.).

In the literature most of the investigated SWIPT network topologies are for specific and fixed configurations. However, as explained above, the efficiency of energy harvesting depends on the interference and also on the locations of all nodes. Thus, it impacts the propagation channels of all links. Therefore, a fundamental question arises: how to incorporate into the investigations the random location of the nodes? The appropriate theoretical framework that has established itself to address such questions regarding both network topology and propagation modelling is stochastic geometry (SG). Stochastic geometry has been introduced as a random and spatial model to analyse the performance of dense networks [19].

This dissertation also addresses the issue of the limited computational capability of wirelessly powered devices due to the low level of energy that can be reasonably obtained through RF-EH. A popular solution to enhance the possibilities of LPDs is the so-called mobile edge computing (MEC) paradigm. This allows the outsourcing of the computation tasks that cannot be performed by the device to an edge server, thus providing cloud-computing capabilities in order to tackle these limitations [20]. The SG methodology proposed in this dissertation will then be used to analyze the advantages sprang from the integration SWIPT and MEC, where the computational tasks can be performed either locally at the device or offloaded to a MEC server and the required power to compute/offload the task is obtained through radio frequency energy harvesting (RFEH).

## 1.1 Major Contributions

Motivated by these considerations, several researchers have recently investigated various issues related to SWIPT networks. Some authors have analysed the performance of SWIPT networks by leveraging SG [21–23] and some authors have studied the SWIPT-enabled MEC networks [24–26]. With this dissertation, our aim is to analyse the system performance of SWIPT-enabled MEC networks under the presence of spatially correlated shadowing by using SG. In order to achieve that, we start analysing the performance trade-offs of an indoor SWIPT-network where shadowing effect is considered. Then we provide an example as an application of SWIPT for IoT systems, and consider a SWIPT-enabled real time mobile computing (MC) system. As a next step, we also consider uplink phase in our model and analyse the performance of SWIPT-enabled MEC system. And finally we consider the shadowing effect and analyse the performance of SWIPT-enabled MEC system under the presence of spatially correlated shadowing. The contributions of this dissertation is listed below:

- An analytical expression of the cumulative distribution function (CDF) of the minimum propagation loss and the multi-user interference is provided for a SWIPT-MIMO indoor network. Multi-dimensional analysis in which the impact of both the network densification and the density of blocking objects on the rate-energy trade-offs are jointly analysed.
- A comprehensive understanding of the rate-energy trade-off on a service basis is provided for a real-time multi-input multi-output (MIMO) SWIPT-MC systems operating in an indoor environment. The connection between the rate-energy trade-off and the computation capacity of the LPDs is investigated.
- A stochastic decision strategy is proposed for a SWIPT-enabled MEC system and the impact of this strategy on a triple trade-off between energy, local computation and offloading is evaluated. Communication-computation trade-offs of the system are characterised and joint success probability of local computation and offloading is investigated.
- The impact of an adaptive offloading technique on the global success probability is evaluated for a SWIPT-enabled MEC system in the presence of spatially correlated shadowing. An approximation is proposed for the distribution of walls in order to obtain a shadowing model that depends only on the distance. The impact of the different system parameters on the trade-off between the energy harvested and the computational task admission rate is analysed.

## 1.2 List of Publications

The work accomplished in this dissertation has led to the following publications:

- (1) **Akin, Ayse Ipek**, Ivan Stupia and Luc Vandendorpe. "On the effect of blockage objects in dense MIMO SWIPT networks." In *IEEE Transactions on Communications*, vol. 67, no. 2, pp. 1059-1069, Feb. 2019, doi: 10.1109/TCOMM.2018.2876308.
- (2) **Akin, Ayse Ipek**, Nafiseh Janatian, Ivan Stupia, and Luc Vandendorpe. "SWIPT-based real-time mobile computing systems: A stochastic geometry

perspective." In *2019 IEEE Wireless Communications and Networking Conference (WCNC)*, Marrakesh, Morocco, 2019, pp. 1-7, doi: 10.1109/WCNC.2019.8885663.

- (3) **Akin, Ayse Ipek**, Hamed Mirghasemi and Luc Vandendorpe. "SWIPT-based mobile edge computing systems: A stochastic geometry perspective." In *2019 IEEE 30th Annual International Symposium on Personal, Indoor and Mobile Radio Communications (PIMRC)*, Istanbul, Turkey, 2019, pp. 1-7, doi:10.1109/ PIMRC.2019.8904282.
- (4) **Akin, Ayse Ipek**, Ivan Stupia, Hamed Mirghasemi, and Luc Vandendorpe. "On the performance of SWIPT MEC systems in the presence of spatially correlated shadowing." In *2020 IEEE Global Communications Conference (GLOBECOM)*, Taipei, Taiwan, 2020, pp. 1-6, doi: 10.1109/GLOBECOM42002.2020. 9347963

## 1.3 Thesis Outline

Following the introductory chapter, this dissertation is organised as follows.

Chapter 2 presents a literature review on the simultanous wireless information and power transfer and mobile edge computing systems. Moreover, we provide an overview on the SG based theoretical analysis of SWIPT enabled systems.

In Chapter 3, we analyse the performance of an indoor multi-input multi-output SWIPT enabled system where power splitting scenario is considered. Effect of the obstacles on the rate-energy trade-off is investigated by utilizing SG approach in which the locations of the network elements are distributed by using Poisson point process. For modelling the obstacles, Manhattan Poisson line process is considered. In order to study the trade-off between rate and energy, we obtain the joint complementary cumulative distribution function of information rate and harvested power. To achieve this, the stochastic behaviour of the signal attenuation and the multi-user interference is studied first. Finally, theoretical results are validated by Monte Carlo simulations. Moreover, as an application of SWIPT we consider a real-time MIMO SWIPT-MC systems. After studying rate-energy trade-offs of indoor MIMO SWIPT-enabled systems, we provide a comprehensive understanding on the rate-energy trade-off on a service basis for MIMO SWIPT-MC systems . Here we propose the use of SWIPT to control distributed computation process. To investigate the operating conditions of real-time computing systems, we study an achievable performance region which guarantees that the central processing unit may perform the task before receiving a new task. In addition, a practicable model for the central processing unit energy consumption is presented. Finally we study the outage probability of the system for different network setups.

The work of this chapter resulted in producing the research outcomes (1) and (2) of Section 1.2.

In Chapter 4, we focus on mobile edge computing and extend the previous study to SWIPT-enabled MEC systems where the energy harvested by the LPDs in the downlink phase is then used to either locally execute the assigned computation task or to offload it to the MEC server. Due to the complex nature of the stochastic geometry analyses, as a first step, only standard power law path-loss model and small-scale fading are considered in this model. Analysing the effect of shadowing is left for the next chapter. In this model, we propose a stochastic decision strategy where an LPD has to decide either to perform local computation or offload. Since interference is the bottleneck in such a MEC system, we introduce a random probability with Bernoulli distribution to overcome the interference issue. And it enables us to analyse the trade-off between local computation and offloading. In order to obtain the total success probability of the system, first the probabilities of offloading and local computation are derived. As a next step, we obtain the success probabilities of local computation and offloading which eventually give us the total success probability of the system. Moreover we present the Monte carlo simulations to corroborate the theoretical results of the offloading/local computation probabilities.

The work of this chapter resulted in producing the research outcomes (3) of Section 1.2.

In Chapter 5, we develop an analytical framework to analyse the performance of the SWIPT-enabled MEC system in the presence of spatially correlated shadowing. To achieve this we consider randomly distributed obstacles following Manhattan Poisson Line Process. In order to simplify the SG analysis, we approximate the blockage attenuation with its expectation to obtain a shadowing model that depends only on the distance between the source and the destination. By leveraging stochastic geometry, the expressions for downlink SINR coverage and success probabilities of offloading and of local computation are derived to characterize the success probability of the system. Moreover, we analyse the impact of different system parameters on the trade-off between the harvested energy and the computational task admission rate.

The work of this chapter resulted in producing the research outcomes (4) of Section 1.2.

Finally, Chapter 6 concludes the dissertation and presents the future work.

# Chapter 2

# Background and Motivations

The rapid development of mobile internet and IoTs has given rise to a serious concern about the cost of deployment and maintenance of the massive number of connected devices as well as the environmental impact of battery replacement due to the ecotoxicity of battery production and disposal. Therefore, power management and environmental sustainability of IoT devices are major issues to be considered in deploying the upcoming networks successfully [27].

In the past decade, Simultaneous Information and Power Transfer (SWIPT) has been identified as a possible solution to reduce the environmental impact of the foreseen massive number of connected devices by removing the need for wires or a battery [11]. The main idea behind SWIPT is to use the same electromagnetic field for both transferring data and energy. Nevertheless, the unavoidable limitations to the energy transfer efficiency due to the path loss associated with the propagation of the electromagnetic waves in the air, together with the legislative norms to preserve public health, restrict the range of application of these devices, limiting their capability to simple computational tasks and posing significant obstacle to the fruition of high demand services by a large number of users [2].

Several solutions addressing the issue of limited computational capability in low power mobile devices have been proposed, delineating a new framework for the design and the optimization of wireless networks in which computation and traditional communication aspects are merged into a unified perspective [28]. An initial idea was to use the concept of mobile cloud computing (MCC) allowing cloud computing for mobile user [29,30]. However, MCC has some major disadvantages, such as high latency and traffic congestion, which makes the offloading unsuitable for delay sensitive applications [2]. To mitigate the effect of latency, the mobile edge computing (MEC) paradigm, which allows outsourcing the computation tasks that cannot be performed by mobile user to an edge server, has been thoroughly investigated [1, 31–33]. Within this context, an enticing emerging research direction is the integration of SWIPT and MEC where the computational tasks can be performed either locally at the device of offloaded to a MEC server and the required power to compute/offload the task is obtained through radio frequency energy harvesting (RFEH).

Though the integration of SWIPT and MEC represents an enticing perspective to provide a sustainable design of IoT devices, it makes the network performance analysis extremely complex due to the emergence of conflicting objectives among power transfer efficiency, data communication and task offloading for the use of the available wireless resources. Therefore, the performance of SWIPT-MEC systems must be characterized by a multidimensional region in which the optimization of one objective may jeopardize the others. To give an example, multi-user interference may be beneficial in increasing the level of energy harvested by a device but detrimental for the data rate of the wireless communication link. In this scenario, the morphology of the network (i.e. density of the nodes, distribution) and the propagation environment (e.g. shadowing) is of paramount importance to define the interplay between power and data transfer at a network level. For this reason, stochastic geometry appears as the perfect methodological tool to the analysis of SWIPT-MEC systems by duly accounting for the randomness of the locations of the network nodes. Moreover, the use of stochastic geometry allows the derivation of closed-form or semi-closed-form expressions without resorting to simulation methods or (possibly intractable or inaccurate) deterministic models [34].

In the remainder of this chapter, we give detailed information about MEC and SWIPT and explain the SG methodology adopted in this dissertation.

## 2.1 Mobile Edge Computing

Mobile Edge Computing is an emerging technique that is used to enhance the computing capability of LPDs and also improve the battery life (Fig. 2.1). The concept of MEC was firstly proposed by the European Telecommunications Standard Institute (ETSI) in 2014 [35] and in [20] it has been defined as:

*"Mobile Edge Computing provides an IT service environment and cloud-computing capabilities at the edge of the mobile network, within the Radio Access Network (RAN) and in close proximity to mobile subscribers."*

Since the benefits of MEC technology reached beyond mobile and into Wi-Fi and fixed access technologies, the ETSI industry group renamed it to Multi-Access Edge Computing (MEC) From 2017. However, the name change conveniently allows ETSI to retain the MEC acronym, which has become widely recognized among stakeholders in the industry [3].

MEC technique allows processing complex data by outsourcing the computation tasks that cannot be performed by the LPD to an edge server. The important part regarding computation offloading is to decide whether to offload or not. Moreover in case of offloading then how much and what should be offloaded [2]. As a result of this decision, user equipments (UEs) can take three different actions (Fig. 2.2):

- Local computation where UEs perform the task execution locally.

- Binary offloading where the task cannot be partitioned and has to be executed as a whole either locally at the mobile device or offloaded to the MEC server.

- Partial offloading where the task can be partitioned into two parts with one executed locally at the mobile device and the other offloaded to the MEC server

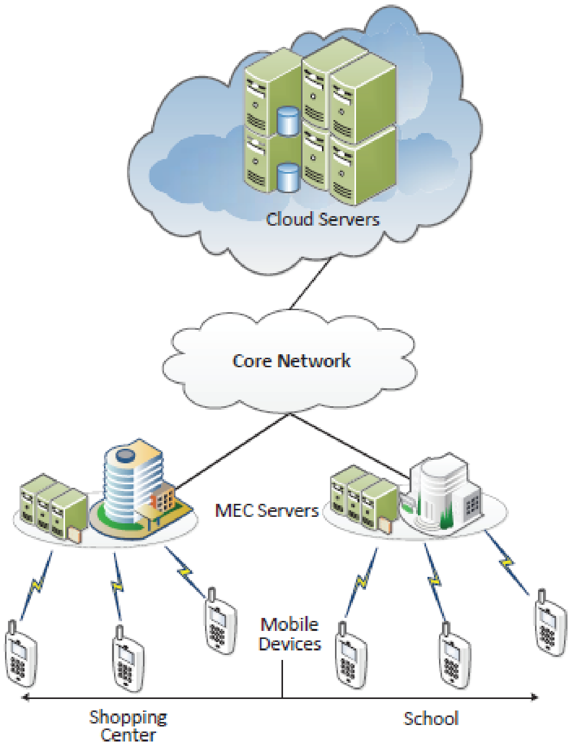


FIGURE 2.1: Mobile Edge Computing Architecture. [1].

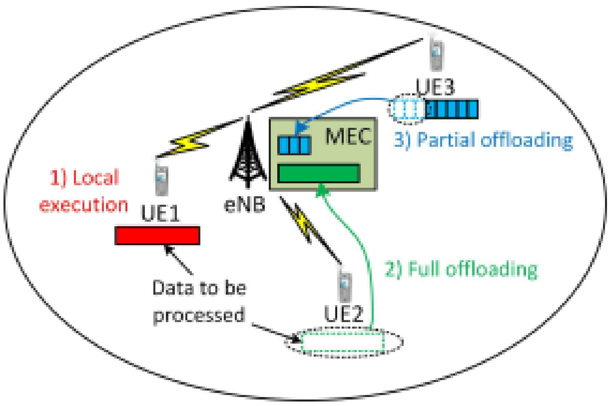


FIGURE 2.2: Possible outcomes of computation offloading decision [2].

Due to advantages of MEC technique such as reducing the latency and the energy consumption at the LPDs, it has attracted growing research interests [31, 36–38]. In [36], the authors have studied the MEC offloading mechanisms in 5G heterogeneous networks (HetNet). In order to minimize the system energy cost under delay constraints, they have jointly optimized the computation offloading. [31] presents a comprehensive overview and research outlook of MEC from the communication perspective. In [37], a MEC-enabled HetNet system has been proposed where the users have different computation task sizes and MEC servers have different computing capacities. Authors have derived the successful edge computing probability. The authors of [38] analysed the performance of MEC network with multi-core edge

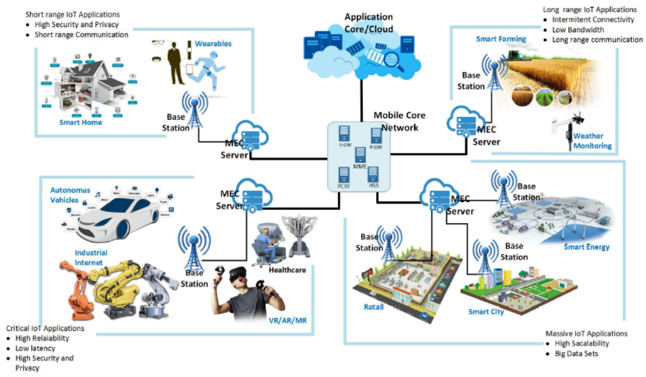


FIGURE 2.3: IoT and MEC application scenarios. [3].

servers by utilizing stochastic geometry (SG) and queueing theory. They have derived the total successful edge computing probability by combining the successful communication probability and the successful computing probability.

#### Practical Applications

There are four service scenarios for MEC that have been considered within ETSI ISG MEC [20]: 1)Augmented Reality, 2)Intelligent Video Acceleration, 3)Connected Cars and 4)Internet of Things Gateway. All these applications require high accuracy which brings the high computational needs with it. Regarding the aforementioned challenges about computational capacity and battery limitation of LPDs, it is not useful to deploy these applications into an LPD. Thus, MEC emerges as a possible solution.

There is mutual advantage between MEC and IoT. While MEC empowers tiny IoT devices with significant additional computational capabilities through computation offloading, IoT expands MEC services to all types of smart objects ranging from sensors and actuators to smart vehicles [3]. Various IoT and MEC application scenarios can be seen in Fig. 2.3.

## 2.2 Simultaneous Wireless Information and Power Transfer

Due to the concerns about the energy storage, power management and increase of the battery life of the mobile device, WPT has drawn attention as a possible solution. In this context, SWIPT is considered as one of the most appealing techniques since it exploits the same electromagnetic field for both transferring data and energy.

### 2.2.1 History

Radio frequency energy transfer has originally been studied by Nicola Tesla in late 1890s. Despite his failure, during his experiments with a particular circuit, he has observed that the energy transfer efficiency has a peak for the transmission of a single sinusoid at a specific frequency depending on the parameters of the circuit.

More than a century later, the concept of transporting power and information simultaneously was proposed by Varshney in [9]. He has studied a fundamental tradeoff, in the information theory sense, between energy harvesting and information decoding (ID) for single-input single-output (SISO) systems corrupted by additive white Gaussian noise (AWGN). The authors of [39] extended the work of Varshney to the more generalised case of SISO frequency-selective fading channels, where the EH/ID trade-off was supposed to be the topic of a hypothetical meeting between Tesla and Shannon. While Tesla would maximize EH by assigning the power to a single frequency, Shannon would obtain information maximization by allocating the power across multiple frequencies according to the seminal "water-filling" approach.

The main idea behind the SWIPT can be explained as, since every RF signal can carry energy as well as information, EH and ID can be performed from the same RF signal. However, recently it has been revealed that using multi-sine waveforms instead of a single tone waveform can increase the efficiency of WPT [40, 41]. A multi-sine is characterized by a high Peak-to-Average Power Ration (PAPR), and the envelope of the transmitted RF signal is designed so that there are large peaks, while the average power is kept the same as in the continuous wave case [42]. The authors of [41], have obtained the SWIPT waveform as the superposition of a WPT waveform (multi-sine) and a WIT waveform (Orthogonal Frequency Division Multiplexing (OFDM)) and optimized it to maximize the rate-energy region of the whole system. Moreover, in [43], an innovative idea has been proposed where multi-sine waveforms are used for energy transfer and their distinct PAPR are for information transmission, both through a single output of the rectifier.

In the literature, concept of SWIPT has been reported in various scenarios such as multi-input multi-output (MIMO) communication systems [44, 45], mmWave networks [46, 47] and non-orthogonal multiple access (NOMA) [48, 49].

### 2.2.2 Receiver Architecture

In the earlier studies it has been assumed that one signal can carry both the energy and information simultaneously without losses [39]. However it is not possible practically due to the fact that decoding the information without destroying the energy content is not possible because of the technological limitations.

In addition, large differences of the power sensitivity values for information reception and RF energy harvesting (e.g.,$-10$dBm for energy harvesters versus $-50$ dBm for information receivers) [50], make them intractable for current receiver architectures.

A considerable effort has been devoted to the study of different SWIPT receiver architectures at the user equipment. Four major types of SWIPT receiver architectures have been considered in the literature, namely, the co-located receiver architecture [50,51], the parallel receiver architecture (also called as antenna switching ) [50], the integrated receiver architecture [51], and the ideal receiver architecture [9,39,52].

#### Co-located Receiver Architecture

In a co-located receiver architecture, the energy harvester and the information receiver share the same antennas. This architecture can be further categorized into two models: time-switching and power-splitting architectures [51].

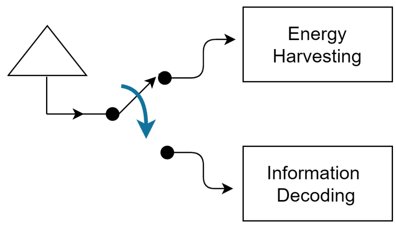


FIGURE 2.4: Co-located Receiver Architecture: Time Switching

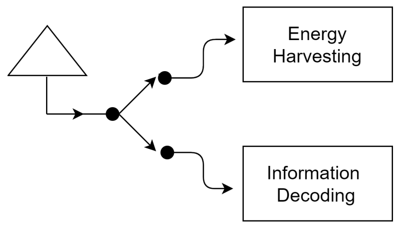


FIGURE 2.5: Co-located Receiver Architecture: Power Splitting.

***Time Switching:*** In a SWIPT-enabled system with time-switching (TS) architecture (see Fig. 2.4), the signal splitting is performed in time domain. The receiver switches in time between ID and EH [50]. The signal received in one time slot is used either for ID or EH. Besides the simple hardware implementation at the receiver for TS, the accuracy of time synchronization and scheduling is very important. TS architecture is one of the techniques that is considered in this dissertation.

***Power Splitting:*** With a power splitting (PS) architecture (Fig. 2.5), the received signal is split into two streams with different power levels by using a power splitting ratio $\rho$, where $0 \leq \rho \leq 1$. While one signal stream is sent to the rectenna circuit for EH, the other stream is used for ID [50].

In comparison with TS technique, PS requires higher receiver complexity since the power splitting ratio should be optimized. However, with PS technique, by varying PS ratios, the information rate and the harvested energy can be balanced according to the system requirements. Overall performance also can be improved by optimizing the combination of the signal and the PS ratios [14]. Moreover, since an instantaneous SWIPT can be achieved, this technique is more suitable for the applications with critical information/energy or delay constraints [11]. PS is another strategy that is considered in this dissertation.

**Parallel Receiver Architecture**

In this architecture, also called as antenna switching (AS), the receiving antennas are divided into two groups where one group is used for information decoding and the other group for energy harvesting [11]. This technique dynamically switches each antenna element between decoding/rectifying to enable the SWIPT [50].

Although this technique requires the solution of an optimization problem in each communication frame in order to decide the optimal assignment of the antenna elements for ID and EH, AS is an easier technique compared to TS and PS techniques and appealing for practical SWIPT architecture designs. Architecture for parallel receiver is shown in Fig. 2.6

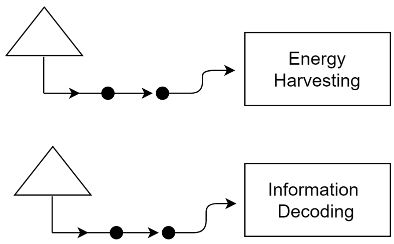


FIGURE 2.6: Parallel Receiver Architecture.

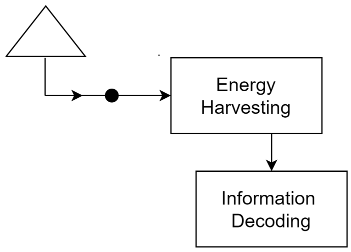


FIGURE 2.7: Integrated Receiver Architecture.

**Integrated Receiver Architecture**

In the integrated receiver architecture (Fig. 2.7), the information receiver does not implement any RF-to-baseband conversion, since this operation is integrated with the energy harvester via the rectifier (i.e. the circuit element that converts the input RF signals into DC voltage). The main advantage of this type of architecture is that it enables to encode the information in the energy signal by varying its power levels over time, thus achieving continuous information transfer without (theoretically) degrading the power transfer efficiency.

**Ideal Receiver Architecture**

In this architecture, it has been assumed that energy can be extracted from the same signal which is used for information decoding. However, as pointed out in [51], the current circuit designs are not yet able to implement this extraction. As mentioned above, energy carried by the RF signal is lost during the information decoding process. In order to evaluate theoretical benchmarks for SWIPT, the ideal receiver architecture has been considered in [9, 39, 52] where it leads to upper bounds on the investigated performance.

It is worth to mention that each particular SWIPT receiver architecture has a considerable impact on the energy harvesting-information decoding trade-off associated with the link [51].

### 2.2.3 Rate-Energy Trade-offs

At the network level, an interesting aspect of SWIPT systems is the ambivalent role of the multi-user interference (MUI). It is important in wireless information systems, because when not handled properly, it can become the ingredient limiting the system performance. It is usually considered as an undesired factor for wireless information transfer [15, 16] due to the negative effect on the coverage probability and the information rate. On the other hand, MUI is beneficial for wireless power transfer since it can be used as an additional source of energy to be harvested [17, 18]. In other words, the beneficial effect of MUI on RF energy harvesting is obtained at the price of a reduced link capacity. For this kind of non-trivial situations in the multi-objective systems where there is a competition between objectives, trade-offs necessarily exist between them. Therefore, SWIPT-enabled systems can be described in terms of achievable trade-offs between the information rate and the harvestable energy. These trade-offs will be analysed by taking advantage of the Joint Complementary Cumulative Distribution Function (J-CCDF) which will be explained in details in the next chapter.

## 2.3 Integration of SWIPT and MEC

The integration of WPT and MEC technologies (can be seen in Fig. 2.8) was first proposed in [53]. In this study, authors have optimized the Central Process Unit (CPU) cycle frequencies, EH and offloading time in order to maximize the probability of satisfying the computation requirements. Resource management is important in enhancing the energy efficiency of mobile device in MEC systems. Thus, several joint resource allocation and offloading strategies for WPT-based MEC were proposed in [54–56]. In [54], authors have investigated the use of cooperative communications in computation offloading for a WPT-MEC system. They aimed to minimize the transmit energy of the access point for completing the computation tasks of the two users and proposed a two-phase method to find the optimal solution. The authors of [55] have studied the problem of resource management and time allocation for multi-user offloading in wirelessly powered MEC systems and proposed an online computation rate maximization (OCRM) algorithm. They have also obtained the closed-form expressions for optimal time allocation and CPU-cycle frequencies of wireless devices. The authors have considered collocated MEC server and energy transmitter to assist single-antenna mobile devices in fully or partially offloading their computational tasks in [56]. In order to minimize the energy consumption at the access point (AP) side, they have optimized the energy transmit covariance matrix and the offloading strategy.

Moreover in [57], [24] and [26] SWIPT-enabled MEC systems have been considered. In [57], the authors have proposed a joint offloading and computing design based on SWIPT and MIMO full-duplex (FD) relay techniques. In [24], a MEC design framework in a SWIPT-based multi-user MEC system has been developed. The authors have jointly optimized offloading strategy and resource allocation in order to minimize the total energy cost of the ultra LPDs. Authors of [26] have formulated a MEC design framework with joint optimization of the CPU frequency, the uplink transmitting power, the uplink rate and computation task in a MEC-based multi-user FD-SWIPT system with the aim to minimize the uplink energy consumption of mobile terminals.

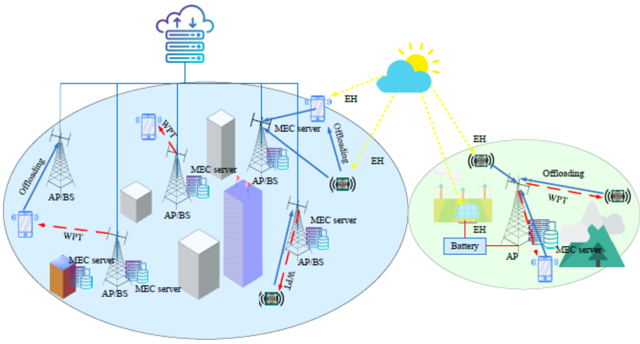


FIGURE 2.8: EH/MEC system. [3].

## 2.4 Stochastic Geometry Approach in SWIPT-enabled systems

In this section, some important constituents of SWIPT-enabled systems are explained. We start with introducing some useful essentials and theorems for stochastic geometry approach and continue with explaining the reasons to utilize SG in SWIPT-enabled systems, then we discuss the impact of shadowing on the system performance.

### 2.4.1 Essentials of Stochastic Geometry Approach

In this section, we provide some definitions and theorems that are used in this dissertation.

#### Homogenous Poisson Point Process

Consider the $d-$ dimensional Euclidean space $\mathbb{R}^d$. A spatial *point process* (p.p.) $\Psi$ is a random, finite or countable-infinite collection of points in the space $\mathbb{R}^d$, without accumulation points.

**Definition 1.** *The Poisson point process $\Psi$ of intensity measure $\Lambda$ is defined by means of its finite-dimensional distributions:*

$$\mathbf{P}\{\Psi(A_1) = n_1, \ldots, \Psi(A_k) = n_k\} = \sum_{i=1}^{k} \left( e^{-\Lambda(A_i)} \frac{\Lambda(A_i)^{n_i}}{n_i!} \right) \tag{2.1}$$

*for every $k = 1, 2, \ldots$ and all bounded, mutually disjoint sets $A_i$ for $i = 1, \ldots, k$. If $\Lambda(dx) = \lambda dx$ is a multiple of Lebesgue measure (volume) in $\mathbb{R}^d$, we call $\Psi$ a homogeneous Poisson p.p. and $\lambda$ is its intensity parameter [19].*

#### Thinning

Consider a function $p : \mathbb{R}^d \mapsto [0, 1]$ and p.p. $\Psi$. A realization of $\Psi^p$ can be constructed from that of $\Psi$ by randomly and independently removing some fraction of points; the probability that a given point of $\Psi$ located at $x$ is not removed (i.e. is retained in $\Psi^p$) is equal to $p(x)$.

**Proposition 1.** *The thinning of the Poisson p.p. of intensity measure $\Lambda$ with the retention probability $p$ yields a Poisson p.p. of intensity measure $p\Lambda$ with $(p\Lambda)(A) = \int_A p(x)\Lambda(dx)$*

*[19].*

#### Probability generating functional (PGFL)

Let $f : \mathbb{R}^d \to \mathbb{R}^+$ be a function. Then the PGFL of the PP with respect to this function is defined as the mean of the product of the function's values at each point of the PP *i.e.* [58]

$$\mathcal{P}_\Psi(f) = \mathbb{E}\left[\prod_{\mathbf{X_i}\in\boldsymbol{\Psi}} f(\mathbf{X_i})\right].$$

#### Campbell's Formula

For a point process $\Psi$ with intensity $\Lambda$ and a measurable function $f : \mathbb{R}^d \to \mathbb{R}$, the sum of $f$ over the point process is given by the equation [59]:

$$\mathbb{E}\left[\sum_{x\in\Psi} f(x)\right] = \int_{\mathbb{R}^d} f(x)\Lambda(dx).$$

#### Slivnyak Meckes Theorem

Slivnyak Meckes theorem states that for a Poisson point process, the distribution of the original process is equal to its reduced Palm distribution. Definition of reduced Palm distribution is given below.

**Definition 2.** *Given a point process with a locally finite mean measure, the distribution $P_x^!(\cdot)$ is called the reduced Palm distribution of $\Psi$ given a point at $x$.*

**Theorem 1.** *Let $\Psi$ be a Poisson point process with intensity measure $\Lambda$. For $\Lambda$ almost all $x \in \mathbb{R}^d$,*

$$P_x^!(\cdot) = \mathbf{P}\{\Psi \in \cdot\}; \tag{2.2}$$

*that is, the reduced Palm distribution if the Poisson p.p. is equal to its (original) distribution [19].*

#### Displacement Theorem

Consider a probability kernel $p(x, B)$ from $\mathbb{R}^d$ to $\mathbb{R}^{d'}$, where $d' \geq 1$, i.e. for all $x \in \mathbb{R}^d$, $p(x, \cdot)$ is a probability measure on $\mathbb{R}^{d'}$.

$\Psi^p$ is obtained by randomly and independently displacing each point of $\Psi$ from $\mathbb{R}^d$ to some new location in $\mathbb{R}^{d'}$ according to the kernel $p$. This operation preserves the Poisson p.p. property as stated in the following theorem.

**Theorem 2.** *The transformation of the Poisson p.p. of intensity measure $\Lambda$ by a probability kernel $p$ is the Poisson p.p. with the intensity measure $\Lambda'(A) = \int_{\mathbb{R}^d} p(x, A)\Lambda(dx), A \subset \mathbb{R}^{d'}$ [19].*

### 2.4.2 Random Network Elements Placement

Network elements' densification leads to a possibility that the achievable rate-energy trade-off is highly dependent on the spatial locations of the network elements. Due to this dependency, Wyner model and the regular hexagonal or square grid models [60, 61] are inadequate to describe SWIPT-enabled systems.

Recently, SG has been introduced as a random and spatial approach for modelling dense networks [15]. SG approach provides a theoretical framework to obtain performance that is spatially averaged by avoiding the possible concerns regarding the repeatability and the transparency of Monte Carlo simulations. In the literature, there have been several studies capitalizing on SG [11, 21, 62–67].

In SG approach, the possible sets of network elements deployed in a given area are modelled as instances of a homogenous Poisson Point process (PPP) $\Psi$ of density $\lambda$. We limit our investigation to a single point located at the origin of the axes, by invoking the Slivnyak-Mecke's theorem, under the assumption of large indoor network [68]. This assumption is justified by the ultra dense scenario considered, i.e. $\frac{1}{\lambda_{\text{ph}}} \ll \pi R_{\text{a}}^2$, where $\lambda_{\text{ph}}$ is the density of the PHs and $R_{\text{a}}$ is the maximum distance at which a PH's contribution to the global interference has a non-negligible impact on the achievable rate-energy trade-offs. This single point located at the origin of the axes will be called as typical LPD and denoted by $\text{LPD}^{(0)}$.

### 2.4.3 Shadowing

In dense networks, it is difficult to predict coverage of networks due to the variations in path loss caused by common obstacles. Moreover, in these networks since the distance between the PHs and the user is very short, the effect of blocking objects is highly correlated in the space. Thus, shadowing becomes more cruel than fast fading in SWIPT-enabled systems.

Ray tracing is one of the popular approaches that has been studied in the literature in order to incorporate blockages on wireless propagation [69, 70]. However, it requires accurate terrain information (e.g. location and size of the blockages in the area) to perform site-specific simulations. Another useful method is to use SG approach to characterize the statistics of blockages that provides acceptable estimation of the blockage effects with only a few parameters. An advantage of stochastic models is that it may be possible to analyse general networks [71].

The authors of [71] have proposed a mathematical framework to model the blockages by using concepts from random shape theory on the urban networks. In this paper, the key idea is to model the random buildings as a Boolean scheme of rectangles, which allows for a comprehensive characterization of the randomness of the blockages, such as sizes, locations, orientations, and heights. However, the Boolean model (take union of (possibly random) sets placed on Poisson points) does not adapt well to random lines, since random lines are not localized [72]. In [68], authors developed a model by making use of SG to analyse the impact of shadowing in urban environments. This work has been extended to indoor systems in [73]. The authors have proposed an analytically tractable model by using Manhattan Poisson line process (MPLP) for handling the effect of walls in 2D indoor environment and in [74] the analysis has been extended to 3D indoor networks. In [75], the authors investigates the performance of wireless communication networks in indoor scenarios by using several wall generation methods. For generating an indoor environment comprising of wall blockages, they have employed several methods ranging from conveniently tractable Boolean schemes to a practical floor plan generation as well as the Manhattan line process. It has been showed that MPLP provides a tight lower bound for a real situation. In particular, the authors employed the signal-to-interference ratio (SIR) as a figure of merit, since it serves as a basis for further metrics such as coverage and rate. Comparing the wall generation methods, the authors found that for similar wall volume, the average attenuation is the same. In contrast to that, the SIR performance varies, which is due to the dynamics in the SIR values for individual realizations. The conclusions of this work show that MPLP wall generation yields the tightest lower bound with respect to the SIR results among all the mathematically tractable wall generation methods. Motivated by this, in this dissertation we focus on MPLP in order to model shadowing effect.

**Manhattan Poisson line process (MPLP)**

**Definition 3 (Poisson Line Process).** *A (stationary) Poisson (undirected) line process of intensity $\lambda > 0$ is obtained from a Poisson point process on $\mathbb{R} \times [0, \pi)$ with intensity $\frac{1}{2}\lambda dr d\theta$ as follows: for each point $(r, \theta)$ in the point process, a line is generated at signed distance $r$ from the origin and making an angle $\theta$ with the x-axis.*

(Stationary) Poisson *directed* line processes can be obtained from undirected Poisson line processes (PLP) by assigning a direction to each line. A natural parameter space would then be $\mathbb{R} \times [0, 2\pi)$ [72].

MPLP is a special case of PLP where the grid-like structure of lines resembles walls for indoor environment. In MPLP model, the plane is divided into rooms of random size. And the variability of room sizes is explained as an essential feature of the model which captures the fact that more users (wireless devices) appear in larger rooms (e.g., conference rooms/halls) than in smaller rooms (e.g., small offices). Moreover, the authors of [73] have mentioned that unit grid model which is a simpler model than MPLP can provide a certain level of insights. However, as the authors showed in the paper, the randomness of the MPLP model creates important properties that do not exist in the aforementioned simple method.

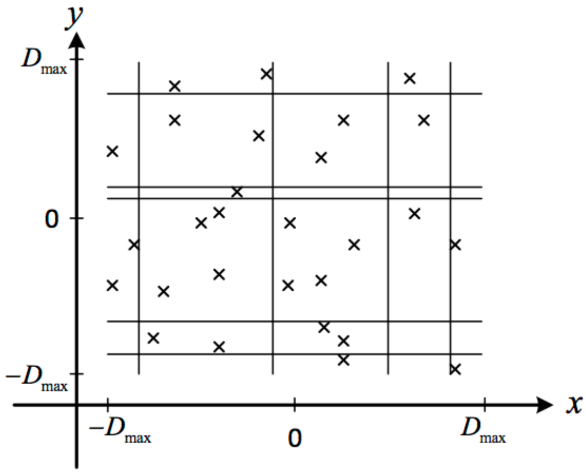


FIGURE 2.9: One realization of the MPL and PP processes.

In MPLP, the orientations of the lines are restricted to $\{0, \pi/2\}$, which means we obtain a set of horizontal and vertical lines in $\mathbb{R}$. In order to generate random lines by using MPLP in an Euclidean space $\mathbb{R}$, we define two homogenous PPPs $\Psi_x, \Psi_y \in \mathbb{R}$ with an identical density $\lambda_w$, over the x-axis and the y-axis, respectively. For illustrative purposes, an instance of a dense SWIPT network over a large area is shown in Fig. 2.9. Here lines represent walls and the markers symbolise PHs.

# Chapter 3

# MIMO SWIPT Networks in the Presence of Spatially Correlated Shadowing

The main target of this chapter is to provide a system-level perspective on the interplay between data and energy transfer in a SWIPT-based system in the presence of spatially correlated shadowing. For analysing the performance of the system in terms of the achievable trade-offs, we will obtain the joint complementary cumulative distribution function of information rate and harvested power. In order to achieve this, we will investigate the stochastic behaviours of the signal attenuation, the multi-user interference and the small scale fading of the serving link. To emphasize the cross-dependences between the deployment of the network elements and the macro parameters that characterise the topology of the venue, rate-energy trade-off will be presented as a function of the density of the obstacles. Finally, we will take advantage of our analysis to obtain the operating conditions of a real-time computing system by putting the achievable performance region in relation with the energy depleted by the central process unit to execute the computational task.

## 3.1 Introduction

Due to its ability to provide useful system-level performance insights, stochastic geometry revealed itself as a useful tool for the modelling and analysis of a variety of wireless networks [76]. In the literature it has been studied to analyse the performance of SWIPT-enabled relay networks [11], ad-hoc networks [21], sensor networks [62] and cellular networks [63], [64]. In particular, the authors of [63] have introduced a new mathematical framework for system-level analysis and optimization for wireless-powered cellular networks. A new mathematical framework for computing the J-CCDF of average harvested energy and average rate is proposed and validated. In their study they have considered two different receiver architectures for SWIPT (TS and PS), a channel model that distinguishes Line-Of-Sight (LOS) and Non-Line-Of-Sight (NLOS) links, and a directional beamforming. In [64], authors extended the work of [63] to MIMO SWIPT-enabled networks. They have introduced a tractable mathematical approach for quantifying the benefits of using MIMO in SWIPT-enabled cellular networks and showed that the use of multiple antennas at both the base stations (BS) and at the low-energy devices is capable of enhancing the achievable rate and increasing the harvested power simultaneously.

Though the methodology that is presented in [63] and [64] is extremely valuable in providing a tool for analysing the performance of stochastic SWIPT-enabled networks, these studies consider an outdoor cellular network that is too sparse to satisfy the constraints on the minimum received power that would enable RF energy harvesting [77]. Moreover, both papers consider distance-based path-loss functions only, thus failing in describing the correlated structure of the signal blockage due to buildings and walls.

Contributions on blockage modelling have been presented in [71], [68] and [73]. The authors of [71] have proposed a mathematical framework to model blockages with random sizes, locations, and orientations in cellular networks using concepts from random shape theory. In [68], a generative model based on stochastic geometry is developed to analyse the shadowing effect in urban environments. This work has been extended to in-building systems in [73] by modelling the walls' distribution as an MPLP. It is worth mentioning that the assumption behind this work is that the blockage-based penetration loss is the dominant factor and free-space propagation loss can be neglected. This model, while convenient for traditional data communication networks, conflicts with the typical operating conditions of SWIPT systems, in which the minimum received energy must be in the order of few microwatts to enable RF harvesting, so that a small difference on the distance can have a huge impact on the achievable rate-energy trade-off.

More realistically, in [75], the authors jointly considered distance-dependent path-loss, wall blockage and small-scale fading in information-only wireless networks and examined the average number of blockages for several wall generation methods, from random and shape theory to semi-deterministic and heuristic approaches. In this study, they considered different fixed transmitter configurations that provide the best scenario with respect to the interference. The conclusions of this work show that MPLP wall generation yields the tightest lower bound with respect to the SIR results among all the mathematically tractable wall generation methods.

In this chapter, we consider a signal propagation model where distance dependent path-loss, wall blockages and small scale fading are considered jointly. In order to model the wall blockages we will adopt MPLP and propose a stochastic geometry analysis for dense in-building MIMO SWIPT networks. The main contributions and results presented in this chapter are summarised as follows:

- In contrast to prior contributions relevant to SWIPT, we consider the effect of randomly located blockage objects like walls. This is of particular importance for any scenario accounting for the realistic levels of incident RF power required to activate the rectifier and produce a serviceable DC voltage at its output.

- We consider joint effect of the distance dependent propagation loss and blockages for a SWIPT-enabled network. The locations of both PHs and walls are modelled through a stochastic process, thus allowing a macro-level investigation of the interactions between the network nodes and the venue in which they are deployed.

- The geographical position of PHs and walls are modelled as Poisson processes. It follows that the characterisation of multi-user interference depends on the density of PHs as well as on the density of blocking objects. This model allows a multi-dimensional analysis in which the impact of both the network densification and the density of blocking objects on the rate-energy trade-offs are jointly analysed.

- The reported numerical results provide important insights on the interplay between the network and the in-building environment from the perspective of the rate-energy trade-off. The potentiality of maximum ratio transmission (MRT)- maximum ratio combining (MRC) processing in improving the rate energy trade-off of the link is also assessed.

- We studied the non-trivial rate-energy trade-off between the PHs' density and the density of the obstacles. Blockage objects can be beneficial in some cases depending on which trade-off is considered. Their effect in reducing the received power is compensated by the decrease of MUI.

- We investigated the effect of power splitting ratio by showing that it has relatively low impact on the maximum achievable information rate while more power can be harvested with its higher values.

- It is shown that multi antenna processing is a valuable strategy to counteract the undesired effect of the densification. Increasing the number of antennas helps improving both harvested energy and information rate.

- We have studied the best CPU utilization with the help of the provided analysis. We accounted for the complexity of the computation tasks as well as the rate at which those tasks are performed to map the rate-energy trade-off onto a value of achievable computation rate. It is shown that the best CPU utilisation is obtained when more complex tasks are performed at a lower rate instead of executing less complex tasks at a higher rate.

## 3.2 System Model

We consider a MIMO power splitted SWIPT-enabled system deployed in a two dimensional area. The SWIPT waveforms are generated by a set of randomly located PHs and each PH has equipped with $n_{\mathrm{t}}$ antenna. The LPD with an integrated SWIPT receiver which operates according to the power splitting is located at the centre of the investigated area and is equipped with $n_{\mathrm{r}}$ antenna. It is worth to mention that our analyses can be straightforwardly extended to a scenario where time switching is considered.

In order to increase the performance of the information transfer process, the received signals captured from the different LPD antennas are processed using MRC, while MRT is implemented at the transmitter side. It is worth mentioning that with such a

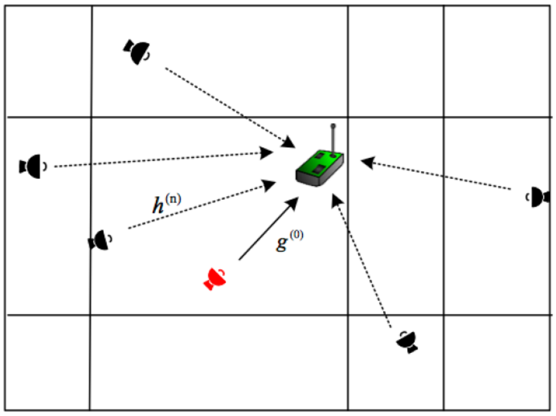


FIGURE 3.1: SWIPT indoor network

limited amount of energy available, there might appear some technical challenges in a practical implementation of MRT. Just to mention a few, the imperfect knowledge of the estimated signal to interference plus noise ratio (SINR), the temporal variations of the propagation environment for LPD with low duty cycle, and so forth. However, since the scope of this dissertation is to analyse the fundamental theoretical limits of the system, we will not address these important issues.

Fig. 3.1 presents an illustration of a SWIPT network in an indoor scenario. Here, the serving PH (the red one) is transmitting data and power towards the typical LPD with power gain $g^{(0)}$. The power wirelessly delivered in the downlink can then be used for enabling all the LPD functionalities, including subsequent uplink communications. Hence, provided that a reliable energy consumption model for the LPD is available, the rate-energy trade-off also defines the operating conditions of the LPD functionalities including computation and uplink communication (e.g. data rates, duty cycles, etc.) that can be supported through SWIPT. In this chapter, we will focus on the energy-computation trade-off originated in the downlink. The impact of this trade-off on the LPD functionalities will be addressed in the next chapters.

As it is mentioned before, one of the objectives of this chapter is to analyse the effect of the randomly located blockage objects like walls on the rate-energy trade-off. Hence our signal propagation model must comprise wall blockages. To achieve this, we assume that the signals are subject to distance dependent path-loss, wall blockages and small scale fading. The path-loss and the wall blockages are jointly modelled through the following log-distance dependent law:

$$l_N(r) = \begin{cases} \frac{\kappa r^{\alpha}}{K^N} & \text{if} \quad r \geq \kappa^{-1/\alpha} \\ 1 & \quad \text{otherwise} \end{cases} \tag{3.1}$$

where $r$ is the distance between the PH and the device, $\alpha$ is the path-loss exponent, $\frac{1}{K}$ is the so called penetration loss where $K \in [0, 1)$, and $N$ is a random variable representing the number of walls between a generic PH and the device. The path-loss constant is defined as $\kappa = (\frac{4\pi f_c}{c_0})^2$, where $f_c$ and $c_0$ being the carrier frequency (Hz) and the speed of light (m/sec), respectively. The small scale fading is modelled through random variables following a Rayleigh distribution to account for the multi-path propagation effect. More accurate fading models, like shadowed $\kappa - \mu$, can be adopted. However, using those models would harm the readability of the analytical results without bringing any additional insights into the spatially correlated structure of the blocking objects. Hence, in this dissertation, we focus on the more tractable Rayleigh fading model.

The locations of the network elements have an important impact on the performance of SWIPT-enabled systems, since they determine the interference distribution. In this system model, we assume that the network infrastructure is modelled by a set of PHs randomly located inside a circular area with radius $R_{\mathrm{a}} \in \mathbb{R} \cup \infty$ . We assume that the PHs have been deployed following a homogeneous PPP distribution, $\Psi_{\mathrm{ph}}$, with density $\lambda_{\mathrm{ph}}$. Moreover the positions of walls are modelled as MPLP with density $\lambda_{\mathrm{w}}$.

Finally we assume that the information transfer towards the typical LPD, denoted by LPD$^{(0)}$, is provided by the PH ensuring the smallest average signal attenuation, also referred to as serving PH. From the information transfer perspective the other PHs are considered as interferers. The set of interfering PHs is denoted by $\Psi^{(\backslash 0)}$. In the next section, we will provide the adopted methodology that will be used to analyse the effects of the obstacles on the SWIPT-enabled system performance.

## 3.3 Performance Analysis

This section presents a methodology to study the effects of the obstacles on the SWIPT performance. Then, we provide an expression for the J-CCDF of information rate and harvested power as a function of the network parameters.

### 3.3.1 Wall Blockage Analysis

The positions of the walls have an important impact on the system performance due to their effect on the interference distribution. Among the other blockage modelling concepts such as Boolean schemes or practical floor plan generation, MPLP is an analytically tractable model that provides a tight lower bound for a real situation. In order to study the effect of blockage objects on the system performance by using MPLP, we first decompose the original PPP, $\Psi$, with density $\lambda_{\mathrm{ph}}$ into the sum of equivalent PPPs whose distribution depends on the specific geographic coordinate (i.e. inhomogenous PPP), $\Psi_N$. Since the number of walls blocking the signal depends on the position of the PHs we need to obtain the spatial distribution of the PHs that experience $N$ blocking objects. Thus displacement theorem (see Section 2.2) is advocated and the densities of the processes $\Psi_N$ are given by

$$\lambda_N(r,\theta) = \lambda_{\mathrm{ph}} P_N(r,\theta) . \tag{3.2}$$

Here $P_N(r,\theta)$ is the probability that $N$ walls are experienced at the point defined by the polar coordinates $(r,\theta)$ and given as

$$P_N(r,\theta) = \frac{\left(\lambda_{\mathrm{w}} r|\cos(\theta)| + \lambda_{\mathrm{w}} r|\sin(\theta)|\right)^N}{N!} \times \exp\left\{-\left(\lambda_{\mathrm{w}} r|\cos(\theta)| + \lambda_{\mathrm{w}} r|\sin(\theta)|\right)\right\} . \tag{3.3}$$

To make it clear, it worths recalling the fact that the number of walls in the intervals $[0, r|\cos(\theta)|]$ and $[0, r|\sin(\theta)|]$ along the x$-$ and y$-$ dimensions, respectively, is a random variable with Poisson distribution since MPLP is utilised in order to model the positions of the walls. Thus, the probabilities of experiencing $N$ walls on x-axis and y-axis can be found as $\frac{(\lambda_{\mathrm{w}} r|\cos(\theta)|)^N}{N!} e^{-\lambda_{\mathrm{w}} r|\cos(\theta)|}$ and $\frac{(\lambda_{\mathrm{w}} r|\sin(\theta)|)^N}{N!} e^{-\lambda_{\mathrm{w}} r|\sin(\theta)|}$, respectively. Since the sum of two independent Poisson random variables is Poisson distributed with density equal to the sum of the two corresponding densities, (3.3) can be easily obtained.

As mentioned before, LPD$^{(0)}$ receives the information from the serving PH which provides the minimum average signal attenuation. However, this choice depends both on the locations of the PHs and the placement of the walls. Thus, in order to analyse the performance of the system, we first need to study the characterization of the stochastic properties of the minimum path-loss, $L^{(0)}$, and the multi-user interference, $\mathcal{I}_{\mathrm{MU}}$.

**Minimum Path-Loss**

Minimum path-loss, $L^{(0)}$, is given as

$$L^{(0)} = \min_{N} \left\{ \min_{\mathrm{n} \in \Psi_N} \left\{ l_N(r^{(\mathrm{n})}) \right\} \right\} \tag{3.4}$$

where n denotes the index of the PHs belonging to the inhomogeneous PPPs associated with $N$ obstacles, $\Psi_N$, and $r^{(\mathrm{n})}$ is the distance between the LPD and the nth PH. By capitalising on displacement theorem we end up with the following proposition.

**Proposition 2.** *Let the minimum path-loss being the one defined in* (3.4) *and define a function* $\chi_\eta(\lambda_w)$ *as*

$$\chi_\eta(\lambda_w) = \lambda_w^\eta \left[ \frac{2^{\frac{\eta}{2}} \sqrt{\pi}\, \Gamma(\frac{\eta+1}{2})}{\Gamma(\frac{\eta+2}{2})} - \frac{\sqrt{2}\, {}_2F_1\left(\frac{1}{2}, \frac{\eta+1}{2}, \frac{\eta+3}{2}, \frac{1}{2}\right)}{\eta+1} \right] \tag{3.5}$$

*where* $\Gamma(\cdot)$ *is the Gamma function,* ${}_2F_1(\cdot)$ *is the Gaussian hypergeometric function [78] and* $\eta \in \mathbb{R}_+$ *is a compound variable (i.e.* $\eta = N + i$*) introduced in Appendix A. Then the cumulative distribution function (CDF) of* $L^{(0)}$ *is given by*

$$F_{L^{(0)}}(\xi) = \Pr\{L^{(0)} \le \xi\} = 1 - \prod_{N=0}^{N_{max}} \exp\{-\Lambda_N([0,\xi))\} \tag{3.6}$$

*where* $N_{max}$ *is the number of walls beyond which the attenuation due to blockage makes negligible the signal contribution to the rate-energy trade-off.*

$$\Lambda_N([0,\xi)) = \begin{cases} \frac{4\lambda_{ph}}{N!} \sum\limits_{\eta=N}^{\infty} \frac{(-1)^{\eta-N} \chi_\eta(\lambda_w)}{(\eta-N)!(\eta+2)} \left(\frac{\xi K^N}{\kappa}\right)^{\frac{\eta+2}{\beta}} & \text{if } 1 \le \xi < \frac{R_a^\alpha \kappa}{K^N} \\ \frac{4\lambda_{ph}}{N!} \sum\limits_{\eta=N}^{\infty} \frac{(-1)^{\eta-N} \chi_\eta(\lambda_w)}{(\eta-N)!(\eta+2)} R_a^{\eta+2} & \text{if } \xi \ge \frac{R_a^\alpha \kappa}{K^N} \end{cases} \tag{3.7}$$

*is the intensity of the process* $L_N = \left\{ l_N(r^{(n)}), n \in \Psi_N \right\}$.

*Proof.* See Appendix A. □

In this proposition, we have studied the statistical characterization of minimum path-loss and obtained the CDF of $L^{(0)}$. By using the expression of CDF, probability density function (PDF) of $L^{(0)}$, *i.e.* $f_{L^{(0)}} = dF_{L^{(0)}}(x)/dx$ can be easily obtained.

TABLE 3.1: Values of $\chi_\eta(\lambda_w)$

| $\lambda_w\backslash\eta$ | 0 | 1 | 2 | 3 | 4 | 5 |
|---|---|---|---|---|---|---|
| 0.01 | 1.5708 | 0.02 | $2.5\times10^{-4}$ | $3.3\times10^{-6}$ | $4.35\times10^{-8}$ | $5.73\times10^{-10}$ |
| 0.02 | 1.5708 | 0.04 | $1\times10^{-3}$ | $2.6\times10^{-5}$ | $6.96\times10^{-7}$ | $1.83\times10^{-8}$ |
| 0.03 | 1.5708 | 0.06 | $2.3\times10^{-3}$ | $9\times10^{-5}$ | $3.5\times10^{-6}$ | $1.39\times10^{-7}$ |
| 0.04 | 1.5708 | 0.08 | $4.1\times10^{-3}$ | $2.1\times10^{-4}$ | $1.1\times10^{-5}$ | $5.87\times10^{-7}$ |
| 0.05 | 1.5708 | 0.1 | $6.4\times10^{-3}$ | $4.1\times10^{-4}$ | $2.7\times10^{-5}$ | $1.79\times10^{-6}$ |

Moreover, as explained in Appendix A, in order to obtain an analytical expression, we make use of Taylor series. It is worth to mention that the fact that the series has to be cut at some point leads an approximation.

From (3.7), it is apparent that the signal attenuation is a process whose intensity can be expressed as the weighted sum of power functions of $\xi$. Interestingly, the effects of the blockage due to the walls are captured by the weights $\chi_\eta(\lambda_w)$ that can be computed offline and tabulated for given values of $\eta$ and $\lambda_w$ as shown in Table 3.1. As we mentioned before, the effect of shadowing does not depend on the topology of the network but depends only on the topology of the venue. Thus, Table 3.1 reports the coefficients associated to the distribution of the blocking objects irrespectively to the distribution of the network nodes. This allows us to use the offline computed results in our further analysis by simply substituting the coefficients reported in Table 3.1 that are associated with the required values of $\eta$ and $\lambda_w$ in (3.7). Since $\chi_\eta(\lambda_w)$ is a decreasing function of $\eta$, from (3.6) and (3.7), above a certain number of obstacles that the signal can encounter, the values of $\chi_\eta(\lambda_w)$ become negligible. Consequently, we can infer that the greater the number of obstacles $N$, the lower the impact of the blockage objects on the CDF of $L^{(0)}$. On the contrary, $\chi_\eta(\lambda_w)$ is an increasing function of $\lambda_w$ and, not surprisingly, the impact of the blockage objects on $F_{L^{(0)}}(\xi)$ increases with $\lambda_w$.

### Multi-User Interference

After studying the characterization of the stochastic properties of minimum path-loss, we continue with analysing the characteristic function of multi-user interference. The normalized (with respect to 1W of transmit power) multi-user interference can be expressed as

$$\mathcal{I}_{\mathrm{MU}} = \sum_{N=0}^{N_{max}} \sum_{\mathrm{n}\in\Psi_N} \frac{h^{(\mathrm{n})}}{l_N(r^{(\mathrm{n})})} \mathbb{1}\left\{l_N(r^{(\mathrm{n})}) > L^{(0)}\right\} \tag{3.8}$$

where $h^{(\mathrm{n})}$ represents the gain of the $n$th interfering link and is an exponentially distributed random variable with unit variance. Here $\mathbb{1}(\cdot)$ is the indicator function.

In order to obtain characteristic function of MUI, we first need to have the CDF of $\mathcal{I}_{\mathrm{MU}}$. They are provided in Proposition 3.

**Proposition 3.** *For a given path-loss $L^{(0)}$, consider the functions $\chi_\eta(\lambda_w)$, $\eta\in\mathbb{R}_+$ as in* (3.5)*, and define the function*

$$
\begin{aligned}
&\Delta_{\eta,N}\left(\omega; L^{(0)}\right) = \\
&\left(\frac{L^{(0)}K^N}{\kappa}\right)^{\frac{\eta+2}{\alpha}} \left(1 - {}_2F_1\left(1, -\frac{\eta+2}{\alpha}, 1 - \frac{(\eta+2)}{\alpha}, \frac{j\omega}{L^{(0)}}\right)\right) \\
&- R_a^{\eta+2}\left(1 - {}_2F_1\left(1, -\frac{\eta+2}{\alpha}, 1 - \frac{(\eta+2)}{\alpha}, \frac{j\omega K^N}{R_a^\alpha \kappa}\right)\right).
\end{aligned} \tag{3.9}
$$

*Then, capitalizing on the Gil-Pelaez inversion theorem, [79], the CDF of $\mathcal{I}_{MU}$ is given by*

$$
F_{\mathcal{I}_{MU}}(z; L^{(0)}) = \Pr\{\mathcal{I}_{MU} \le z | L^{(0)}\} = 1/2 - \int_0^\infty \frac{1}{\pi\omega} \operatorname{Im}\left\{e^{-j\omega z}\prod_{N=0}^{N_{max}} \Phi_N\left(\omega; L^{(0)}\right)\right\} d\omega \tag{3.10}
$$

*where $\Phi_N\left(\omega; L^{(0)}\right)$ is the characteristic function of the multi-user interference produced by the PHs whose signals are subject to the attenuation of $N$ obstacles to reach the typical LPD and shown as*

$$
\Phi_N\left(\omega; L^{(0)}\right) = \begin{cases} \exp\left\{\frac{4\lambda_{ph}}{N!}\sum\limits_{\eta=N}^{\infty}\frac{(-1)^{\eta-N}\chi_\eta(\lambda_w)}{(\eta-N)!(\eta+2)}\Delta_{\eta,N}\left(\omega; L^{(0)}\right)\right\} & \text{if } L^{(0)} < \frac{R_a^\alpha\kappa}{K^N} \\ 1 & \text{if } L^{(0)} \ge \frac{R_a^\alpha\kappa}{K^N}. \end{cases} \tag{3.11}
$$

*Proof.* See Appendix B. □

### 3.3.2 SWIPT Performance Analysis

As explained in the previous chapter, due to the multi objective nature of SWIPT, the performance of SWIPT-enabled systems can be described in terms of achievable trade-offs between the average throughput (bits/sec), $R$, and the average harvested power (in Watt), $Q$. These rate-energy trade-offs are analysed through the J-CCDF of the achievable information rate and the average harvested power:

$$
F_c(R^*, Q^*) = \Pr\{R \ge R^*, Q \ge Q^*\} \tag{3.12}
$$

where $R^* \ge 0$ and $Q^* \ge 0$ represent the minimum desired rate and the sensitivity of the energy harvester, respectively. Assuming that the transmission bandwidth is equal to $W$ and that each PH transmits with average power $P$, we have

$$
\begin{aligned}
R &= W\log_2\left(1 + \frac{Pg^{(0)}/L^{(0)}}{P\mathcal{I}_{\mathrm{MU}} + \sigma_{\mathrm{n}}^2 + \sigma_{\mathrm{c}}^2/(1-\rho)}\right), \\
Q &= \rho\mu P\left(\frac{g^{(0)}}{L^{(0)}} + \mathcal{I}_{\mathrm{MU}}\right)
\end{aligned} \tag{3.13}
$$

in which $\rho$ is the power splitting ratio and $\mu$ is the energy harvesting efficiency factor. The variance of the thermal noise is denoted by $\sigma_{\mathrm{n}}^2$, while $\sigma_{\mathrm{c}}^2$ indicates the variance of the noise due to the conversion of the received signal from radio frequency to baseband [51].

As known, RFEHs are non-linear devices. Therefore the efficiency of the harvesting process would actually depend on the particular SWIPT waveform adopted and on the incident Rx power. However, for the sake of tractability, we make the hypothesis that the system adopts an optimised waveform which provides an almost constant efficiency across all the operating region of the RFEH. Thus, it has been assumed that the harvested power is a linear function of the received power in (3.13) [77].

In order to obtain J-CCDF of the achievable information rate and the average harvested power, we need to study the characterization of stochastic properties of the random variables that have an impact on the performance of the system i.e. minimum path-loss, multi-user interference and small scale fading of the serving link. In the previous chapter, we have provided the characteristic functions of the minimum path-loss, $L^{(0)}$, and the multi-user interference, $\mathcal{I}_{\mathrm{MU}}$. Now we will discuss about another source of randomness which is the small scale fading $g^{(0)}$ of the link between the serving PH and the LPD$^{(0)}$. It comprises the small scale fading experienced by the serving PH's signal and the effect of both the MRT and the MRC processing at the transmitter and the receiver side, respectively. As mentioned in [80], the MRT-MRC processing minimizes the induced bit- or symbol- error probability and therefore maximizes the output SNR. This maximization yields to $g^{(0)}$, which is the largest eigenvalue of the Hermitian matrix, $\mathbf{H}^H\mathbf{H}$ where $\mathbf{H} = \left[g_{i,j}^{(0)}\right]_{i,j=1}^{n_t,n_r}$, representing the small scale fading. The probability density function (PDF) of $g^{(0)}$ is given as [80],

$$f_{g^{(0)}}(\zeta) = \mathcal{K}_{m,n} \sum_{s=1}^{m} \sum_{t=n-m}^{(n+m-2s)s} a_{s,t}\zeta^t \exp(-s\zeta) \tag{3.14}$$

where $m = \min(n_t, n_r)$ and $n = \max(n_t, n_r)$. Here $\mathcal{K}_{m,n} = \prod_{k=1}^{m}((m-k)!(n-k)!)^{-1}$ is a normalising factor and $a_{s,t}$ are some coefficients that can be easily obtained by using [80, Algorithm 1].

A convenient reformulation of the J-CCDF has been proposed in [64]. It amounts to computing the probability that the multi-user interference belongs to an interval for which a minimum SINR $\beta$ can be achieved conditioned to a minimum amount of received power $q_*$. It can be shown as

$$\begin{aligned} F_{\mathrm{c}}(R^*, Q^*) = \mathbb{E}_{L^{(0)}} &\left\{ \int_{(\mathcal{T}_*/P)L^{(0)}}^{+\infty} F_{\mathcal{I}_{MU}} \left( x\beta/L^{(0)} - \sigma_*^2/P \,\middle|\, L^{(0)} \right) f_{g^{(0)}}(x)dx \right\} \\ - \mathbb{E}_{L^{(0)}} &\left\{ \int_{(\mathcal{T}_*/P)L^{(0)}}^{+\infty} F_{\mathcal{I}_{MU}} \left( -x/L^{(0)} + q_*/P \,\middle|\, L^{(0)} \right) f_{g^{(0)}}(x)dx \right\} \end{aligned} \tag{3.15}$$

where $\sigma_*^2 = \sigma_{\mathrm{n}}^2 + \sigma_{\mathrm{c}}^2(1-\rho)^{-1}$, $q_* = Q^*/(\rho\mu)$, $\mathcal{T}_* = (q_* + \sigma_*^2)/(\beta+1)$ and $\beta = 1/\left(2^{R^*/W} - 1\right)$.

After analysing the statistical characterisations of minimum path-loss, multi-user interference and the power gain of the serving link, we now obtain J-CCDF in Proposition 4.

**Proposition 4.** *Let us define,*

$$\begin{aligned}\Phi\left(\omega; L^{(0)}\right) &= \prod_{N=0}^{\infty} \Phi_N\left(\omega; L^{(0)}\right), \\ \Lambda([0,\xi)) &= \sum_{N=0}^{\infty} \Lambda_N([0,\xi)),\end{aligned} \tag{3.16}$$

*and $\widehat{\Lambda}([0,\xi))$ as the derivative of $\Lambda([0,\xi))$ with respect to $\xi$, whose expression is provided by* (B.3) *in Appendix B.*

*Given the statistical characterisation of $L^{(0)}$, $\mathcal{I}_{MU}$, and $g^{(0)}$ expressed as in* (3.6), (B.5), *and* (3.14), *respectively, the J-CCDF $F_c(R^*, Q^*)$ can be computed as [64],*

$$F_c(R^*, Q^*) = \mathcal{K}_{m,n} \sum_{s=1}^{m} \sum_{t=n-m}^{(n+m-2s)s} a_{s,t}\left(J_{s,t}^{(1)} - J_{s,t}^{(2)}\right) \tag{3.17}$$

*where the functions $J_{s,t}^{(1)}$ and $J_{s,t}^{(2)}$ are defined as*

$$\begin{aligned}&J_{s,t}^{(1)} = \\ &\int_1^\infty \int_0^\infty \frac{1}{\pi w} \operatorname{Im}\left\{ \exp\left(-jw\frac{q_*}{P}\right)\left(s - \frac{jw}{y}\right)^{-(1+t)} \Gamma\left(1+t, \frac{\mathcal{T}_*}{P}(sy - jw)\right)\Phi(w;y)\right\} \\ &\times \left(\widehat{\Lambda}([0,\xi)) \exp\left\{-\Lambda([0,\xi))\right\}\right) dwdy\end{aligned} \tag{3.18}$$

$$\begin{aligned}&J_{s,t}^{(2)} = \\ &\int_1^\infty \int_0^\infty \frac{1}{\pi w} \operatorname{Im}\left\{ \exp\left(jw\frac{\sigma_*^2}{P}\right)\left(s + \frac{jw\beta}{y}\right)^{-(1+t)} \Gamma\left(1+t, \frac{\mathcal{T}_*}{P}(sy + jw\beta)\right)\Phi(w;y)\right\} \\ &\times \left(\widehat{\Lambda}([0,\xi)) \exp\left\{-\Lambda([0,\xi))\right\}\right) dwdy\end{aligned} \tag{3.19}$$

*Proof.* See Appendix C □

Using Proposition 4 the J-CCDF can be numerically computed for illustrating the average trade-off between the information rate and the harvested power without the need of time consuming Monte Carlo simulations.

## 3.4 Numerical Results

This section shows the performance of a SWIPT-enabled indoor network by means of numerical results. The analytical findings presented in previous sections will be validated through Monte Carlo simulations.

### 3.4.1 Setup

The parameters are set as given in Table 3.2 unless otherwise specified. The PHs are assumed to be deployed with a density $\lambda_{\text{ph}} = 1/(\pi d_{\text{ph}}^2)$, where $d_{\text{ph}}$ is half of the

TABLE 3.2: System Parameters for Chapter 3

| | |
|---|---|
| The radius of the investigated region, $R_a$ | $60m$ |
| Average transmit power, $P$ | 1W |
| Signal bandwidth, $W$ | 200kHz |
| Carrier frequency, $f_c$ | 2.1GHz |
| Thermal noise variance, $\sigma_n^2$ | $-174 + 10log_{10}(W) + \mathcal{F}_n$ |
| Noise figure, $\mathcal{F}_n$ | 10dB |
| RF/DC conversion noise variance, $\sigma_c^2$ | $-70$dBm |
| Energy harvesting efficiency, $\mu$ | 0.8 |
| Path-loss exponent, $\alpha$ | 2.5 |
| Power splitting ratio, $\rho$ | 0.5 |
| Number of receive antennas, $n_r$ | 2 |
| Number of transmit antennas, $n_t$ | 4 |
| Penetration loss, $K$ | $-10$dB [81, Table 3] |

average distance between PHs. It worths to mention that, the methodological tool proposed in this dissertation does not depend on the values of the link parameters. As a matter of fact, though the results of numerical analysis may be changed, the qualitative behaviour of the trade-off with respect to MUI remains the same when the channel condition varies. For instance, in this study, frequency has been chosen as cellular network frequency in order to be consistent with the existing studies in literature which allows us to validate our numerical results. Nevertheless, when different frequencies are considered (e.g. ISM or subGHz bands), from Proposition 4 and assuming the same penetration loss for all frequencies, only the relative impact of distance-based path loss on the MUI will change, but not the ambivalent role of the interference on the rate-energy trade-off.

### 3.4.2 Results

In Fig. 3.2 and Fig. 3.3 we validate our analytical findings through Monte Carlo simulations. Specifically, In Fig. 3.2 we present the rate-energy trade-off parametrised with respect to $\lambda_{ph}$ when $F_c(R^*, Q^*) = 0.75$. The results are presented for different values of $d_{ph} = 3, 5, 7$ meters $\left(\text{i.e. } \lambda_{ph} = \frac{1}{28}, \frac{1}{79}, \frac{1}{154}\right)$, while the density of the walls is kept fixed to $\lambda_w = 0.05$. The analytical results (solid lines) are compared to the ones obtained through Monte Carlo simulations (squares). Despite of the approximation due to the fact that the series in (3.7) and (3.11) has to be cut at some point, an almost perfect match between theoretical results and simulations is apparent. Clearly, the harvested power always benefits from the increase of the PHs' density $\lambda_{ph}$, while the maximum achievable information rate decreases because of the larger level of multi-user interference. We can therefore identify a first compromise to be achieved when the network elements are densified. For example, if a minimum harvested energy of $-23$dBm is required, the optimum PHs' density is the one corresponding to $d_{ph} = 3$ meters (blue line), while if a harvested energy of $-28$dBm is sufficient, it would be better to have a less dense network, $d_{ph} = 5$ meters, to benefit from a higher information rate (red line).

Fig. 3.3 investigates the effect of the walls on the SWIPT performance when $F_c(R^*, Q^*)$ $= 0.75$ and $d_{ph} = 5$ meters. In this figure Monte Carlo simulations are represented with markers and theoretical results are with solid lines. The blue curve is used as a benchmark and represents the case in which all the blockage objects have been

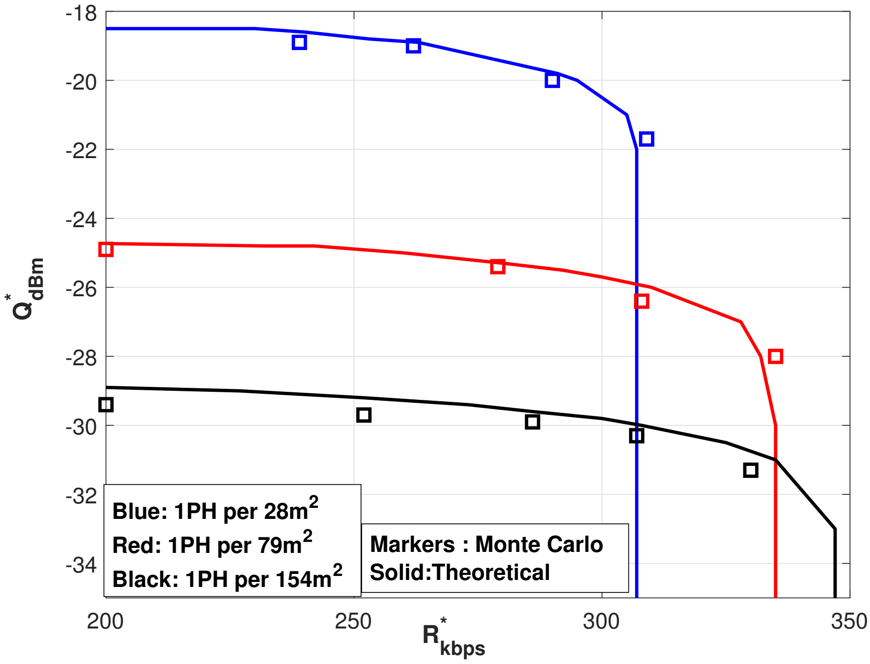


FIGURE 3.2: Monte Carlo simulations and theoretical results of rate-energy trade-off for different $\lambda_{\mathrm{ph}}$ when $\lambda_{\mathrm{w}} = 0.05$, $n_{\mathrm{t}} = 4$, $n_{\mathrm{r}} = 2$.

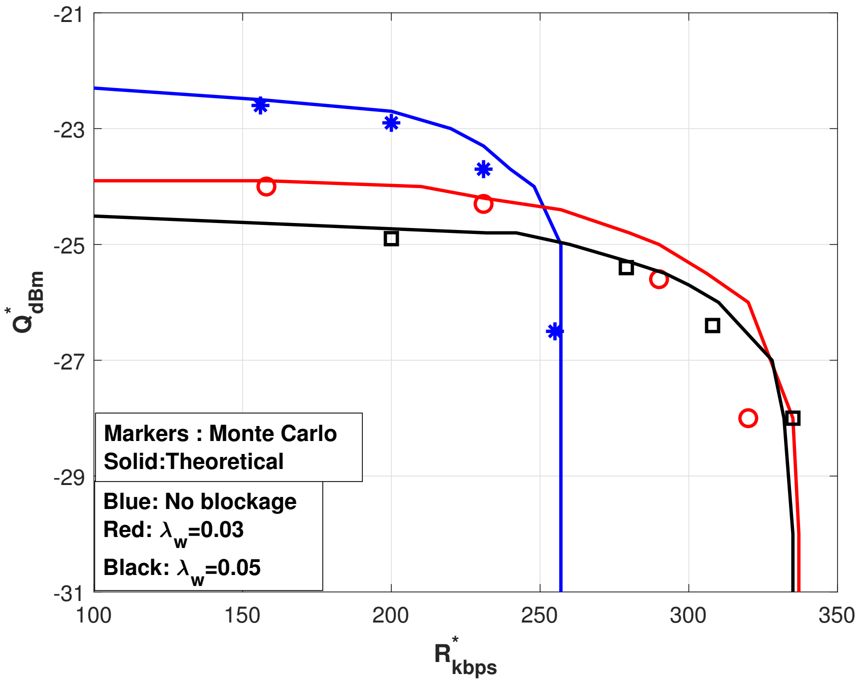


FIGURE 3.3: Monte Carlo simulations and theoretical results of rate-energy trade-off for different $\lambda_{\mathrm{w}}$ when $d_{\mathrm{ph}} = 5m$, $n_{\mathrm{t}} = 4$, $n_{\mathrm{r}} = 2$.

removed. The red and black curves are associated with two different values of $\lambda_{\mathrm{w}}$: $\lambda_{\mathrm{w}} = 0.03$ and $\lambda_{\mathrm{w}} = 0.05$, respectively. It is apparent that an increment of the density of blockage objects is beneficial for the maximum achievable information

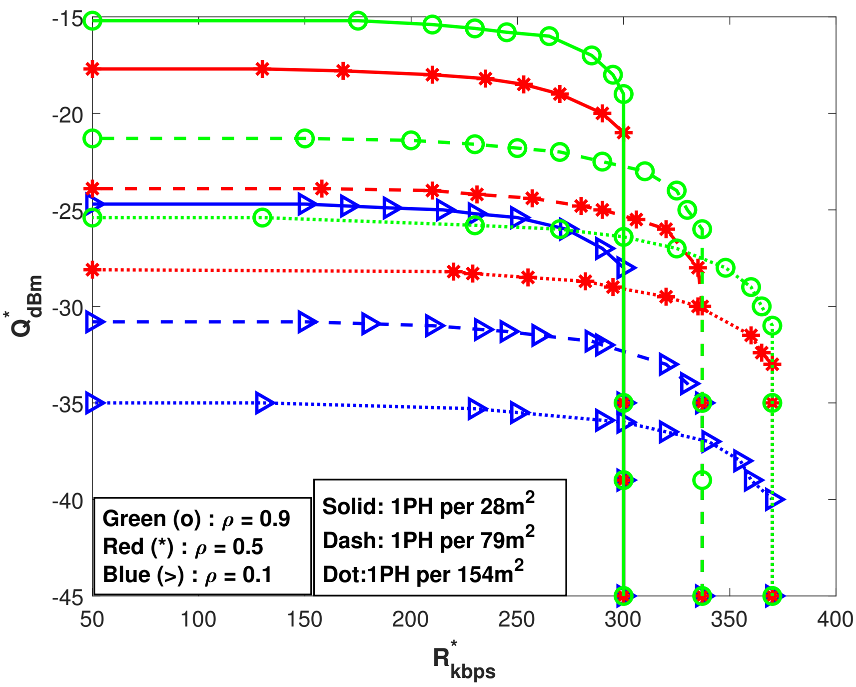


FIGURE 3.4: Theoretical results of rate-energy trade-off for different $\rho$ values when $F_c(R^*, Q^*) = 0.75$, $\lambda_w = 0.03$, $n_t = 4$ and $n_r = 2$.

rate because of the reduced multi-user interference. On the other side, we notice a reduction of the harvestable power level when $\lambda_w$ increases. We can conclude, that the topology of the venue impacts the achievable rate-energy trade-off in view of the ambivalent role of the multi-user interference in SWIPT networks. Morever, it worths to mention that, for $\lambda_w = 0.03$, theoretical result (solid line) provides a better performance compared to Monte Carlo simulations (marker) in terms of the information rate. It can be explained with the fact that theoretical result gives an underestimated interference level due to the approximation related to Taylor series.

In Fig. 3.4, we analyse the role of the SWIPT receiver architecture on the achievable performance. The rate-energy trade-offs for different values of the power splitting ratio when $F_c(R^*, Q^*) = 0.75$ are presented. The curves are provided for 3 different values of $\lambda_{ph}$ when $\lambda_w = 0.03$. Obviously, the receiver harvests more power with higher power splitting ratio for all cases. More interestingly, we obtain the same value of maximum achievable information rate for all values of $\rho$. This can be explained with the fact that, with the level of densification required to receive a total power belonging to the microwatt region, the system is essentially interference limited and the SINR has a negligible effect on $\rho$ for realistic levels of noise. For instance, considering the case $d_{ph} = 3$m (solid lines), with an information rate of 300 kbps, $-27$dBm of harvested power can be achieved when $\rho = 0.1$, while we can obtain $-20$dBm and $-17$dBm of harvested power when $\rho$ is equal to 0.5 and 0.9, respectively. We can conclude that the power splitting ratio must be as large as possible and its fine tuning is of limited interest in the design of ultra-dense SWIPT networks. It is worth remarking that this conclusion is radically different from previous works (see [64]) in which the authors consider values of harvested power below $-60$dBm. In that case, multi-user interference has a limited role while the optimisation of the power splitting ratio is paramount. On the contrary, we show that the technological

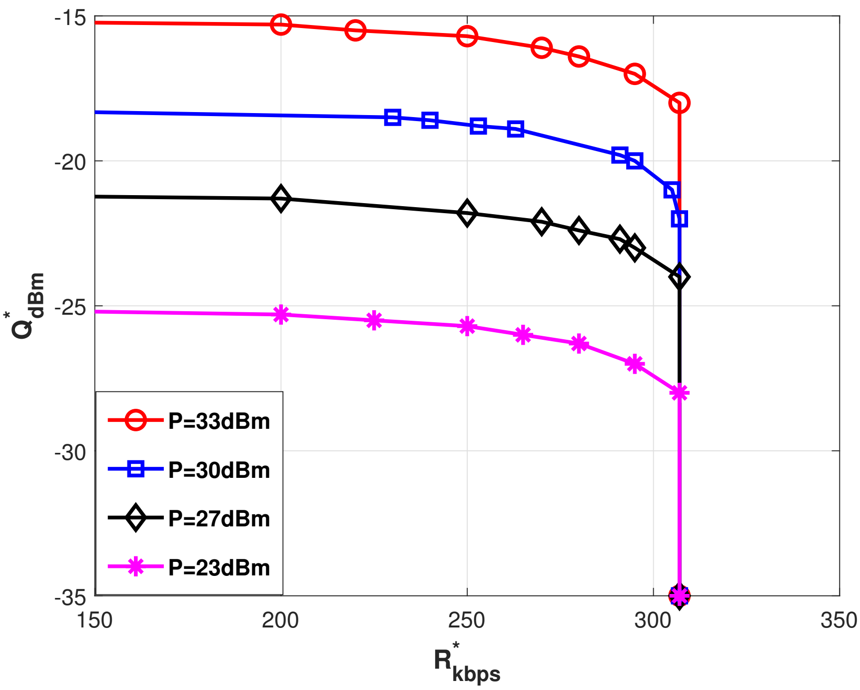


FIGURE 3.5: Theoretical results of rate-energy trade-off for different $P$ values when $F_c(R^*, Q^*) = 0.75$, $d_{ph} = 3$ and $\lambda_w = 0.05$.

limitations of the harvesting process make the topology of the venue and its effect on the interference the most important parameters in defining the achievable rate-energy trade-off.

Fig. 3.5 illustrates the rate-energy trade-off for different values of the transmit power when $n_t = 4$ and $n_r = 2$ in order to see the effect of the transmit power. As expected, more energy is harvested with higher values of transmit power. On the other hand, since the system is interference limited and the SINR is not affected by the change on values of $P$, the same maximum achievable information rate is obtained for all the considered cases.

In the previous figures we showed impact of the ambivalent role of the interference on the rate-energy trade-off. However, both harvested energy and information rate can be improved by increasing the power gain from the serving PH to the typical LPD. To achieve this antenna array gain can be increased. It is worth mentioning that in this study we refer exclusively to the rate-energy trade-off of the link while the additional energy consumption required to implement MRC at the LPD is not considered in the performance metrics. In order to illustrate the benefits of MIMO on the SWIPT performance in such a dense interference-limited scenario, Fig. 3.6 provides the rate-energy trade-off for different numbers of transmit antennas when $F_c(R^*, Q^*)$ is 0.75 and $n_r = 2$. The proposed results show how increasing the number of antennas is of great help in dealing with the MUI while improving the level of harvestable power. Here, for illustrative purposes, we present numerical results only for $\lambda_w = 0.03$, but the same trend has been observed for all the tested densities of walls.

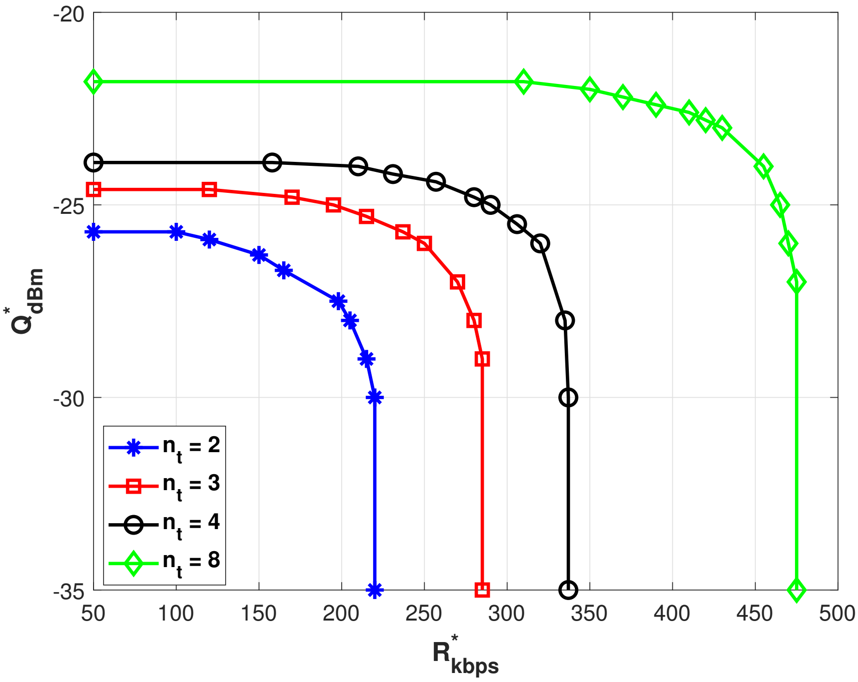


FIGURE 3.6: Theoretical results for rate-energy trade-off as a function of $n_t$ when $n_r = 2$, $\lambda_w = 0.03$ and $d_{ph} = 5m$.

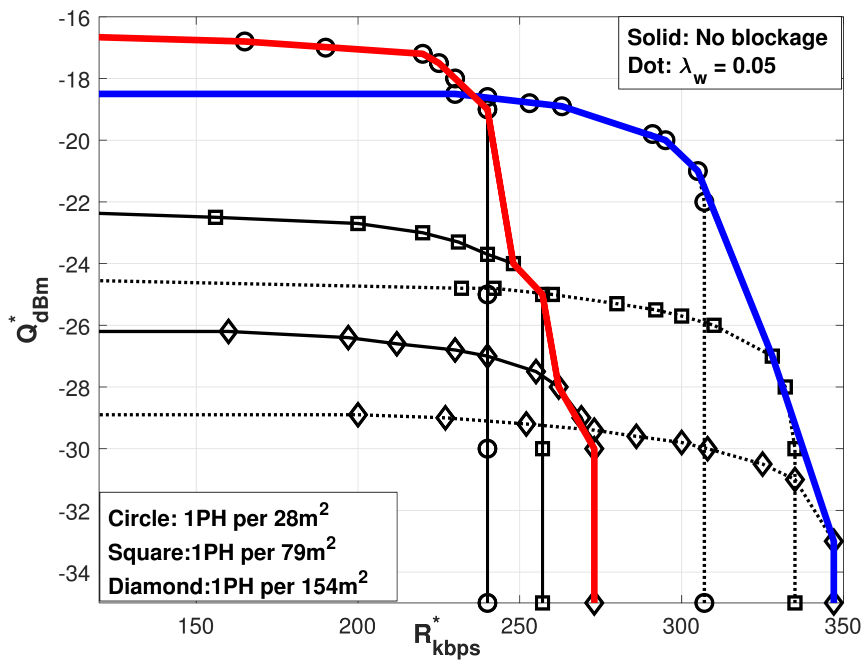


FIGURE 3.7: Theoretical results for the envelope of rate-energy trade-off for different $\lambda_{ph}$ and $\lambda_w$ when $F_c(R^*, Q^*) = 0.75$, $n_t = 4$, $n_r = 2$.

Finally, we focus on how the the level of network densification must be wisely chosen in accordance with the topological characteristic of the indoor environment. To this purpose, Fig. 3.7 shows the envelopes of the rate-energy trade-offs relevant to

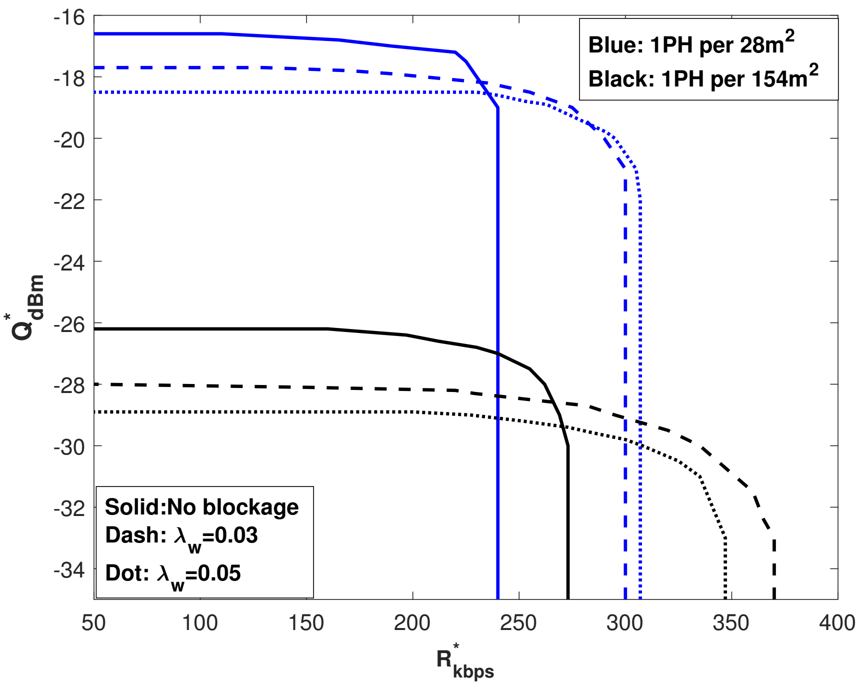


FIGURE 3.8: Theoretical results of rate-energy trade-off for different $\lambda_{\text{ph}}$ and $\lambda_{\text{w}}$ when $F_{\text{c}}(R^*, Q^*) = 0.75$, $n_{\text{t}} = 4$ and $n_{\text{r}} = 2$.

different values of $\lambda_{\text{ph}}$ and for a J-CCDF equal to 0.75. In particular, the red curve represents a situation in which all blockage objects have been removed, while the blue curve is associated with the presence of walls with density equal to $\lambda_{\text{w}} = 0.05$. It is apparent that the additional attenuation of walls is beneficial for the achievable trade-off and rate. For example, an information rate of 300 kbps can be achieved with $-20$dBm of harvested power in the presence of blockages, while this value is reduced to 240 kbps when those obstacles are removed.

In Fig. 3.8 we plotted the rate-energy trade-off for different values of $\lambda_{\text{w}}$ with $d_{\text{ph}} =$ 3m and $d_{\text{ph}} =$ 7m. In the denser case, the information rate always benefit from the reduced MUI due to the presence of walls. On the contrary, when the network elements are less dense, the blockage experienced by the serving PH is not compensated by the MUI reduction. Hence, neither the harvested power nor the information rate benefits from the interference. Therefore, we can argue that the best achievable trade-off is a multidimensional factor in which the cross-dependences between the network infrastructure and the topology of the venue have a major impact.

## 3.5 SWIPT-based Real Time Computation

In this section, we provide an application of SWIPT-enabled systems as an example for utilisation of the analysis provided in the previous sections.

### System Model

In the system model that is investigated in the previous sections, we only assume that the power enabling both computation and communication tasks at the LPD are wirelessly delivered in the downlink. The harvested energy can then be used for

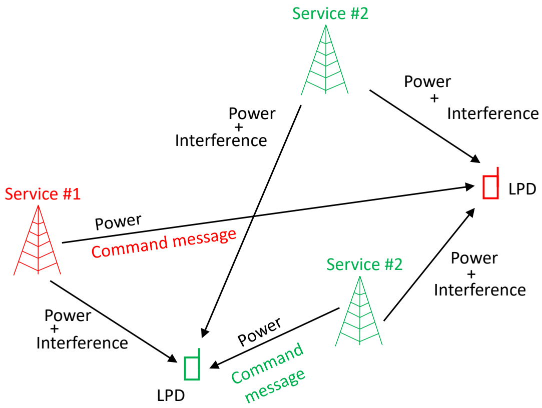


FIGURE 3.9: SWIPT-MC system model

transmitting data from the LPD to an access point. In this sense, an harvest then-transmit procedure is compatible with our analysis. However, the trade-off curve in the downlink is agnostic to the uplink transmission parameters. We analyse the probability that a given value of energy is harvestable by the LPD for different values of data rate in the downlink. This energy is then used for enabling all the LPD functionalities, including uplink communications.

In this section we will present an indoor MIMO real-time mobile computing (MC) system as an application of SWIPT. We will provide a comprehensive understanding of the rate-energy trade-off on a service basis. The objective of this MC system is to provide a set of services $\mathcal{S}$, where the attributes of a generic service $s \in \mathcal{S}$ are a collection of computation tasks. Each computation task processes $L_{\text{task}}$ bits representing contextual information (e.g. sensed data, information on the activity of a human user, mobility patterns) locally collected and stored at the LPD. The SWIPT waveform received is used to simultaneously decode the control signal that will select the computation tasks to be executed and extract the power needed to perform those tasks. According to this model, instead of considering the signal propagation as the sole restriction, we recognise that the SWIPT signals are sent with the purpose of enabling the execution of computation tasks.

Since it is a real-time MC system, the trade-off between the information rate and the harvestable energy must be carefully chosen to guarantee that the CPU may perform tasks of given complexity before receiving the next task. By using the analyses that we have presented in Section 3.3.2, we will investigate the operating conditions of real-time computing systems and study the outage probability of the system for different network setups.

We have considered the same network model as in Section 3.2 and the same propagation model as in (3.1). In our system, at each time slot, a generic PH is associated with the service $s$ with probability $q_s$. We denote with $\mathcal{P}_s$ the subset of PHs allocated to the service $s$. During an initial discovery phase, the LPDs broadcast a packet containing a message indicating their associated services. Then, each LPD establishes a communication link with the PH $p \in \mathcal{P}_s$ ensuring the minimum average signal attenuation. We also assume that all the PHs share the same radio resources, so that all the PHs but $p$ are considered as interferers for the information transfer process. An illustration of the SWIPT-MC system is provided in Fig. 3.9. In this figure, red and green PHs are allocated to 'Service #1' and 'Service #2', respectively. $\text{LPD}^{(0)}$, which is associated with 'Service #2' and illustrated in green, establishes a communication link with the closest PH that is associated with 'Service #2'. The serving PH sends a command message to trigger the execution of a specific task. In this example, the farther green PH and the red PH which is allocated to another service act as interferers for $\text{LPD}^{(0)}$ in terms of information decoding.

**Rate-Energy Trade-off Analysis**

Typically, the PH experiencing the minimum signal attenuation is assumed to be the serving PH for the $\text{LPD}^{(0)}$. However, assuming that the $\text{LPD}^{(0)}$ is only associated with a subset of services $\mathcal{S}_{\text{LPD}} \subseteq \mathcal{S}$, it may not be able to answer to the PH's request. In such a case, the PH will initiate a communication with another LPD, thus creating interference to the $\text{LPD}^{(0)}$. It follows that the serving PH shall belong to the subset of PHs that were allocated to a service $s \in \mathcal{S}_{\text{LPD}}$. Therefore, we introduce the concept of hit probability, $q_{\text{hit}} = \sum_{s\in\mathcal{S}_{\text{LPD}}} q_s$, defined as the probability that a generic PH is allocated to one of the services implemented by the $\text{LPD}^{(0)}$. The original PPP, $\Psi$, is then partitioned into two homogeneous PPPs: $\Psi_{q_{\text{hit}}}$ with density $q_{\text{hit}}\lambda_{\text{ph}}$ and $\Psi_{\bar{q}_{\text{hit}}}$ with density $\bar{q}_{\text{hit}}\lambda_{\text{ph}}$, where $\bar{q}_{\text{hit}} = 1 - q_{\text{hit}}$. By replacing $\lambda_{\text{ph}}$ with $q_{\text{hit}}\lambda_{\text{ph}}$ and $\bar{q}_{\text{hit}}\lambda_{\text{ph}}$, in the characteristic functions of $L^{(0)}$ and $g^{(0)}$ given in Section 3.3.2, they can be adapted to the considered system model. However differently from (3.8), due to the proposed hit probability concept, $\mathcal{I}_{\text{MU}}$ is composed of two parts:

$$\mathcal{I}_{\text{MU}} = \sum_{N=0}^{N_{max}} \left( \sum_{\text{n}\in\Psi^{(\setminus 0)}_{N,q_{\text{hit}}}} \frac{h^{(\text{n})}}{l_N(r^{(\text{n})})} \mathbb{1}\left\{ l_N(r^{(\text{n})}) > L^{(0)} \right\} + \sum_{\text{n}\in\Psi_{N,\bar{q}_{\text{hit}}}} \frac{h^{(\text{n})}}{l_N(r^{(\text{n})})} \right). \tag{3.20}$$

The first part represents the interference produced by all PHs belonging to $\Psi^{(\setminus 0)}_{N,q_{\text{hit}}}$, while the second one refers to the interference generated by the PH belonging to $\Psi_{N,\bar{q}_{\text{hit}}}$. As we know from the previous sections, in order to obtain J-CCDF we also need the characteristic function of $\mathcal{I}_{\text{MU}}$ which is given as

$$\Phi_N\left(\omega; L^{(0)}\right) = \Phi_{N,q_{\text{hit}}}\left(\omega; L^{(0)}\right) \Phi_{N,\bar{q}_{\text{hit}}}(\omega). \tag{3.21}$$

In order to avoid repetition, we do not show the details step by step to obtain the J-CCDF. By replacing $\lambda_{\text{ph}}$ with $q_{\text{hit}}\lambda_{\text{ph}}$ the characteristic function of the first term of $\mathcal{I}_{\text{MU}}$ can easily be obtained. For the second term, in addition to replacement of $\lambda_{\text{ph}}$ with $\bar{q}_{\text{hit}}\lambda_{\text{ph}}$, we substitute $L^{(0)} = 1$ in the closed form of $\Phi_N\left(\omega; L^{(0)}\right)$ (see (B.4)) and then J-CCDF can trivially be obtained.

**Computation Model**

As mentioned above, the objective of our MC system is to provide a set of services $\mathcal{S}$. To achieve this, the generic PH $p \in \mathcal{P}_s$ transmits a command message with a fixed length of $L_{\text{com}}$ bits to trigger the execution of a specific task to process the data gathered locally. It is worth mentioning that in this study, we consider only the first phase of the system (downlink) and study the impact of the computation requirements on the achievable rate-energy trade-offs in the downlink. Each computation task is characterised by $k$ logical operations per bit. The primary engine for local computation at the LPD is the CPU, where the energy consumption per logical operation depends on the CPU clock speed. Therefore, under the assumption of low CPU voltage, the energy consumed by the CPU to execute a task can be modelled as [82]

$$E_C = \sum_{i=1}^{kL_{task}} c_e f_i^2 \tag{3.22}$$

in which, $c_e$ is the effective capacitance coefficient and $f_i$ denotes the CPU frequency (i.e. the clock speed) for each CPU cycle $i \in \{1, ..., kL_{task}\}$.

Upon decoding the $L_{com}$ bits of the command message, the LPD exploits the harvested energy to perform the computation tasks requested and the triggered tasks must be executed prior to the reception of the next message. In other words, the information rate of the wireless link determines the maximum time that can be devoted to the computation $\left(\text{i.e. } \sum_{i=1}^{kL_{task}} \frac{1}{f_i} \leq \frac{L_{com}}{R}\right)$. At the same time, larger values of rate correspond to smaller values of energy harvested. From (3.22), this amounts to saying that the CPU must perform less cycles or reduce its clock speed. Clearly, this causes a conflict between communication and computation performance. The following describes a procedure to determine the best compromise between communication and computation for a given J-CCDF.

The computation capacity can be determined by optimising the clock frequencies to minimise the CPU energy consumption. Minimizing the energy consumption, considering the fact that execution of the triggered task must be finished before next command message arrives, will result in equal frequencies of $f_i = \frac{kL_{task}R}{L_{com}}, \forall i$ as shown in [56]:

$$\begin{aligned} \underset{f_i}{\text{Minimize}} \quad & E_C = \sum_{i=1}^{kL_{task}} c_e f_i^2 \\ \text{subject to} \quad & \sum_{i=1}^{kL_{task}} \frac{1}{f_i} \leq \frac{L_{com}}{R} \\ & f_i \in (0, f_{max}] \end{aligned} \tag{3.23}$$

where the feasibility region is obtained when

$$R \leq \frac{f_{max} L_{com}}{kL_{task}}, \tag{3.24}$$

with $f_{max}$ representing the maximum CPU clock speed. Hence, it is found that the optimal point is achieved when all the frequencies are equal to $f_i = \frac{kL_{task}R}{L_{com}}, \forall i$.

By substituting $f_i$ into (3.22) the minimum power needed to support real-time operations is obtained as

$$Q = \frac{E_C R}{L_{com}} = c_e \left(\frac{kL_{task}R}{L_{com}}\right)^3. \tag{3.25}$$

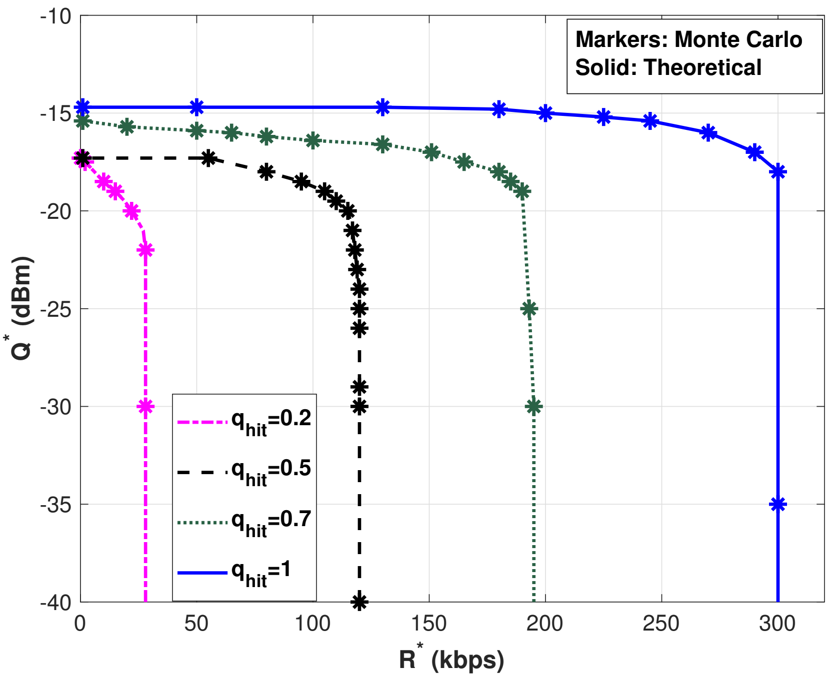


FIGURE 3.10: Rate-energy trade-off: theoretical results and Monte Carlo simulations for different values of $q_{\text{hit}}$.

Finally, we can define the outage probability of the real-time SWIPT-MC system as a function of the targeted information rate as

$$P_{\text{out}} = 1 - F_{\text{c}}\left(R, c_{\text{e}}\left(\frac{kL_{\text{task}}R}{L_{\text{com}}}\right)^3\right). \tag{3.26}$$

Interestingly, the information rate can also be interpreted as the rate at which the local data must be updated before initiating a new computation. Hence, (3.26) provides also insights into the maximum task complexity given the rate, $R$ (see (3.13)), of the data gathered at the LPD.

### Results

In addition to the parameters given in Table 3.2, we fix the half of the average minimum distance between PHs to $d_{\text{ph}} = 3$m and the density of the walls to $\lambda_{\text{w}} = 0.3$ except otherwise stated. Moreover, the effective capacitance coefficient is set to $c_{\text{e}} = 10^{-28}$ [56]. Regarding the fact that the system is essentially interference limited and the SINR does not depend on realistic levels of noise (see Section 3.4.2), the power splitting ratio must be as large as possible and it is set to $\rho = 0.99$. The length of command messages is fixed to $L_{\text{com}} = 32$bits and the number of the bits at the LPD is assumed to be $L_{\text{task}} = 0.6$kb.

Fig. 3.10 shows the trade-off between the information rate and the harvested power for several values of $q_{\text{hit}}$ when $F_{\text{c}}(R^*, Q^*) = 0.75$. In order to validate our analysis, both theoretical results (lines) and Monte Carlo simulations (markers) are reported. An almost perfect match between the Monte Carlo simulations and the analytical curves is observed. Besides, it can be observed how the hit probability impacts the

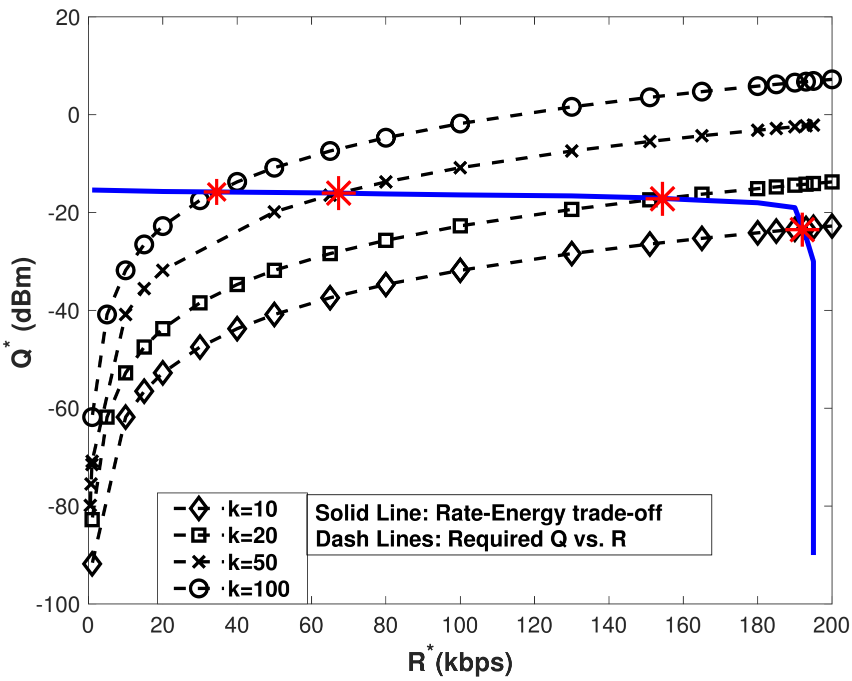


FIGURE 3.11: Operating points on the rate-energy trade-off for different values of $k$.

rate-energy trade-off. In fact, when the hit probability increases, more PHs will be allocated to one of the services implemented by the $\mathrm{LPD}^{(0)}$. As a result, the probability of experiencing a relatively moderate signal attenuation between the PH and the $\mathrm{LPD}^{(0)}$ will be larger, which, in turns will give rise to higher values of signal to SINR at the SWIPT receiver. For instance, by increasing $q_{\mathrm{hit}}$ from 0.2 to 1, the information data rate increases from 28kbps to 300kbps for $-25$dBm of harvested power.

From Fig. 3.10 we can also observe that the maximum harvested power increases when $q_{\mathrm{hit}}$ increases. This is mainly due to the fact that serving PH which takes the advantage of MRT process has a greater probability of being closer to the $\mathrm{LPD}^{(0)}$. For example at 22kbps of information rate, with $q_{\mathrm{hit}} = 1$, the power harvested is 5.3dB greater than the one relevant to $q_{\mathrm{hit}} = 0.2$.

Fig. 3.11 indicates the operating points associated with different computation loads (expressed in number of logical operations per bit processed). The number of logical operations per bit is set to $k = 10, 20, 50, 100$, $F_{\mathrm{c}}(R^*, Q^*) = 0.75$ and $q_{\mathrm{hit}} = 0.7$. Required powers (dash lines) are obtained with the help of (3.25). Not surprisingly, for fixed information rates, more harvested power is required for performing more complex tasks. It can be observed that if $k = 10$ operations per bit are required we need $Q^* = -23.5$dBm of power to perform $R^*/L_{\mathrm{com}} = 192/32 = 6$ kilotasks/second. However, if $k = 100$, we can only execute 1 kilotasks/second by using $Q^* = -15.8$dBm of harvested power.

Fig. 3.12 illustrates the outage probability against the number of tasks per second, $\frac{RL_{\mathrm{task}}}{L_{\mathrm{com}}}$, to be executed for $k = 10, 20, 50$. It is apparent that, for the same outage probability, the number of tasks per second decreases when the number of operations per bit increases. As an example, with a fixed outage probability of $P_{\mathrm{out}} = 0.4$, we

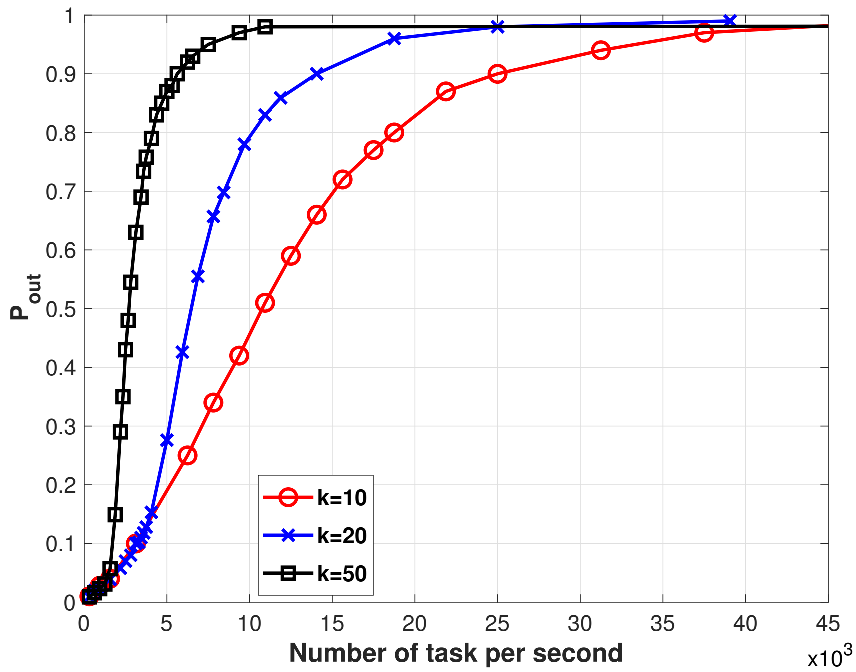


FIGURE 3.12: Outage probability versus the number of tasks per second for different values of $k$.

can perform 9 kilotasks/second with $k = 10$ operations per bit, while for $k = 20$ and $k = 50$ only 5 and 2 kilotasks/second can be executed, respectively. However, as shown in Fig. 3.13, executing more tasks per second does not necessarily mean that we better utilise the CPU.

In fact, from Fig. 3.13 we observe that for a fixed number of CPU cycles per second, $\frac{kL_{\text{task}}R}{L_{\text{com}}}$, the outage probability decreases when $k$ increases. This is mainly due to the fact that the data rate is interference limited, so it is not always possible to perform low complexity tasks at a very high rate. Therefore, it can be more efficient to perform more complex tasks at low rate to optimise the CPU usage. Stated otherwise, it would be more efficient to trigger a large number of tasks with the same command message rather than sending command messages at a very high rate to select only a small number of tasks.

Finally, the effect of network densification is made clear in Fig. 3.14 and Fig. 3.15. Fig. 3.14 shows the total number of CPU cycles per second and the number of tasks per second for different values of $d_{\text{ph}} = 3, 5, 7$m for $q_{\text{hit}} = 1$ and $k = 20$. In this case, network densification is helpful in increasing the SWIPT-MC performance. However, if only $k = 1$ logical operation per bit is considered (Fig. 3.15) (e.g. a simple comparison of the local data with a reference value), the CPU is better utilised for a less dense network. This can be explained by the fact that each task consumes very little power and that the limiting factor is not the harvested power but the rate at which the tasks can be performed. It follows that it would be better to have a less dense network to reduce the multi-user interference and increase the information rate at the expense of the harvestable power level.

In this section, we have provided an application of SWIPT-enabled system. After

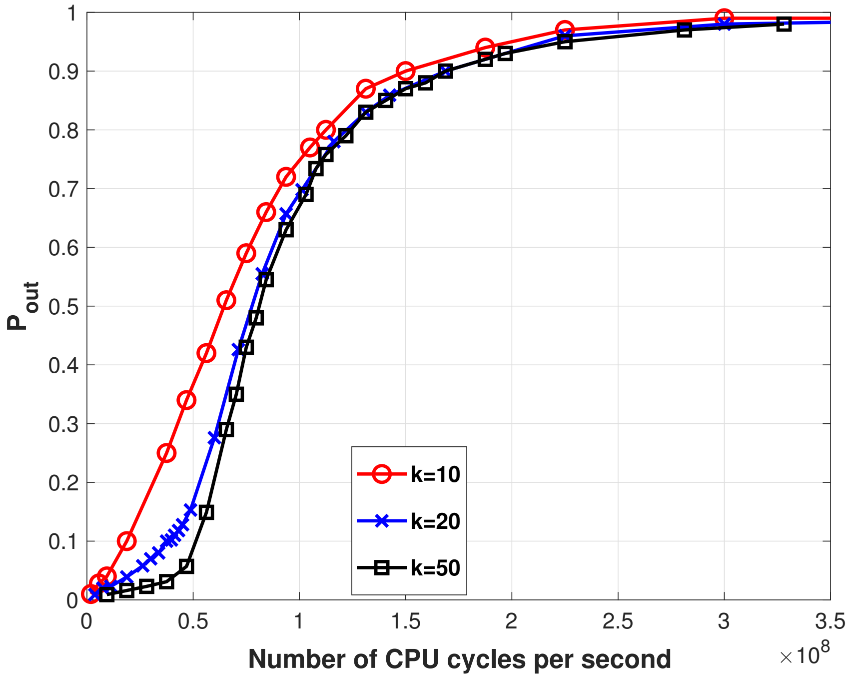


FIGURE 3.13: Outage probability versus the number of CPU cycles per second for different values of $k$.

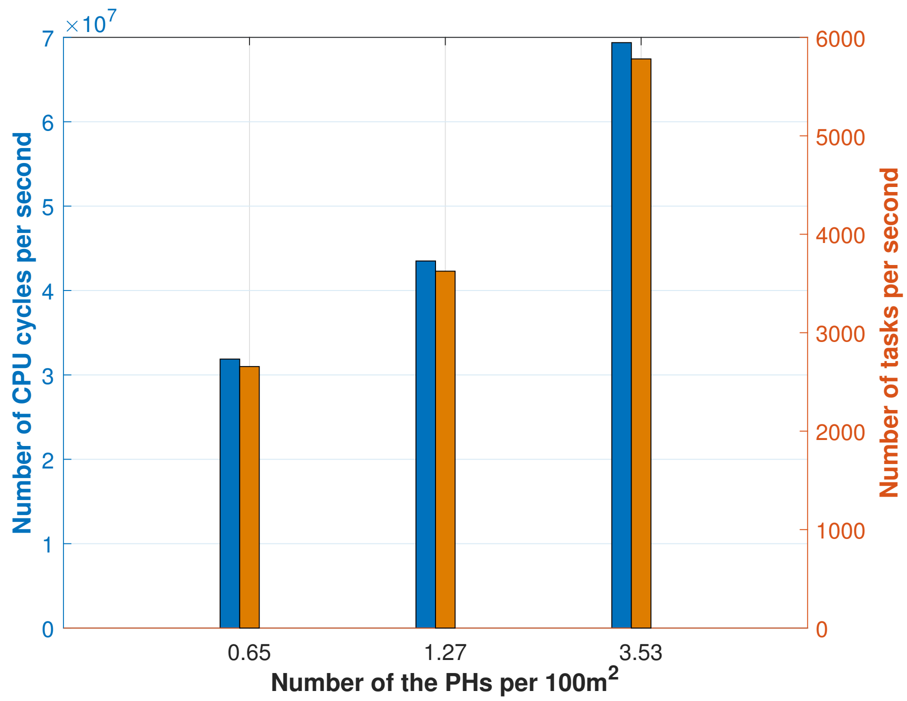


FIGURE 3.14: Effect of the PHs' densities for $k = 20$ operations per bit.

studying the characterization of the rate-energy trade-offs in the previous sections, here we have presented the operating conditions of real-time computing system as well as the outage probabilities.

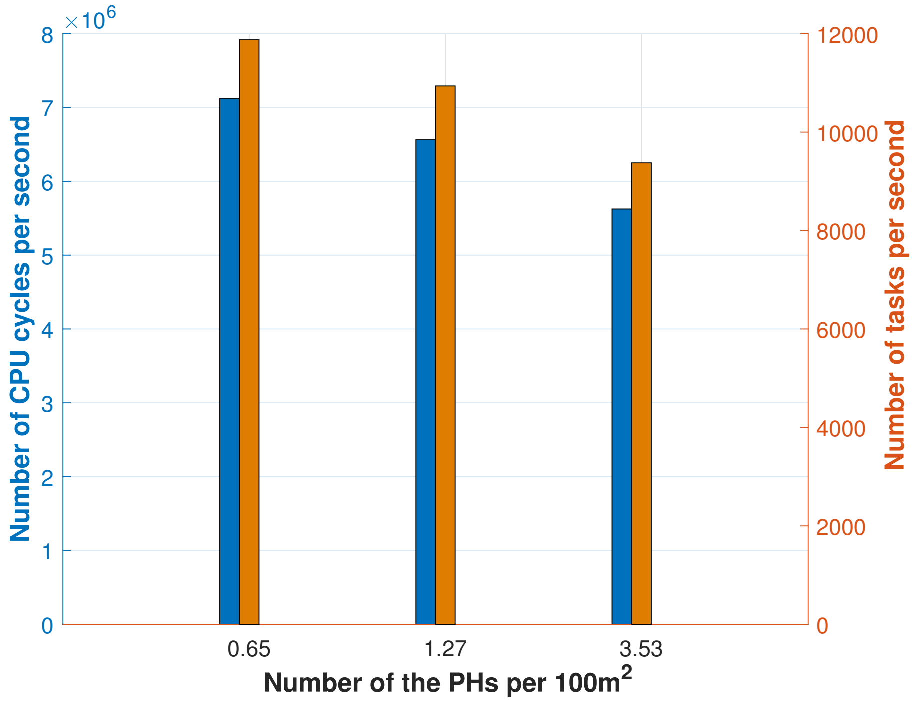


FIGURE 3.15: Effect of the PHs' densities for $k = 1$ operation per bit.

## 3.6 Summary

In this chapter we have proposed a stochastic geometry analysis to model the impact of blockages on the performance of an indoor SWIPT-enabled MIMO system. In this scenario, we have addressed the issue of MUI in relation with both the network infrastructure and the topology of the venue. An analytical expression of the cumulative distribution function of the multi-user interference as a function of the density of walls is provided. A similar result is also obtained for the distribution of the minimum propagation loss. With the help of characteristic functions of MUI, minimum propagation loss and the serving channel gain we obtained the J-CCDF of information rate and the harvestable energy in order to define the rate-energy trade-offs of the system.

After providing the analyses for MIMO-SWIPT indoor network, we have presented a real-time SWIPT-MC system as an application of SWIPT. We have proposed the use of SWIPT to control distributed computation process while delivering power to perform the computation tasks requested. Moreover, operating points that guarantee real-time processing of the locally generated data for given task complexities have been provided. Finally, we have studied the outage probability of the system.

In the next chapter we will extend our analyses to a SWIPT-MEC system where we both consider local computation and offloading.

# Chapter 4

# SWIPT-based Mobile Edge Computing Systems

In the previous chapter, we have analysed the information-energy trade-off and presented an application of SWIPT for an IoT system. In this chapter, we focus on mobile edge computing and investigate the performance of SWIPT-based MEC systems where the complex data that can not be performed by LPD is offloaded to the edge server. In particular, we will propose a decision strategy for a SWIPT-MEC system where LPD has to decide either to perform local computation or offloading. We will provide insights on the design of the decision strategy and will evaluate the impact of this strategy on a triple trade-off between energy, local computation and offloading. In order to provide a system-level perspective on the performance of a SWIPT-MEC network, we will make use of SG for characterising the trade-offs between communication and computation. Moreover, joint success probability of local computation and offloading will be studied.

## 4.1 Introduction

In SWIPT-based mobile edge computing systems, LPD offloads the data to the MEC server when the harvested energy is not enough to compute the data locally. Thus, in order to analyse the performance of SWIPT-based MEC system, we have to jointly address the downlink (DL) and the uplink (UL). Here DL term is used for the link between the PH and the LPD (information decoding) and UL is used for the link between the LPD and the MEC server (offloading the computational task/uploading the results of local computation).

In the literature, most of the previous works on SG based analyses of cellular networks with energy harvesting are either focused on uplink [65, 83, 84] or downlink [62, 85, 86]. A first study dealing with joint UL/DL coverage probability of cellular-based ambient RF energy harvesting IoT is reported in [66]. In order to derive the joint coverage probability, first the probability distribution of interference should be obtained. However, the probability distribution of interference is only computable for simple scenarios and not known in general. Thus, the authors of [66] developed a dominant base station (BS)-based approach to derive a tight approximation for the joint coverage probability. Following the same approach to approximate the density of interfering users as in [66], an analytical framework to evaluate and optimise the performance of an energy-efficient joint DL/UL RF wake-up strategy for IoT devices over cellular networks has been presented in [67].

In this chapter, we make use of stochastic geometry to analyse a MEC system in which SWIPT is used to simultaneously deliver power and a command message to an LPD. This command message is used to select computation tasks to be executed by the LPD. Harvested energy is deployed by the LPD device for information decoding (ID) and either to perform local computation or to offload the computations to the MEC server. Therefore, each time frame is divided into orthogonal time slots, one for energy harvesting (EH), one for ID and the other for local computation or offloading. In this model, LPDs have to decide either to perform the computation locally or to offload to the MEC server. The main contributions and results of this work are summarised as follows:

- In this chapter, our aim is to evaluate the impact of the decision strategy and computation rate on a triple trade-off between energy, communication and computation.

- In contrast to the SWIPT mobile computing system analysed in the previous chapter, where only local computation is considered, in this model, based on the amount of the harvested energy, LPDs have to decide either to perform the computation locally or to offload to the MEC server. Thus, we propose a simple stochastic decision strategy which allows to exploit different local computation-offloading (communication-computation) trade-offs at the network level.

- In such a MEC system, we confront interference in the offloading and the uploading phases as a bottleneck. In order to overcome this obstacle, we will propose a decision strategy and validate it.

- We use dominant BS-based approach to approximate the harvested energy and the amounts of interference in downlink, offload and upload phases.

- Theoretical results are provided for offloading/local computing probabilities and verified by means of Monte Carlo simulations. It has been shown that the probability of local computation increases with the increment on SINR target in the uploading phase while the probability of offloading decreases.

- Finally, we present success probabilities of offloading/local computing and total success probability as functions of tuning parameters. Results show that for small values of tuning parameters, system performance is better for higher values of task complexity.

## 4.2 System Model

We consider a SWIPT-enabled MEC system composed of a set of multiple LPDs, PHs and MEC servers, as shown in Fig. 4.1. The aim of this system is to perform some tasks by using the energy harvested in the DL. Since the amount of harvested energy

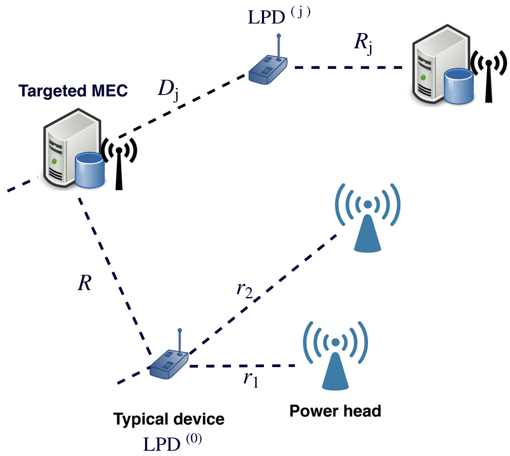


FIGURE 4.1: SWIPT-MEC system model 1

is limited, it may not be enough to perform the task locally. Thus, in contrast to the system model studied in the Section 3.5 where only local computation is considered, here we consider MEC and LPDs have to decide either to perform the computation locally or offload it to the MEC server.

Since it has been assumed that the LPDs are battery-less and do not have any storage capability, each LPD has to harvest the energy in order to enable the information decoding. Thus we have considered time-switching SWIPT scheme as a receiver architecture. It is worth to mention that our analyses can be straightforwardly extended to a scenario where power splitting is considered. A generic LPD receives energy and command message, with length of $L_{\text{com}}$ bits, from its associated PH through the time-switching SWIPT scheme. This command message indicates the specific task that is needed to be executed by the LPD. For the sake of simplicity, we assume that the size and the complexity of tasks are constant, denoted by $L_{\text{task}}$ bits and $k$ operations per bit, respectively. Based on the location of the MEC server and the amount of harvested energy, the LPD node decides whether to offload the assigned task to its associated MEC server or not. If not, the LPD executes the computation task locally and sends the result with length $L_{\text{res}}$ bits to its associated MEC server. Without loss of generality and for the sake of readability, it has been assumed that $L_{\text{com}} = L_{\text{res}} = m\,L_{\text{task}}$ where $m \ll 1$ is a constant. It is worthy to mention that in this model, the MEC servers are considered to be the endpoint of this computation process.

We also assume that time is slotted with a fixed slot duration, denoted by $T$. As shown in Fig. 4.2, each time slot is further divided into energy harvesting, information (i.e. command message) decoding and local computation/offloading sub-slots with durations $\tau_{\text{eh}}$, $\tau_{\text{id}}$ and $\tau_{\text{off}}$, respectively. During the energy harvesting sub-slot, the LPDs harvest energy from the RF-signal transmitted by PHs which will be used to perform information decoding and task execution in the next two sub-slots. In the information decoding sub-slot, the LPDs decode the command messages transmitted by their associated PHs. In the third sub-slot with duration of $\tau_{\text{off}}$, the LPDs execute their scheduled tasks either locally or by offloading to their associated MEC servers. In the case of offloading, the whole duration $\tau_{\text{off}}$ is used by the LPD to transmit the task to the MEC server. On the other hand, in the case of local computation,

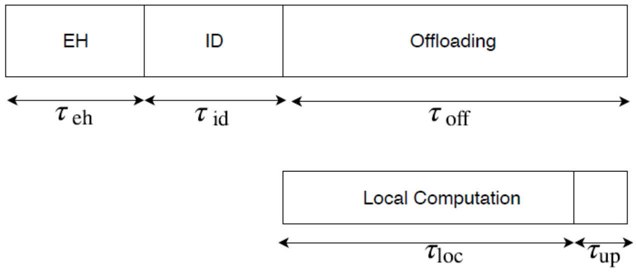


FIGURE 4.2: Time frame structure

the third sub-slot needs to be further divided into two sub-slots: computation sub-slot, with duration of $\tau_{loc}$ in which the task is executed and the uploading sub-slot, with duration of $\tau_{up}$ in which the LPD transmits the obtained result to its associated MEC server.

As a first step we will just consider the effect of path-loss and small-scale fading. Spatially correlated shadowing will be considered in next chapter. Therefore, we assume that the transmitted signals are subject to the standard power law path-loss model with exponent $\alpha > 2$ and small-scale fading modelled by the Rayleigh distribution. The path-loss model is given as:

$$l(r) = \begin{cases} \kappa r^{\alpha} & \text{if} \quad r \geq \kappa^{-1/\alpha} \\ 1 & \quad \text{otherwise,} \end{cases} \tag{4.1}$$

where $r$ is the distance between the PH and the LPD, $\alpha$ is the path-loss exponent, $\kappa = \left(\frac{4\pi}{v}\right)^2$ is the path loss constant, where $v = c_0/f_c$ is the transmission wavelength, $f_c$ and $c_0$ being the carrier frequency in Hz and the speed of light in m/sec, respectively.

For any link j, fading coefficients in the energy harvesting sub-slot, the information decoding sub-slot, the offloading sub-slot and the uploading sub-slot are denoted by $g_{\text{j}}$, $h_{\text{j}}$, $w_{\text{off,j}}$ and $w_{\text{up,j}}$, respectively. All these channel coefficients are assumed to be independent and identically distributed exponential random variables with unit mean.

Regarding the network structure, it has been assumed that the possible sets of PHs, LPDs and MEC servers, deployed in a circular area with radius $R_{\text{a}} \in \mathbb{R} \cup \infty$, are modelled as instances of three independent homogeneous Poisson Point Processes $\Psi_{\text{ph}}$, $\Psi_{\text{lpd}}$ and $\Psi_{\text{mec}}$ of density $\lambda_{\text{ph}}$, $\lambda_{\text{lpd}}$ and $\lambda_{\text{mec}}$, respectively. The typical LPD, denoted by LPD$^{(0)}$ is located at the origin of the $x-$ and $y-$ axes. Regarding the association policy, we assume that each LPD is associated with its nearest PH and nearest MEC server.

### 4.2.1 Energy Harvesting

During the EH sub-slot, LPD$^{(0)}$ harvests energy which will be used for locally computing/offloading the task to the MEC server. Assuming that all PHs transmit with the same power $P$, the amount of energy harvested by the LPD$^{(0)}$ over this sub-slot is:

$$E_{\mathrm{h}} = \tau_{\mathrm{eh}} \mu P \sum_{\mathrm{j} \in \Psi_{\mathrm{ph}}} g_{\mathrm{j}} \kappa^{-1} r_{\mathrm{j}}^{-\alpha}, \tag{4.2}$$

where $r_{\mathrm{j}}$ denotes the distance from the j-th PH, denoted by $\mathrm{PH}^{(\mathrm{j})}$, to the $\mathrm{LPD}^{(0)}$, $\mu < 1$ is the efficiency of the RFEH and $g_{\mathrm{j}} \sim \exp(1)$ is the fading gain between $\mathrm{LPD}^{(0)}$ and $\mathrm{PH}^{(\mathrm{j})}$.

### 4.2.2 Information Decoding

In this sub-slot, $\mathrm{LPD}^{(0)}$ receives a command message with a fixed length of $L_{\mathrm{com}}$ bits sent by its serving PH which triggers the execution of a specific computation task. In contrast with the energy harvesting, the other PHs are considered as interferers for the command message decoding. Denoting the set of interfering PHs by $\Psi_{\mathrm{ph}}^{(\backslash 1)}$, the SINR at the $\mathrm{LPD}^{(0)}$ is:

$$\mathrm{SINR}_{\mathrm{id}} = \frac{P h_1 \kappa^{-1} r_1^{-\alpha}}{\sigma_{\mathrm{id}}^2 + \mathcal{I}_{\mathrm{id}}} \tag{4.3}$$

where $r_1$ is the distance from the serving PH to the $\mathrm{LPD}^{(0)}$ , $h_1 \sim \exp(1)$ is the fading coefficient of the serving link, $\sigma_{\mathrm{id}}^2$ is the thermal noise power, and $\mathcal{I}_{\mathrm{id}}$ denotes the interference at the typical user, given by:

$$\mathcal{I}_{\mathrm{id}} = \sum_{\mathrm{j} \in \Psi_{\mathrm{ph}}^{(\backslash 1)}} P h_{\mathrm{j}} \kappa^{-1} r_{\mathrm{j}}^{-\alpha}, \tag{4.4}$$

where $h_{\mathrm{j}} \sim \exp(1)$ is the channel gain between $\mathrm{PH}^{(\mathrm{j})}$ and $\mathrm{LPD}^{(0)}$.

### 4.2.3 Local Computation/Offloading

After decoding the command message and based on its decision, in the third sub-slot, $\mathrm{LPD}^{(0)}$ processes the data locally or offloads it to the nearest MEC server, referred hereafter as the targeted MEC server and denoted by $\mathrm{MEC}^{(1)}$. The energy consumption for local computation and task offloading, denoted by $E_{\mathrm{loc}}$ and $E_{\mathrm{off}}$, are given by:

$$\begin{aligned} E_{\mathrm{loc}}(R) &= c_{\mathrm{e}} \frac{(k L_{\mathrm{task}})^3}{(\tau_{\mathrm{loc}})^2} + \tau_{\mathrm{id}} c_{\mathrm{dec}} \log(1 + \beta_{\mathrm{id}}) + \tau_{\mathrm{up}} \kappa R^{\alpha} \eta, \\ E_{\mathrm{off}}(R) &= \tau_{\mathrm{id}} c_{\mathrm{dec}} \log(1 + \beta_{\mathrm{id}}) + \tau_{\mathrm{off}} \kappa R^{\alpha} \eta, \end{aligned} \tag{4.5}$$

respectively. Here $R$ denotes the distance from the $\mathrm{LPD}^{(0)}$ to the $\mathrm{MEC}^{(1)}$, $\eta$ is the MEC server sensitivity (i.e. the minimum required power for succesfully decoding the message), $c_{\mathrm{dec}}$ is a constant and measures the required energy to decode one bit (Joule/bit), $c_{\mathrm{e}}$ is the effective capacitance coefficient and $\beta_{\mathrm{id}}$ is the SINR target in the downlink. Here, first term of $E_{\mathrm{loc}}(R)$ represents the energy that is needed for the local computation which has been explained in Section 3.5. Second term which is also the first term of $E_{\mathrm{off}}(R)$, is for the required energy to decode $L_{\mathrm{com}}$ bits and finally the energy that is needed for uploading the results to the MEC server is given in the last term of $E_{\mathrm{loc}}(R)$ where it also appears as the second term of $E_{\mathrm{off}}(R)$ and represents the energy needed to offload the data to MEC server. The SINRs for offloading and uploading sub-slots at the $\mathrm{MEC}^{(1)}$ can be expressed as:

$$\mathrm{SINR_i} = \frac{w_{\mathrm{i},1}\eta}{\sigma_{\mathrm{i}}^2 + \mathcal{I}_{\mathrm{i}}}, \;\; \mathrm{i} \in \{\mathrm{off,up}\}, \tag{4.6}$$

in which $\sigma_{\mathrm{i}}^2$ denotes thermal noise power and $w_{\mathrm{i},1} \sim \exp(1)$ is the channel gain of the link between the LPD$^{(0)}$ and the MEC$^{(1)}$. Moreover, $\mathcal{I}_{\mathrm{i}}$ denotes the interference at the MEC$^{(1)}$, given by:

$$\mathcal{I}_{\mathrm{i}} = \sum_{\mathrm{j}\in\Psi_{\mathrm{lpd,i}}^{(\backslash 0)}} w_{\mathrm{i,j}}\eta R_{\mathrm{i,j}}^{\alpha} D_{\mathrm{i,j}}^{-\alpha}, \tag{4.7}$$

where $\Psi_{\mathrm{lpd,i}}^{(\backslash 0)}$ represents the point process of all the interfering LPDs that perform offloading/uploading and are scheduled on the same time-frequency resource as LPD$^{(0)}$, $D_{\mathrm{i,j}}$ is distance from LPD$^{(\mathrm{j})}$ to the MEC$^{(1)}$, $R_{\mathrm{i,j}}$ is the distance from LPD$^{(\mathrm{j})}$ to its associated MEC server and $w_{\mathrm{i,j}} \sim \exp(1)$, for any $\mathrm{j} \in \Psi_{\mathrm{lpd,i}}$. As can be seen here, due to uplink power control, the transmission power of each device is a function of its distance to its associated MEC server (e.g. the transmitted power of LPD$^{(\mathrm{j})}$ to its associated MEC server MEC$^{(j)}$ is $\eta R_{\mathrm{j}}^{\alpha}$). Moreover, $w_{\mathrm{j}} D_{\mathrm{j}}^{-\alpha}$ is the attenuation that the signal encounters between the device and the targeted MEC server.

### 4.2.4 Timing Parameters

In this section we present the timing parameters. By defining $B(\mathrm{s})$ as the required time to transmit $L_{\mathrm{task}}$ with the rate $W\log(1+\beta_{\mathrm{s}})$ and fixing $T$ and $\tau_{\mathrm{eh}}$, the time durations of the sub-slots are given as

$$\tau_{\mathrm{id}} = mB(\mathrm{s}),\; \tau_{\mathrm{up}} = mB(\mathrm{s}),\; \tau_{\mathrm{off}} = B(\mathrm{s}), \tag{4.8}$$

where $B(\mathrm{s}) = \frac{L_{\mathrm{task}}}{W\log(1+\beta_{\mathrm{s}})}$, $\mathrm{s} \in \{\mathrm{id}, \mathrm{up}, \mathrm{off}\}$, $W$ is the signal bandwidth and $\beta_{\mathrm{s}}$ is the SINR target in the considered phase (i.e. $\beta_{\mathrm{id}}$ for the downlink, $\beta_{\mathrm{off}}$ for the offloading and $\beta_{\mathrm{up}}$ for uploading). Here $\tau_{\mathrm{off}} = \tau_{\mathrm{loc}} + \tau_{\mathrm{up}}$ and $\tau_{\mathrm{eh}} + \tau_{\mathrm{id}} + \tau_{\mathrm{off}} = T$.

## 4.3 Successful Computation Probability

In this section, we will evaluate the successful computation probability defined as the probability of successfully computing a given task either locally or remotely at the MEC server via task offloading:

$$P_{\mathrm{suc}} = P_{\mathrm{suc}}^{\mathrm{loc}} + P_{\mathrm{suc}}^{\mathrm{off}} \tag{4.9}$$

where

$$P_{\mathrm{suc}}^{\mathrm{s}} = \mathbb{E}\left[\mathbb{1}(\mathrm{SINR_{id}} \geq \beta_{\mathrm{id}})\mathbb{1}(\mathrm{SINR_{i(s)}} \geq \beta_{\mathrm{i(s)}})\mathbb{1}(\delta = \mathrm{s})\right] \tag{4.10}$$

in which $\mathrm{s} \in \{\mathrm{loc,off}\}$, $\mathrm{i(loc)} = \mathrm{up}$, $\mathrm{i(off)} = \mathrm{off}$ and $\delta$ is a random variable denoting the offloading/local computation decision. Here $\mathbb{1}(\cdot)$ denotes the indicator function. In this section, we evaluate the success probability through the characterization of the success probabilities of local computation and task offloading (see (4.9)). Success probabilities of local computation and task offloading (given in (4.10)) depend on the SINR coverages in the downlink and offloading/uploading phases. Moreover, it is obvious that the system performance depends also on the offloading/local computation decision strategy. In the following subsection, we describe our energy-based offloading/local computation decision strategy.

### 4.3.1 Decision Strategy

After LPD$^{(0)}$ harvests energy and receives the command message, it has to decide whether to perform local computation or to offload. Based on the amount of harvested energy $E_{\rm h}$, the following possibilities arise:

- $E_{\rm h} \leq \min\{E_{\rm loc}, E_{\rm off}\}$, i.e. the harvested energy is not enough either for offloading or local computation, leading to an outage happening with probability $P_{\rm out}$.
- $E_{\rm loc} \leq E_{\rm h} \leq E_{\rm off}$, i.e. the only feasible mode is local computation.
- $E_{\rm off} \leq E_{\rm h} \leq E_{\rm loc}$, i.e. the only feasible mode is offloading.
- $E_{\rm h} \geq \max\{E_{\rm loc}, E_{\rm off}\}$, i.e. both modes are feasible in terms of energy. In this case, with probability of $q$, the LPD offloads the task and with probability of $\bar{q} \stackrel{\rm def}{=} 1 - q$ performs local execution.

The objective of the proposed decision strategy is maximizing the total success probability. Thus, $q$ as a tuning parameter enables us to apportion the interference between offloading and uploading sub-slots according to $\beta_{\rm off}$ and $\beta_{\rm up}$ in order to increase the success probability. Based on this decision strategy, the probabilities of offloading and local computation are given as:

$$P(\delta = {\rm off}) = \mathbb{P}(E_{\rm off} < E_{\rm h} < E_{\rm loc}) + q\,\mathbb{P}(E_{\rm h} \geq \max\{E_{\rm loc}, E_{\rm off}\})\,, \tag{4.11}$$

$$P(\delta = {\rm loc}) = \mathbb{P}(E_{\rm loc} < E_{\rm h} < E_{\rm off}) + \bar{q}\,\mathbb{P}(E_{\rm h} \geq \max\{E_{\rm loc}, E_{\rm off}\})\,. \tag{4.12}$$

### 4.3.2 Conditional Probabilities

To evaluate the success probabilities of local computation and offloading, we need to characterize the probabilities of two SINR coverage events in uploading and offloading phases $\{{\rm SINR}_{\rm up} \geq \beta_{\rm up}\}$ and $\{{\rm SINR}_{\rm off} \geq \beta_{\rm off}\}$, given in (4.6), the SINR coverage in the downlink $\{{\rm SINR}_{\rm id} \geq \beta_{\rm id}\}$, given in (4.3), and the chosen strategy $\{\delta = {\rm loc}\}$ and $\{\delta = {\rm off}\}$. From (4.7), the evaluation of SINR coverage probabilities in the uploading and offloading phases requires the characterization of the set of active LPDs in the uploading and offloading phases, $\Psi_{\rm lpd,i}$.

Due to the MEC association and the time-frequency resource allocation inside each MEC server coverage region and by following the same approach as in [66], we approximate the locations of active LPDs in uploading/offloading phase by independently thinning $\Psi_{\rm mec}$ with probability $P_{\rm loc}/P_{\rm off}$, which makes these two SINR coverage events dependent on $\Psi_{\rm mec}$. On the other hand, the SINR downlink success event, $\{{\rm SINR}_{\rm id} \geq \beta_{\rm id}\}$, is dependent on $\Psi_{\rm ph}$. Finally, we note that the decision random variable $\delta$, which depends on $\Psi_{\rm ph}$ through $E_{\rm h}$ and on $\Psi_{\rm mec}$ through $E_{\rm loc}(R)$ and $E_{\rm off}(R)$, couples the downlink and upload/offload SINR coverage events which consequently necessitates the joint analysis of these three events.

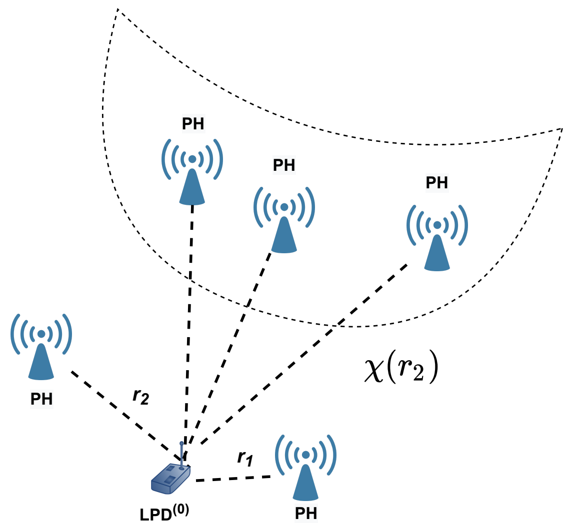


FIGURE 4.3: Dominant BS approach

Obviously, these three events become independent when conditioned on $\Psi_{\mathrm{ph}}$ and $\Psi_{\mathrm{mec}}$ since all channel gains in energy harvesting, downlink and uplink phases are independent. Following the procedure proposed in [66], we first derive conditional probabilities of SINR coverages and local computation and offloading probabilities by approximating the amount of harvested energy and the amounts of interference in downlink, offload and upload phases. The total success probability can be, then, obtained by unconditioning the product of these conditional probabilities with respect to $r_1$, $r_2$ and $R$.

In order to approximate the total energy harvested by the typical device (see (4.2)), we use dominant BS-based approach which is proposed in [66]. This approach is useful when the exact analysis is either too difficult or leads to unwieldy results. Here the idea is approximating the total energy that the LPD$^{(0)}$ harvests from all PHs by the energy harvested from the nearest two PHs (located at distances $r_1$ and $r_2$ from the typical device and the conditional mean (conditioned on the location of the nearest 2 PHs) of the rest of the terms (Fig. 4.3). Thus, the overall amount of energy harvested by the LPD$^{(0)}$ conditioned on $\Psi_{\mathrm{ph}}$ can be approximated by:

$$\begin{aligned} E_{\mathrm{h}} &= \tau_{\mathrm{eh}} \eta P \sum_{\mathrm{j} \in \Psi_{\mathrm{ph}}} g_{\mathrm{j}} \kappa^{-1} r_{\mathrm{j}}^{-\alpha} \\ &\approx \tau_{\mathrm{eh}} \eta P \left( g_1 \kappa^{-1} r_1^{-\alpha} + g_2 \kappa^{-1} r_2^{-\alpha} + \chi(r_2) \right). \end{aligned} \tag{4.13}$$

Here $\chi(r_2)$ is the mean that is conditioned on the location of the second closest PH and can be found as,

$$\begin{aligned} \chi(r_2) &= \mathbb{E}\left[ \sum_{\mathrm{j} \in \Psi_{\mathrm{ph}}^{(\backslash 1,2)}} g_{\mathrm{j}} \kappa^{-1} r_{\mathrm{j}}^{-\alpha} | r_1, r_2 \right] \\ &\overset{(a)}{=} \frac{2\pi\lambda_{\mathrm{ph}}}{\kappa} \int_{r_2}^{R_{\mathrm{a}}} r^{(1-\alpha)} dr \\ &= \frac{2\pi\lambda_{\mathrm{ph}}}{\kappa(\alpha-2)} \left( \frac{1}{r_2^{(\alpha-2)}} - \frac{1}{{R_a}^{(\alpha-2)}} \right) \end{aligned} \tag{4.14}$$

where (a) follows from Campbell's theorem [76].

### Local Computation/Offloading

In the previous subsection, we have presented our decision strategy which depends on the probabilities of offloading/ local computation. Thus, in order to compute the successful computing probabilities given in (4.10), we first need to derive these conditional offloading/ local computing probabilities.

**Theorem 3.** *Let us define a function $Z_s(r_2, R)$ as*

$$Z_s(r_2, R) \stackrel{def}{=} \frac{E_s(R)\kappa}{\tau_{eh}\eta P} - \chi(r_2), \tag{4.15}$$

*where $s \in \{off,loc\}$ and $E_{off}(R)$, $E_{loc}(R)$ are defined in* (4.5). *Then the conditional probabilities can be approximated as,*

$$\mathbb{P}(E_h \geq max\{E_{loc}, E_{off}\}|\Psi_{ph}, \Psi_{mec}) = \sum_{s\in\{off,loc\}} \frac{r_2^\alpha exp\left(-r_1^\alpha Z_s^+(r_2, R)\right) - r_1^\alpha exp\left(-r_2^\alpha Z_s^+(r_2, R)\right)}{r_2^\alpha - r_1^\alpha}, \tag{4.16}$$

$$\begin{aligned}\mathbb{P}(E_{off} < E_h < E_{loc}|\Psi_{ph}, \Psi_{mec}) = {} & \frac{r_1^\alpha \left[exp\left(-r_2^\alpha Z_{loc}^+(r_2, R)\right) - exp\left(-r_2^\alpha Z_{off}^+(r_2, R)\right)\right]}{r_2^\alpha - r_1^\alpha} \\ & - \frac{r_2^\alpha \left[exp\left(-r_1^\alpha Z_{loc}^+(r_2, R)\right) - exp\left(-r_1^\alpha Z_{off}^+(r_2, R)\right)\right]}{r_2^\alpha - r_1^\alpha},\end{aligned} \tag{4.17}$$

$$\begin{aligned}\mathbb{P}(E_{loc} < E_h < E_{off}|\Psi_{ph}, \Psi_{mec}) = {} & \frac{r_1^\alpha \left[exp\left(-r_2^\alpha Z_{off}^+(r_2, R)\right) - exp\left(-r_2^\alpha Z_{loc}^+(r_2, R)\right)\right]}{r_2^\alpha - r_1^\alpha} \\ & - \frac{r_2^\alpha \left[exp\left(-r_1^\alpha Z_{off}^+(r_2, R)\right) - exp\left(-r_1^\alpha Z_{loc}^+(r_2, R)\right)\right]}{r_2^\alpha - r_1^\alpha}\end{aligned} \tag{4.18}$$

*where $[x]^+ = max\{0, x\}$.*

*Proof.* See Appendix D □

By substituting these probabilities into (4.11) and (4.12), conditional probabilities of offloading and local computation, respectively, can be obtained. Moreover, for a given $q$, the probabilities of offloading and local computation can be found by unconditioning these conditional probabilities with respect to the joint distribution of $r_1$ and $r_2$ and the distribution of $R$.

**Remark 1.** *It is obvious that if $\mathbb{P}(E_h \geq max\{E_{loc}, E_{off}\}|\Psi_{ph}, \Psi_{mec})$, then the success probability of the energy harvesting MEC system is equal to that of the regularly powered network in which LPDs have unlimited and reliable access to the energy. Using* (4.15) *and* (4.16), *this condition can be shown to be equivalent to:*

$$r_2 \leq \left[\lambda_{ph} \frac{2\pi\eta\tau_{eh}}{(\alpha-2)\kappa \max\{E_{loc}(R), E_{off}(R)\}}\right]^{1/\alpha-2}, \tag{4.19}$$

*which means that as long as $r_2$, the location of the second nearest PH is smaller than right hand side of* (4.19)*, in other words, if $r_2$ is monotonically increasing with the density of PHs, then the harvested energy is enough for both local computation and offloading and therefore, the performance of the energy harvesting MEC system approaches that of the regularly powered network.*

**SINR Coverages**

It is worth to remark that in order to obtain the expression of the success probabilities of offloading/local computation, we have to jointly decondition on all the coverage events at the end. In the previous subsection we have presented the local computing/offloading probabilities. It is useful to derive conditional SINR coverages (i.e. downlink, offloading and uploading) also in terms of $r_1$ and $r_2$. In order to do that, we use the same dominant BS-based approach that we used in the previous subsection. In particular, the interference in the denominator of SINR in (4.3) is approximated by the interference from the second nearest PH (strongest interferer) and the expectation of the interference from the rest of the PHs. Under this approximation, the conditional downlink SINR coverage probability and offloading/uploading SINR coverage probability become

$$\mathbb{P}(\mathrm{SINR_{id}} \geq \beta_{\mathrm{id}} || r_1, r_2) = \exp\left\{-\frac{\beta_{\mathrm{id}} r_1^{\alpha}}{\kappa^{-1}}\left(\frac{\sigma_{\mathrm{id}}^2}{P} + \chi(r_2)\right)\right\}\left(\frac{1}{1+\beta_{\mathrm{id}}\frac{r_1^{\alpha}}{r_2^{\alpha}}}\right) \tag{4.20}$$

and

$$\mathbb{P}(\mathrm{SINR_{i(s)}} \geq \beta_{\mathrm{i(s)}} || R) =$$
$$\exp\left(\frac{-\beta_{\mathrm{s}}\sigma_{\mathrm{s}}^2}{\eta}\right)\exp\left(-2\pi\lambda_{\mathrm{mec}}P_{\mathrm{s}}\int_0^{R_{\mathrm{a}}}\int_0^{x^2}\frac{\pi\lambda_{\mathrm{mec}}P_{\mathrm{s}}\exp(-\pi\lambda_{\mathrm{mec}}P_{\mathrm{s}}u)}{1+\left(\frac{1}{\beta_{\mathrm{s}}}\right)u^{\frac{-\alpha}{2}}x^{\alpha}}du x dx\right) \tag{4.21}$$

respectively. Here $\chi(r_2)$ is given in (4.14) and s $\in$ {off,loc}, i(loc) = up, i(off) = off. The derivations can be found in [66] and are included in the Appendix E for the sake of completeness.

### 4.3.3 Success Probabilities

Now we have all the conditional probabilities (i.e. downlink/offloading/uploading SINR coverages and probability of offloading/local computation ) in order to obtain the success probabilities. By substituting all these probabilities into the expression given in (4.10) and unconditioning it with respect to $r_1$, $r_2$ and $R$, $P_{\mathrm{suc}}^{\mathrm{s}}$ is found as,

$$P_{\mathrm{suc}}^{\mathrm{s}} = \int_0^{R_{\mathrm{a}}} \int_0^{R_{\mathrm{a}}} \int_0^{r_2} \left( \exp\left( -\frac{\beta_{\mathrm{id}} \kappa \sigma_{\mathrm{id}}^2 r_1^{\alpha}}{P} - \frac{2\pi\lambda_{\mathrm{ph}} \beta_{\mathrm{id}} r_1^{\alpha} r_2^{(2-\alpha)}}{\alpha - 2} \right) \frac{1}{1 + \beta_{\mathrm{id}} \left(\frac{r_1}{r_2}\right)^{\alpha}} \right.$$
$$\times \left( \exp\left( \frac{-\beta_{\mathrm{s}} \sigma_{\mathrm{s}}^2}{\eta} \right) \exp\left( -2\pi\lambda_{\mathrm{mec}} P_{\mathrm{s}} \int_0^{R_{\mathrm{a}}} \int_0^{x^2} \frac{\pi\lambda_{\mathrm{mec}} P_{\mathrm{s}} \exp(-\pi\lambda_{\mathrm{mec}} P_{\mathrm{s}} u)}{1 + \left(\frac{1}{\beta_s}\right) u^{\frac{-\alpha}{2}} x^{\alpha}} du x dx \right) \right)$$
$$\left. \times P(\delta = \mathrm{s} | \Psi_{\mathrm{ph}}, \Psi_{\mathrm{mec}}) f(r_1, r_2) f(R) dr_1 dr_2 dR \right), \quad \mathrm{s} \in \{\text{off,loc}\} \tag{4.22}$$

where the joint distribution of $r_1$ and $r_2$ and the distribution of $R$ are given as,

$$\begin{aligned} f(r_1, r_2) &= (2\pi\lambda_{\mathrm{ph}})^2 r_1 r_2 \exp\{-\pi\lambda_{\mathrm{ph}} r_2^2\}, \\ f(R) &= 2\pi\lambda_{\mathrm{mec}} R \exp\{-\pi\lambda_{\mathrm{mec}} R^2\} \end{aligned} \tag{4.23}$$

respectively. The first term of (4.22) is the conditional SINR coverage probability in the downlink (see (4.20)) and second term is the conditional probability of offloading/uploading SINR coverage (see (4.21)). Here, the last term represents the offloading/local computation probability and is given in (4.11)/ (4.12), respectively. Note that the integrals in (4.22) can be easily and accurately computed by standard mathematical software packages such as Mathematica©, Matlab©, and MapleT.

Finally, the total success probability can be found as given in (4.9).

## 4.4 Numerical Results

This section shows the performance of a SWIPT-enabled MEC system by means of numerical results.

### 4.4.1 Setup

The parameters are set as given in Table 4.1 unless otherwise specified. In the numerical results part, the figures have been presented for different values of upload target SINR $\beta_{\mathrm{up}}$, tuning parameter $q$, density of PHs $\lambda_{\mathrm{ph}}$ and the task complexity $k$.

### 4.4.2 Results

In Fig.4.4, the probabilities of offloading (red) and local computation (blue) i.e. $P_{\mathrm{off}}$ and $P_{\mathrm{loc}}$, are plotted as functions of $\beta_{\mathrm{up}}$ for $q = 0$, complexity $k = 400$ and two different values of $\lambda_{\mathrm{ph}} = \{0.1, 0.2\}$ when $R_{\mathrm{a}} = 600$m. The nearly perfect match between our theoretical results (markers) and the Monte Carlo simulations (lines) verifies the accuracy of two PH dominant-based approach used to approximate harvested energy $E_{\mathrm{h}}$. As expected, in both cases $\lambda_{\mathrm{ph}} = 0.1$ (solid lines) and $\lambda_{\mathrm{ph}} = 0.2$ (dash lines), the probability of local computation increases with $\beta_{\mathrm{up}}$. This can be explained with the fact that by increasing $\beta_{\mathrm{up}}$, duration for uploading the results to the MEC server, $\tau_{\mathrm{up}}$, decreases which leads to increase in $\tau_{\mathrm{loc}} = \tau_{\mathrm{off}} - \tau_{\mathrm{up}}$, hence decreasing the required energy for local computation $E_{\mathrm{loc}}$, given in (4.5), and consequently increasing the probability of local computation.

TABLE 4.1: System Parameters for Chapter 4

| | |
|---|---|
| Density of the MEC servers, $\lambda_{\text{mec}}$ | 0.2 |
| Average transmit power, $P$ | 3W |
| MEC server sensitivity, $\eta$ | $-55$dBm |
| Noise variance for information decoding, $\sigma_{\text{id}}^2$ | $-105$dB |
| SNR in offloading/uploading, $\eta/\sigma_{\text{i}}^2$ | 20dB |
| Carrier frequency, $f_c$ | 2.1GHz |
| Signal bandwidth, $W$ | 1MHz |
| Effective capacitance coefficient, $c_e$ | $10^{-27}$ |
| Energy harvesting efficiency, $\mu$ | 0.4 |
| Length of the task, $L_{\text{task}}$ | 1 kbits |
| Path loss exponent, $\alpha$ | 2.5 |
| Total time duration, $T$ | $10^{-2}$s |
| Energy harvesting time duration, $\tau_{\text{eh}}$ | $0.25 \times T$ |
| Target SINR for information decoding, $\beta_{\text{id}}$ | $-10$dB |
| Length ratio, $m$ | 0.05 |
| Constant, $c_{\text{dec}}$ | $10^{-3}$ J/bit [66] |

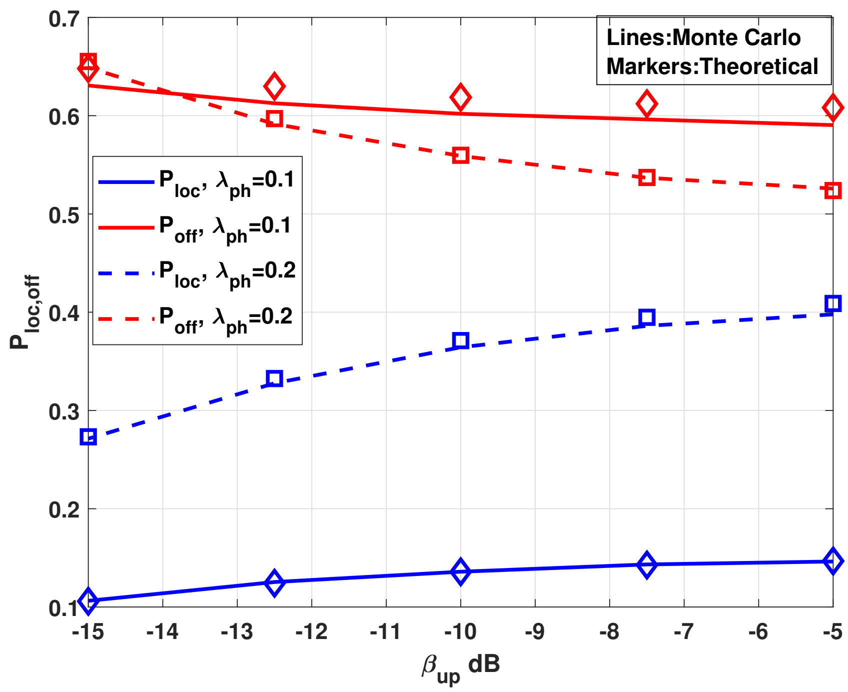


FIGURE 4.4: Probability of offloading and local computation: theoretical results and Monte Carlo simulations for different values of $\beta_{\text{up}}$ when $q = 0$ and $k = 400$.

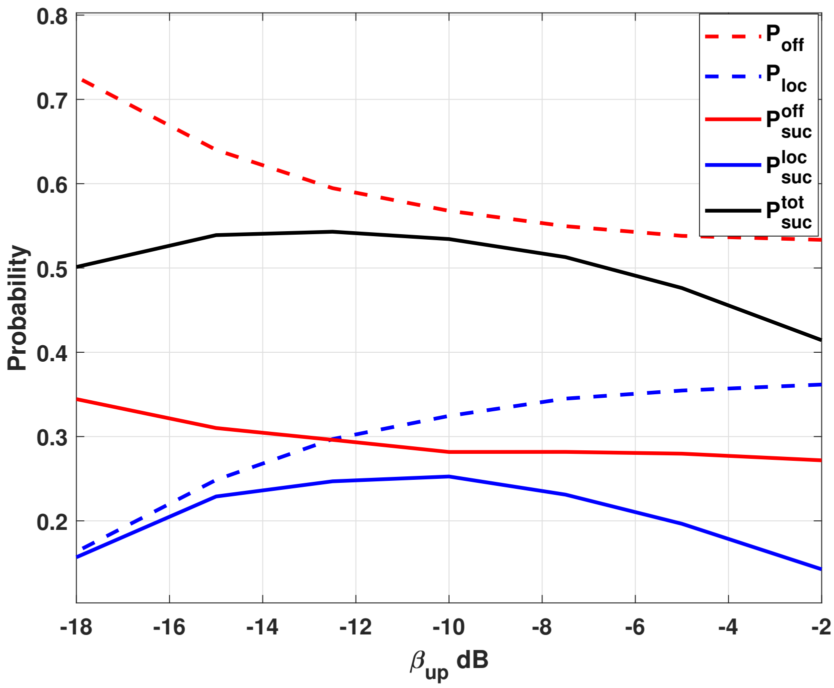


FIGURE 4.5: Success probabilities of offloading, local computation and total offloading-local computation for different values of $\beta_{up}$ when $q = 0$ and $k = 400$.

For offloading, since $q = 0$, then $P_{off} = \mathbb{P}\{E_{off} \leq E_h \leq E_{loc}\}$, and therefore increasing $\beta_{up}$ decreases $E_{loc}$ and consequently the probability of offloading. By comparing these two probabilities for $\lambda_{ph} = \{0.1, 0.2\}$, we can see that as the density of PHs increases, as expected, the outage probability decreases. More interestingly, we can observe that the rate of increasing (resp. decreasing) in $P_{loc}$ (resp. $P_{off}$) with $\beta_{up}$, respectively, is higher for higher values of $\lambda_{ph}$: for $q = 0$, increasing $\lambda_{ph}$ and therefore $E_{off}$ and decreasing $E_{loc}$ (by increasing $\beta_{up}$) leads to double increase in probability of local computation $P_{loc}$ and double decrease in probability of offloading $P_{off}$.

Success probabilities of offloading (red), local computation (blue) and total offloading-local computation (black) have been presented for different values of $\beta_{up}$ in Fig.4.5 when $R_a = 30$m, $\lambda_{ph} = 0.2$ and $k = 400$. For the local computation, as we can see, the success probability of local computation initially increases with $\beta_{up}$ until it becomes decreasing starting from about $\beta_{up} = -10$dB. This is due to the fact that, as explained before, $P_{loc}$ is increasing in $\beta_{up}$, however, the upload SINR coverage is decreasing. Our numerical evaluation suggests that for lower values of $\beta_{up}$ (e.g. between $-10$dB and $-18$dB), the increment rate of $\mathbb{P}\{\delta = \text{loc}\}$ is higher than the decrement rate of the upload SINR coverage, however, in the region between $-10$dB and $-2$dB, the increment rate of $P^{loc}_{suc}$ decreases: thus, the upload SINR coverage starts to become the limiting factor.

Considering the offloading case, as previously explained, probability of offloading decreases with $\beta_{up}$, however, the offload SINR coverage increases as $P_{off}$ decreases. The numerical results show that for $\beta_{off} = -10$dB, the increment rate of offload SINR coverage is slightly smaller than the decrement rate of $P_{off}$, and therefore, the success probability of offloading is decreasing in $\beta_{up}$. Moreover, the total success

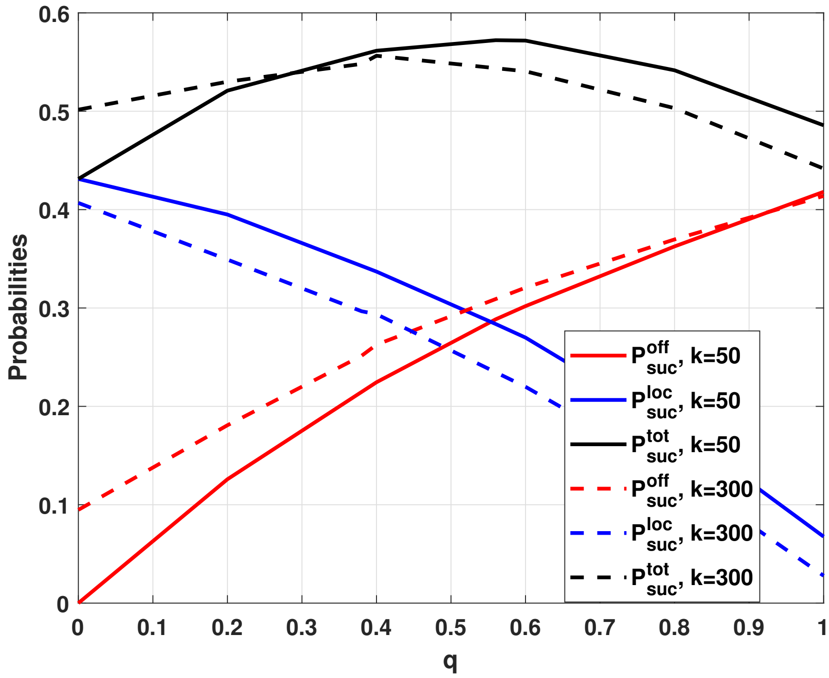


FIGURE 4.6: Success probabilities of offloading, local computation and total offloading-local computation for different values of complexity, $k$, as a function of $q$ when $\beta_{\text{up}} = -10$dB.

probability as the summation of success probabilities of local computation and offloading is presented. As we can see, due to the decreasing monotonicity of $P^{\text{off}}_{\text{suc}}$, the total success probability attains its maximum in a smaller value than the success probability of local computation.

In Fig.4.6, we have presented the success probabilities of offloading (red), local computation (blue) and total offloading-local computation (black) for two different values of complexity, $k = 50$ (solid lines) and $k = 300$ (dash lines), as a function of $q$. Here $R_{\text{a}} = 30$m, $\beta_{\text{up}} = -10$dB and $\lambda_{\text{ph}}$ is chosen as 0.2. From (4.11) and (4.12), it is clear that the probabilities of offloading and local computation are increasing and decreasing, respectively, with $q$. Our numerical results suggest that for $\beta_{\text{off}} = \beta_{\text{up}}$, the offloading/local computation probability is dominating in success probabilities compared to offload/upload SINR coverage probabilities and thus, the success probabilities of offloading and local computation are increasing and decreasing, respectively, with $q$.

Moreover, as we can see, the success probability of local computation is higher for smaller $k$, which is due to the fact that LPD$^{(0)}$ needs less energy to perform local computation for less complex tasks (see (4.5)) which leads to increase in $P_{\text{loc}}$. More interestingly, we can see that for small values of $q$, the performance of the system is better for higher values of task complexity which is due to the fact that increasing $k$ decreases the difference between the local computation and offloading probabilities which leads to a better splitting of interfering LPDs and consequently, a higher success probability. Also we can see that the success probability initially increases with $q$ until it becomes decreasing starting from about $q^*(k)$, beyond which the offloading probability starts to become higher than the local computation probability. Assuming $\beta_{\text{up}} = \beta_{\text{off}}$, $q^*(k)$ is the point at which the local computation and offloading probabilities are equal, and therefore, can be computed as : $q^*(k) = 0.5\Big(1 - \frac{\mathbb{P}\{E_{\text{off}} \leq E_{\text{h}} \leq E_{\text{loc}}\} - \mathbb{P}\{E_{\text{loc}} \leq E_{\text{h}} \leq E_{\text{off}}\}}{\mathbb{P}\{E_{\text{h}} \geq \max\{E_{\text{loc}}, E_{\text{off}}\}\}}\Big)$.

After analysing the rate-energy trade-offs for SWIPT-enabled systems in previous chapter, in this chapter we have focused on the mobile edge computing systems and have analysed the performance of SWIPT-enabled MEC system. We have proposed a decision strategy where a tuning parameter $q$ enables us to apportion the interference between offloading and uploading sub-slots in order to increase the success probability. Numerical results have showed that the system has a better performance for higher values of $q$ which justifies our decision strategy. Moreover, we have seen that the task complexity has also impact on the system performance. For higher values of the tuning parameter, increasing the complexity of the tasks leads to a better splitting of interfering LPDs and consequently a higher success probability.

## 4.5 Summary

In this chapter, we have studied a SWIPT-enabled MEC system where an LPD has to decide either for performing local computation or offloading. We have provided the theoretical results for probabilities of offloading and local computation, as well as their corresponding success probabilities. These success probabilities consequently characterise the total success probability. Moreover, in order to capture the trade-off between computation and communication in local computation mode, we have presented Monte Carlo simulations for different values of SINR target in uploading phase. In addition, the probabilities of local computation and offloading are expressed as a function of a tuning parameter $q$ which enables us to analyse the existing trade-off between local computation and offloading.

As it has been explained before, SWIPT systems are suitable for indoor scenario, thus, in the next chapter, we will investigate the performance of the SWIPT-MEC system under the presence of spatially correlated shadowing.

# Chapter 5

# SWIPT MEC Systems in the Presence of Spatially Correlated Shadowing

After analysing the performance of the SWIPT-enabled MEC system operating in outdoor environment, now in this chapter, we will study the impact of blocking obstacles on the system performance. In particular, we will provide an analytical expression of the joint energy and SINR coverage probability. After that, total success probability which is defined as the probability of either successfully computing given task locally or offloading it to the associated MEC server, will be evaluated. Moreover, we will analyse the impact of the different system parameters on the trade-off between the energy harvested and the computational task admission rate. Regarding the decision strategy, differently from our previous work, we assume energy minimization strategy where the LPD chooses to perform the operation (local computing or offloading) which requires less energy.

## 5.1 Introduction

In the previous chapters, we have explained the importance of considering effect of blockage objects on the system performance. In this chapter, we make use of SG to have a comprehensive analysis of SWIPT-based MEC system where the blockage effect is integrated on our analysis. Here, SWIPT is used to simultaneously deliver power and command message to the LPDs. This command message is used to select a computational task to be executed by the LPD. In order to have a systematic view point on the trade-off between power transfer, communication and computation, we include in our SG analysis a realistic CPU energy consumption model in which the frequency of the CPU can be adapted according to the time available for computation.

- As interference can be beneficial for wireless power transfer, we assume that interference can be exploited in the downlink to increase the amount of energy harvested while the task offloading in the uplink is performed over orthogonal frequency bands.

- Differently from the previous chapter, we consider a decision strategy with the energy minimization decision. Moreover, since the blocking objects are considered in the system model, we use power control in the uplink in order to mitigate the detrimental effect of the shadowing.

- In order to simplify the SG analysis, we approximate the wall attenuation. The authors of [87] used an approximation which is obtained by averaging over the wall distribution and over all the possible angles. However this simple procedure gives a poor approximation of the performance. Thus, we consider a different approximation and average the attenuation over the number of the walls and orientation for a given distance.

- We derive the expression of downlink SINR coverage as well as the expressions of success probabilities for offloading and for local computation.

- The impact of an adaptive offloading technique on the global success probability is evaluated. The accuracy of the proposed analysis is validated by means of Monte Carlo simulations.

- The trade-off between the energy harvested and the energy needed to perform the computation task is investigated. Results show that by increasing the harvesting time the offloading energy coverage probability increases while the energy coverage for local computation first increases and then starts to decrease.

- We also present the effects of the energy minimization strategy on the system performance. We see that the system has better performance when LPDs can choose either to perform local computation or offloading rather than always performing one of them.

## 5.2 System Model

Similarly what has been considered in the previous chapter, in the SWIPT-based MEC system PHs simultaneously deliver command messages of $L_{\text{com}}$ bits and power to the LPDs. We assume that, at the LPD side, SWIPT is implemented through the time-switching scheme. The command message is therefore decoded after the energy harvesting phase and used to trigger a specific computation task on local data. The computation task is characterized by the number of bits to be processed $L_{\text{task}}$ and its complexity $k$ expressed in CPU cycles/bit. Each LPDs executes a task upon reception of the command message by either performing it locally or offloading the task to a MEC server, according to the energy minimization strategy. In case of local computation, a message of $L_{\text{res}}$ bits containing the result of the computation is eventually sent to a data aggregation node. In order to simplify the notation, we assume that $L_{\text{com}} = n\, L_{\text{task}}$ and $L_{\text{res}} = m\, L_{\text{task}}$ with $n < m \ll 1$. We also assume that time is slotted with a fixed slot duration, denoted by $T$. As shown in Fig. 4.2, each time slot is then divided into energy harvesting, information (i.e. command message) decoding and local computation/offloading sub-slots with time durations of $\tau_{\text{eh}}$, $\tau_{\text{id}}$ and $\tau_{\text{off}}$, respectively. In the case of offloading, the whole duration $\tau_{\text{off}}$ is used by the LPD to transmit the task to the associated MEC server. On the other hand, in the case of local computation, the third sub-slot needs to be further divided into two sub-slots:

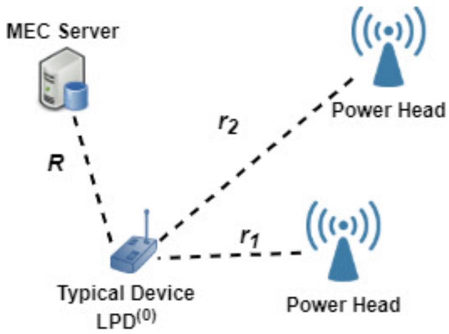


FIGURE 5.1: SWIPT-MEC system model 2.

computation slot, with duration of $\tau_{\text{loc}}$ in which the task is executed and the uploading sub-slot, with duration of $\tau_{\text{up}}$ in which the LPD transmits the obtained result to the aggregation node. In order to simplify the notation and improve the readability of the equations we further assume that the aggregation nodes and the MEC servers are co-localized. In the remainder of this chapter, the term MEC server is also used to refer to the aggregation node.

Differently from the previous chapter, as mentioned above, here it is assumed that $L_{\text{com}} = nL_{\text{task}}$ with $n << 1$ . In this case we can adapt the time parameters that are given in (4.8) as,

$$\tau_{\text{id}} = nB(\text{s}), \ \tau_{\text{up}} = mB(\text{s}), \ \tau_{\text{off}} = B(\text{s}), \tag{5.1}$$

where $B(\text{s}) = \frac{L_{\text{task}}}{W \log(1+\beta_{\text{s}})}$, $\text{s} \in \{\text{id}, \text{mec}\}$, $W$ is the signal bandwidth and $\beta_{\text{s}}$ is the SINR target in the considered phase (i.e. $\beta_{\text{id}}$ for the downlink, $\beta_{\text{mec}}$ for the offloading/uploading).

Regarding the network model, as in the previous system models, we assume that the PHs and MEC servers have been deployed over a circular area with radius $R_{\text{a}} \in \mathbb{R} \cup \infty$ following a homogeneous PPP distribution, $\Psi_{\text{ph}}$, with density $\lambda_{\text{ph}}$ and $\Psi_{\text{mec}}$, with density $\lambda_{\text{mec}}$, respectively. Typical LPD, LPD$^{(0)}$, is located at the centre of the given area. We adopt a common association policy in which each LPD connects to its nearest PH and its nearest MEC server. Fig. 5.1 illustrates the considered SWIPT-based MEC system.

### Wall Blockage Analyses

Since we want to analyse the impact of the obstacles on the performance, we assume that the transmitted signals are subject to distance dependent path loss, wall blockages and small scale fading and consider the propagation model given in (3.1).

However differently from Chapter 3, in order to study the system performance, we have to analyse the uplink and downlink jointly. Thus, in order to simplify the SG analysis, we will approximate the wall attenuation. The authors of [87] assumed an approximation by averaging over the wall distribution, i.e. $(\mathbb{E}[N])$, and over all the possible angles, $\theta$, where the final expression for wall attenuation becomes $K^{\mathbb{E}[N]}$. Interestingly, the result of this approximation is a shadowing with log normal distribution. Unfortunately, this simple procedure gives a poor approximation to the

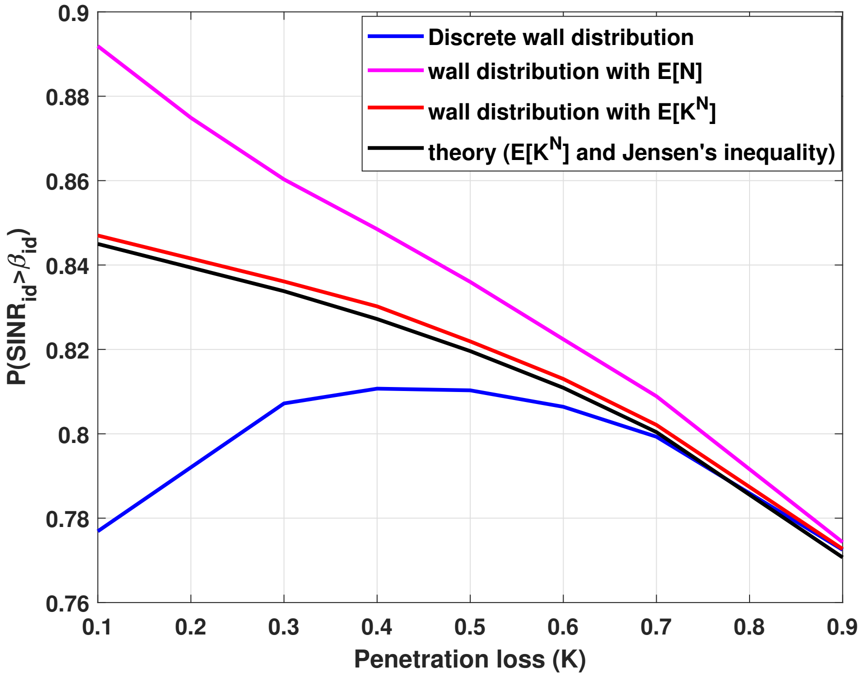


FIGURE 5.2: Downlink SINR coverage for different values of penetration loss.

discrete wall distribution as it is apparent from Fig. 5.2 in which Monte Carlo simulation results for the discrete wall distribution (blue curve) and Monte Carlo simulations results for this approximation (pink curve) have been presented. In order to solve this problem we consider a different approximation to obtain a shadowing model that depends only on the distance between the source and the destination. Therefore, we average the attenuation $\left(\mathbb{E}[K^N]\right)$ over the number of the walls and orientation for a given distance, i.e.

$$\mathbb{E}[K^N|r] = \mathbb{E}_\theta[\mathbb{E}_{N_{xy}}[K^{N_{xy}}|r,\theta]]. \tag{5.2}$$

where $N_{xy}$ is a Poisson distributed random variable with mean $\lambda_{\mathrm{w}} r(|\cos(\theta)| + |\sin(\theta)|)$, [73]. Hence, the average attenuation due to the shadowing can be found as

$$\begin{aligned}
&\mathbb{E}_{N_{xy}}[K^{N_{xy}}|r,\theta] = \\
&\sum_{N=0}^{\infty} K^N \frac{(\lambda_{\mathrm{w}} r\,|\cos(\theta)| + \lambda_{\mathrm{w}} r\,|\sin(\theta)|)^N}{N!} \exp\{-(\lambda_{\mathrm{w}} r\,|\cos(\theta)| + \lambda_{\mathrm{w}} r\,|\sin(\theta)|)\} \\
&\overset{(a)}{=} \exp\{\lambda_{\mathrm{w}} r(K-1)(|\cos(\theta)| + |\sin(\theta)|)\},
\end{aligned} \tag{5.3}$$

where (a) follows the Taylor series representation of exponential function.

In order to obtain the final expression of the average attenuation, we need to take an integral over the variable $\theta$

$$\mathbb{E}[K^N|r] = \mathbb{E}_\theta[K^N|r,\theta] = \int_0^{2\pi} \exp\{\lambda_{\mathrm{w}} r(K-1)\,(|\cos(\theta)| + |\sin(\theta)|)\} f(\theta) d\theta. \tag{5.4}$$

where orientation, $\theta$, is uniformly distributed in $(0, 2\pi]$ and $f(\theta)$ is the probability density function of $\theta$.

Unavailability of closed form expression for this integral motivates us to search for a lower bound. The derivation of this bound follows the approach used in [88] which is a new sharpened version of Jensen's inequality

$$\inf_{x\in(a,b)}\{h(x;\eta)\}\mathrm{var}(X)+e^{t\eta}\leq\mathbb{E}[e^{tX}], \tag{5.5}$$

where

$$h(x;\eta)=\frac{e^{tx}-e^{t\eta}}{(x-\eta)^2}-\frac{te^{t\eta}}{x-\eta},$$

and $\eta$ is the mean value of any random variable $X$ supported on $(a,b)$. By defining $X=|\cos(\theta)|+|\sin(\theta)|$ and $t=\lambda_{\mathrm{w}}r(K-1)$, we can apply (5.5) to our case and the lower bound for the average attenuation is given as,

$$\mathbb{E}[K^N|r]\geq\mathrm{J}(r):=\\ \left(\frac{e^{\lambda_{\mathrm{w}}r(K-1)\sqrt{2}}-e^{\lambda_{\mathrm{w}}r(K-1)\frac{4}{\pi}}}{(\sqrt{2}-\frac{4}{\pi})^2}-\frac{\lambda_{\mathrm{w}}r(K-1)e^{\lambda_{\mathrm{w}}r(K-1)\frac{4}{\pi}}}{\sqrt{2}-\frac{4}{\pi}}\right)\left(1+\frac{2}{\pi}-\frac{16}{\pi^2}\right)+e^{\lambda_{\mathrm{w}}r(K-1)\frac{4}{\pi}}. \tag{5.6}$$

In order to justify our approximation, we have provided downlink SINR coverages in Fig. 5.2. Here, blue curve represents the Monte Carlo simulation results for the discrete wall distribution which has been been discussed in section 3.3.1. We also present Monte Carlo simulation results for the approximation that has been used in [87] (pink curve) and for our proposed approximation where we average the attenuation (red curve). It can be clearly seen that our proposed model provides a better approximation to the discrete wall distribution. Moreover, we have also provided the theoretical results (black curve) where we have used Jensen's inequality in order to validate the proposed approximation. Figure shows that Monte Carlo simulation results and the theoretical results are matching.

## 5.3 Success Probability

In this section, we will derive the success probabilities of offloading/local computation as well as the total success probability. In order to achieve it, we first present the harvested energy, SINR in the downlink and the required energies for local computation and offloading.

**Energy Harvesting**

In the energy harvesting phase, LPD$^{(0)}$ harvests energy in order to use it for locally computing/offloading the task to its associated MEC server. Assuming that all PHs transmit with the same power $P$, the amount of energy harvested by the LPD$^{(0)}$ over this sub-slot is

$$E_{\mathrm{h}}=\tau_{\mathrm{eh}}\mu P\sum_{\mathrm{i}\in\Psi_{\mathrm{ph}}}g_{\mathrm{i}}\kappa^{-1}r_{\mathrm{i}}^{-\alpha}\mathrm{J}(r_{\mathrm{i}}), \tag{5.7}$$

where $r_{\mathrm{i}}$ denotes the distance from the i-th PH, denoted by PH$^{(\mathrm{i})}$, to the LPD$^{(0)}$, $\mu<1$ is the efficiency of the RF energy harvester and $g_{\mathrm{i}}\sim\exp(1)$ is the fading gain between LPD$^{(0)}$ and PH$^{(\mathrm{i})}$.

### Information Decoding

In this phase, LPD$^{(0)}$ receives a command message with a fixed length of $L_{\mathrm{com}}$ bits sent by its serving PH which triggers the execution of a specific computation task. In this phase, the other PHs are considered as interferers for the command message decoding. Denoting the set of interfering PHs by $\Psi_{\mathrm{ph}}^{(\setminus 1)}$, the SINR at the LPD$^{(0)}$ is

$$\mathrm{SINR}_{\mathrm{id}} = \frac{P w_1 \kappa^{-1} r_1^{-\alpha} \mathrm{J}(r_1)}{\mathcal{I}_{\mathrm{id}} + \sigma_{\mathrm{id}}^2}, \tag{5.8}$$

where $r_1$ is the distance from the serving PH to the LPD$^{(0)}$ , $w_1 \sim \exp(1)$ is the fading coefficient of the serving link, $\sigma_{\mathrm{id}}^2$ is the thermal noise power, and $\mathcal{I}_{\mathrm{id}}$ denotes the interference at the typical user, given by

$$\mathcal{I}_{\mathrm{id}} = \sum_{\mathrm{i} \in \Psi_{\mathrm{ph}}^{(\setminus 1)}} P w_{\mathrm{i}} \kappa^{-1} r_{\mathrm{i}}^{-\alpha} \mathrm{J}(r_{\mathrm{i}}), \tag{5.9}$$

where $w_{\mathrm{i}} \sim \exp(1)$ is the channel gain between LPD$^{(0)}$ and PH$^{(\mathrm{i})}$.

### Local Computation/Offloading

After decoding the command message and based on the decision, in the third phase, LPD$^{(0)}$ processes the data locally or offloads it to the associated MEC server. In the previous chapter, we have considered the interference in the uplink, thus the success probabilities of offloading/local computation depended on the SINR coverages in the uplink. However, in this chapter, we analyse SWIPT-enabled MEC system in the presence of spatially correlated shadowing. Shadowing may be detrimental for the MEC systems in the offloading/uploading phases and leads an outage in the uplink. Therefore, here we assume that each LPD performs channel inversion power control in order to have a certain SNR in the uplink. By doing this, we ensure that the LPD performs the offloading only if it has enough harvested energy to successfully offload the task. As we mentioned above, in the offloading as well as the uploading phases, each LPD is assumed to perform channel inversion power control in which the transmitted power is $\frac{\beta_{\mathrm{mec}} \sigma_{\mathrm{mec}}^2 R^{\alpha} \kappa}{h_{\mathrm{mec}}\, \mathrm{J}(R)}$, where $\sigma_{\mathrm{mec}}^2$ is the thermal noise power, $R$ denotes the distance from the LPD$^{(0)}$ to its associated MEC server and $h_{\mathrm{mec}} \sim \exp(1)$ is the fading coefficient of the link. Consequently, the energy consumption for task offloading and local computation, denoted by $E_{\mathrm{off}}$ and $E_{\mathrm{loc}}$, respectively, are given by

$$E_{\mathrm{off}}(R, h_{\mathrm{mec}}) = c_{\mathrm{dec}} \tau_{\mathrm{id}} \log(1 + \beta_{\mathrm{id}}) + (\tau_{\mathrm{loc}} + \tau_{\mathrm{up}}) \frac{\beta_{\mathrm{mec}} \sigma_{\mathrm{mec}}^2 R^{\alpha} \kappa}{h_{\mathrm{mec}}\, \mathrm{J}(R)}, \tag{5.10}$$

$$E_{\mathrm{loc}}(R, h_{\mathrm{mec}}) = c_{\mathrm{e}} \frac{(k L_{\mathrm{task}})^3}{(\tau_{\mathrm{loc}})^2} + \tau_{\mathrm{id}} c_{\mathrm{dec}} \log(1 + \beta_{\mathrm{id}}) + \tau_{\mathrm{up}} \frac{\beta_{\mathrm{mec}} \sigma_{\mathrm{mec}}^2 R^{\alpha} \kappa}{h_{\mathrm{mec}}\, \mathrm{J}(R)}. \tag{5.11}$$

Here $c_{\mathrm{dec}}$ is a constant and measures the required energy to decode one bit and $c_{\mathrm{e}}$ is the effective capacitance coefficient.

Now, we capitalize on a stochastic geometry approach to characterize the success probability which is defined as the probability of successfully computing a given task either locally or offloading it to the associated MEC server

$$P_{\rm suc} = P_{\rm suc}^{\rm off} + P_{\rm suc}^{\rm loc}, \tag{5.12}$$

where

$$P_{\rm suc}^{\rm s} = \mathbb{E}\left[\mathbb{1}\left(\mathrm{SINR}_{\rm id} \leq \beta_{\rm id}\right)\mathbb{1}\left(E_{\rm s} \leq E_{\rm h}\right)\mathbb{1}\left(\delta = {\rm s}\right)\right], \tag{5.13}$$

in which s $\in$ {loc,off} and $\delta$ is a random variable denoting the offloading/local computation decision. As seen in (5.13), success probability of offloading/local computation is expressed as the joint downlink SINR and energy coverage probability which requires the evaluation of the following three probabilities: (i) $\mathbb{P}\left(\mathrm{SINR}_{\rm id} \leq \beta_{\rm id}\right)$ (ii) $\mathbb{P}\left(E_{\rm s} \leq E_{\rm h}\right)$ (iii) $\mathbb{P}\left(\delta = {\rm s}\right)$. It is worth to mention that since LPDs perform channel inversion power control and uplink transmission is assumed to be interference-free, the uplink success rate coincides with $\mathbb{P}\left(E_{\rm s} \leq E_{\rm h}\right)$ for s $\in$ {loc,off}.

As what have been done in the previous chapter, following the procedure proposed in [66], we first derive conditional probabilities of downlink SINR coverage, energy coverage and local computation and offloading probabilities by approximating the amount of harvested energy and the amount of interference in the downlink.

**Conditional Downlink SINR coverage**

The probability that the downlink SINR is higher than a given threshold is

$$P_{\rm c} = \mathbb{P}(\mathrm{SINR}_{\rm id} \geq \beta_{\rm id}\,|r_1, r_2) = \exp\left\{-\beta_{\rm id}\frac{\kappa r_1^{\alpha}}{\mathrm{J}(r_1)}\left(\chi(r_2) + \frac{\sigma_{\rm id}^2}{P}\right)\right\}\left(\frac{1}{1+\beta_{\rm id}\frac{r_1^{\alpha}\mathrm{J}(r_2)}{r_2^{\alpha}\mathrm{J}(r_1)}}\right). \tag{5.14}$$

Derivation can be easily done by following the steps in Appendix E. As given in (4.14), $\chi(r_2)$ is the mean of $\mathcal{I}_{\rm id}/P$ conditioned on the location of the second nearest PH. In this case with the effect of the blockages it becomes,

$$\chi(r_2) = \mathbb{E}\left[\sum_{{\rm i}\in\Psi_{\rm ph}^{(\backslash 1,2)}} w_{\rm i}\kappa^{-1} r_{\rm i}^{-\alpha}\mathrm{J}(r_{\rm i})\,|r_2\right]$$

and can be found as,

$$
\begin{aligned}
\chi(r_2) = \frac{2\pi\lambda_{\mathrm{ph}}}{\kappa}\Bigg\{ & \left(\frac{\pi^2+2\pi-16}{2\pi^2-8\sqrt{2}+16}\right) \\
\times \Bigg( & r_2^{(2-\alpha)}\mathrm{Ei}[-1+\alpha,(1-K)\frac{\sqrt{2}\pi}{4}\beta r_2] - R_a^{(2-\alpha)}\mathrm{Ei}[-1+\alpha,(1-K)\frac{\sqrt{2}\pi}{4}\beta R_a] \\
& - r_2^{(2-\alpha)}\mathrm{Ei}[-1+\alpha,(1-K)\beta r_2] + R_a^{(2-\alpha)}\mathrm{Ei}[-1+\alpha,(1-K)\beta R_a] \\
& - \frac{\sqrt{2}\pi}{4}\beta(K-1)\left(r_2^{(3-\alpha)}\mathrm{Ei}[-2+\alpha,(1-K)r_2\beta] - R_a^{(3-\alpha)}\mathrm{Ei}[-2+\alpha,(1-K)R_a\beta]\right) \\
& + \beta(K-1)\left(r_2^{(3-\alpha)}\mathrm{Ei}[-2+\alpha,(1-K)r_2\beta] + R_a^{(3-\alpha)}\mathrm{Ei}[-2+\alpha,(1-K)R_a\beta]\right)\Bigg) \\
& + r_2^{(2-\alpha)}\mathrm{Ei}[-1+\alpha,(1-K)\beta r_2] - R_a^{(2-\alpha)}\mathrm{Ei}[-1+\alpha,(1-K)\beta R_a]\Bigg\},
\end{aligned}
\tag{5.15}
$$

where $\mathrm{Ei}[\cdot]$ is Exponential integral function [78].

**Conditional Energy coverage**

By following the same steps in Appendix D, the probability that $\mathrm{LPD}^{(0)}$ has harvested enough energy to perform either local computation or offloading can be expressed as

$$
\begin{aligned}
&\mathbb{P}(E_{\mathrm{s}} \le E_{\mathrm{h}}|r_1,r_2,R,h_{\mathrm{mec}}) = \\
&\quad \frac{\mathrm{J}(r_2)r_1^{\alpha}\exp\left\{-\frac{r_2^{\alpha}Z_{\mathrm{s}}^{+}(r_2,R,h_{\mathrm{mec}})}{\mathrm{J}(r_2)}\right\}}{\mathrm{J}(r_2)r_1^{\alpha}-\mathrm{J}(r_1)r_2^{\alpha}} - \frac{\mathrm{J}(r_1)r_2^{\alpha}\exp\left\{-\frac{r_1^{\alpha}Z_{\mathrm{s}}^{+}(r_2,R,h_{\mathrm{mec}})}{\mathrm{J}(r_1)}\right\}}{\mathrm{J}(r_2)r_1^{\alpha}-\mathrm{J}(r_1)r_2^{\alpha}},
\end{aligned}
\tag{5.16}
$$

where

$$Z_{\mathrm{s}}(r_2,R,h_{\mathrm{mec}}) = \frac{E_{\mathrm{s}}\kappa}{\tau_{\mathrm{eh}}\mu P} - \chi(r_2)\kappa.$$

From (5.16), it is obvious that $\mathbb{P}(E_{\mathrm{s}} \le E_{\mathrm{h}}|r_1,r_2,R,h_{\mathrm{mec}}) = 1$ when $Z_{\mathrm{s}}(r_2,R,h_{\mathrm{mec}}) < 0$.

**Conditional Local Computation/Offloading Probabilities**

Following the strategy of minimizing the consumption energy in each task execution, i.e. $\delta = \mathrm{argmin}\{E_{\mathrm{off}},E_{\mathrm{loc}}\}$, the conditional probability of local computation is given by

$$P\left(\delta = \mathrm{loc}\right) = \mathbb{P}(E_{\mathrm{loc}} < E_{\mathrm{off}}|R,h_{\mathrm{mec}}), \tag{5.17}$$

where

$$
\begin{aligned}
&\mathbb{P}(E_{\mathrm{loc}} < E_{\mathrm{off}}|R,h_{\mathrm{mec}}) \\
&= \mathcal{H}\left[\frac{R^{\alpha}}{\mathrm{J}(R)} - c_{\mathrm{e}}\left(\frac{kL_{\mathrm{task}}}{\tau_{\mathrm{loc}}}\right)^3\frac{h_{\mathrm{mec}}}{\beta_{\mathrm{mec}}\sigma_{\mathrm{mec}}^2\kappa}\right].
\end{aligned}
\tag{5.18}
$$

Here $\mathcal{H}[\cdot]$ denotes the Heaviside function. The offloading probability can be easily found as

$$
\begin{aligned}
P(\delta = \text{off}) &= 1 - P(\delta = \text{loc}) \\
&= 1 - \mathcal{H}\left[\frac{R^{\alpha}}{\mathrm{J}(R)} - c_{\mathrm{e}}\left(\frac{kL_{\text{task}}}{\tau_{\text{loc}}}\right)^{3}\frac{h_{\text{mec}}}{\beta_{\text{mec}}\sigma_{\text{mec}}^{2}\kappa}\right].
\end{aligned}
\tag{5.19}
$$

For derivation refer to Appendix F.

Conditional success probability of offloading/local computation can be obtained by substituting (5.14), (5.16) and (5.18)/(5.19) into (5.13). Then, the success probability of offloading/local computation can be obtained by unconditioning the product of these conditional probabilities with respect to joint distribution of $r_1$ and $r_2$, the distribution of $R$ and the distribution of $h_{\text{mec}}$,

$$
\begin{aligned}
P_{\text{suc}}^{\text{s}} = &\int_0^{\infty}\int_0^{R_{\text{a}}}\int_0^{R_{\text{a}}}\int_0^{r_2} \exp\left\{-\beta_{\text{id}}\frac{\kappa r_1^{\alpha}}{\mathrm{J}(r_1)}\left(\chi(r_2) + \frac{\sigma_{\text{id}}^2}{P}\right)\right\}\left(\frac{1}{1+\beta_{\text{id}}\frac{r_1^{\alpha}\mathrm{J}(r_2)}{r_2^{\alpha}\mathrm{J}(r_1)}}\right) \\
&\times \left[\left(\frac{\mathrm{J}(r_2)r_1^{\alpha}\exp\left\{-\frac{r_2^{\alpha}Z_{\text{s}}^{+}(r_2,R,h_{\text{mec}})}{\mathrm{J}(r_2)}\right\} - \mathrm{J}(r_1)r_2^{\alpha}\exp\left\{-\frac{r_1^{\alpha}Z_{\text{s}}^{+}(r_2,R,h_{\text{mec}})}{\mathrm{J}(r_1)}\right\}}{\mathrm{J}(r_2)r_1^{\alpha} - \mathrm{J}(r_1)r_2^{\alpha}}\right)\right. \\
&\times \left.\left(1 - \mathcal{H}\Big[\chi(r_2) - \gamma_{\text{s}}(R,h_{\text{mec}})\Big]\right) + \mathcal{H}\Big[\chi(r_2) - \gamma_{\text{s}}(R,h_{\text{mec}})\Big]\right] \\
&\times P(\delta = \text{s}|R,h_{\text{mec}})\, f(r_1,r_2) f(R) f(h_{\text{mec}})\, dr_1\, dr_2\, dR\, dh_{\text{mec}}, \quad \text{s} \in \{\text{off},\text{loc}\}
\end{aligned}
\tag{5.20}
$$

where

$$
\gamma_{\text{s}}(R,h_{\text{mec}}) = \frac{E_{\text{s}}(R,h_{\text{mec}})}{\tau_{\text{eh}}\mu P},
$$

and the distributions are given in (4.23). It worths to remind that the integrals in (5.20) can be easily and accurately computed by standard mathematical software packages such as Mathematica©, Matlab©, and MapleT.

Finally, as given in (5.12), the total success probability is simply the sum of these two success probabilities.

## 5.4 Numerical Results

In this section the analytical findings presented in this study are validated through the comparison with Monte Carlo simulations. System parameters are given in Table 5.1 and they are compatible with the parameters given in the previous chapter.

The proposed SWIPT-based MEC system is characterized by a trade-off between the amount of harvested energy and the amount of needed energy to execute a task. This trade-off is illustrated in Fig. 5.3 where the energy coverage probability for each LPD's strategy is illustrated as a function of the harvesting time $\tau_{\text{eh}}/T$. As a matter of fact, by increasing the harvesting time, the LPDs can harvest more energy to perform either the local computation or the offloading. However, when $\tau_{\text{eh}}$ increases, the time devoted to the LPD's operations decreases. It follows that either the task must be performed with a higher CPU rate or the data rate for outsourcing

TABLE 5.1: System Parameters for Chapter 5

| | |
|---|---|
| Radius of the area, $R_a$ | 90m |
| Average transmit power, $P$ | 4dB |
| Penetration loss, $K$ | 0.3 |
| Noise variance, $\sigma^2_{\text{id/mec}}$ | $-75$dB |
| Carrier frequency, $f_c$ | 2.1GHz |
| Signal bandwidth, $W$ | 1MHz |
| Effective capacitance coefficient, $c_e$ | $10^{-27}$ |
| Energy harvesting efficiency, $\mu$ | 0.4 |
| Length of the task, $L_{\text{task}}$ | 1 kbits |
| Total time duration, $T$ | 0.1s |
| Length ratio for command message, $n$ | 0.01 |
| Length ratio for results, $m$ | 0.05 |
| Constant, $c_{\text{dec}}$ | $10^{-3}$ J/bit [66] |

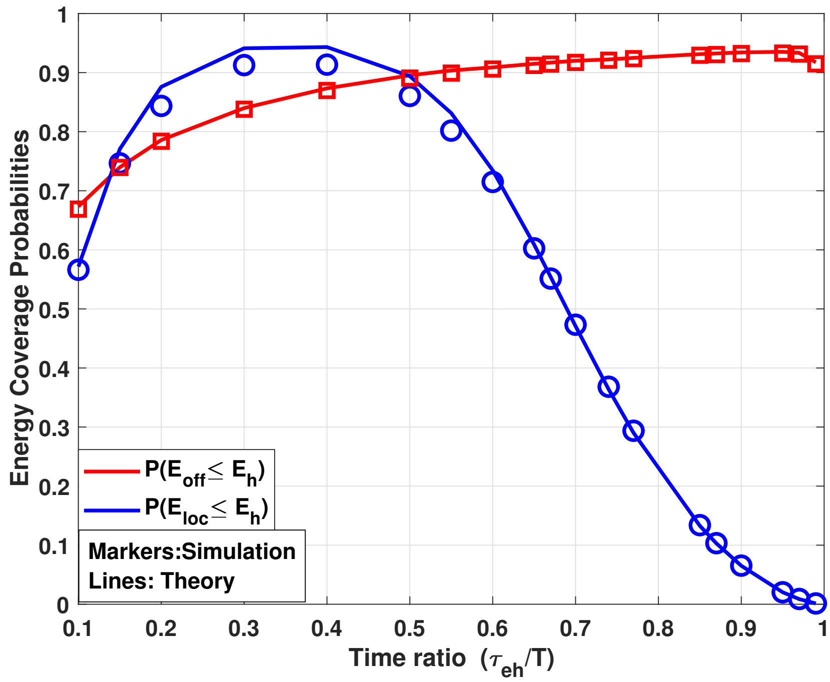


FIGURE 5.3: Energy coverage probabilities of offloading and local computation versus $\tau_{\text{eh}}/T$.

the task must increase. In both cases, this would inflate the total power consumption of the LPD. This energy trade-off has been evaluated for a fixed density of PHs and MEC servers, $\lambda_{\text{mec}} = 0.1$, $\lambda_{\text{ph}} = 0.1$, and for a given task complexity $k = 2000$ bits when path loss exponent $\alpha = 2.5$. It is worth remarking that Monte Carlo simulations (markers) and theoretical results (lines), obtained for different values of the harvesting time $\tau_{\text{eh}}/T$, match almost perfectly, thus validating the accuracy of our proposed analytical expressions.

The probability that the LPDs harvest enough energy to perform data offloading is represented by the red curve. It can be observed that by increasing the harvesting time, the offloading success probability increases despite of the fact that the offloading time decreases and the data rate must then increase. In other words, for the given setup, the additional transmit power due to a larger required data rate for offloading data is compensated by the amount of additional energy harvested by the device. This is true for almost all points. However, when the time ratio is very close to 1 and the allowed time for offloading is very small, the increment on $E_{\text{off}}$ is not balanced by the increase of $E_{\text{h}}$ and the energy coverage curve starts decreasing.

The blue curve represents the energy coverage for local computation. In this case, the energy coverage first increases and then starts to decrease. In fact, for values of $\tau_{\text{eh}}/T \leq 0.4$, the CPU works at low speed and the increment of $E_{\text{h}}$ is greater than the additional CPU energy consumption. On the other hand, for the values of $\tau_{\text{eh}}/T > 0.4$, despite of the higher time devoted to energy harvesting, the energy needed for locally executing the task increases more rapidly than $E_{\text{h}}$. In fact, the dominant part of the required energy for local computation is the energy used by the CPU (first term in (5.11)) while the energy that LPD$^{(0)}$ needs for uploading the results to the associated MEC server is almost negligible. Hence, for higher values of $\tau_{\text{eh}}$, LPD$^{(0)}$ has less time for executing the task, $\tau_{\text{loc}}$, thus leading to larger values of $E_{\text{loc}}$ and decreasing energy coverage.

Fig. 5.4 illustrates the success probability of the computation task for different values of the SINR threshold $\beta_{\text{id}}$ when $\lambda_{\text{mec}} = 0.01$, $\lambda_{\text{ph}} = 0.05$, $\alpha = 2.5$ and $k = 400$ bits. The pink curve represents the SINR coverage in the downlink, while the black curve shows the total success probability (See (5.12)) when LPD$^{(0)}$ can choose to perform either offloading or local computation based on the energy minimization strategy. It can be observed that the total success probability decreases for higher values of $\beta_{\text{id}}$ due to the reduction of the downlink SINR coverage. In order to show the effects of the energy minimization strategy, the success probabilities for offloading and local computation are also reported in Fig. 5.4. The blue curve is associated with the case that LPD$^{(0)}$ always perform local computation, while the red curve represents the case that LPD$^{(0)}$ always offloads the task to the associated MEC server.

Fig. 5.5 shows the probability that the LPD chooses one of the possible strategies to successfully perform the given task when $\lambda_{\text{ph}} = 0.05$, $k = 400$ and $\tau_{\text{eh}}/T = 0.95$ for 3 different values of $\alpha$. It is apparent that, by deploying the MEC servers more densely, the distance between the LPD$^{(0)}$ and the associated MEC server decreases and the offloading probability (red curves) increases. Concurrently, the local computation probability (blue curves) decreases. This is due to the fact that the energy consumption for the uploading phase does not play a major role on $E_{\text{loc}}$ and it plays negligible role on the probability $\mathbb{P}(E_{\text{off}} < E_{\text{loc}})$. As a consequence, the LPD chooses more frequently to offload the tasks rather than to execute them locally.

Not surprisingly the success probability decreases for the higher values of path loss exponent. Moreover for a denser deployment of the MEC servers, due to a reduced distance between the LPD$^{(0)}$ and the associated MEC server, path loss does not play a major role on the performance. Hence, the gap between the curves for different values of $\alpha$ is decreasing.

After analysing the performance of SWIPT-enabled MEC systems in the previous chapter, here we have focused on the impact of the blocking objects on the SWIPT-enabled MEC systems. Numerical results have showed that the performance of the

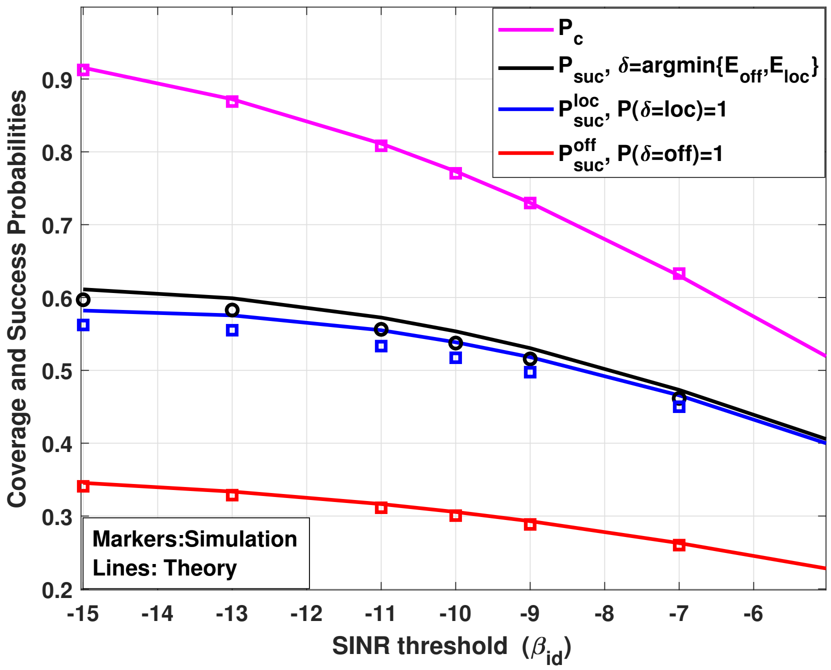


FIGURE 5.4: Downlink SINR coverage, total success, success offloading and success local computation probabilities versus $\beta_{\text{id}}$.

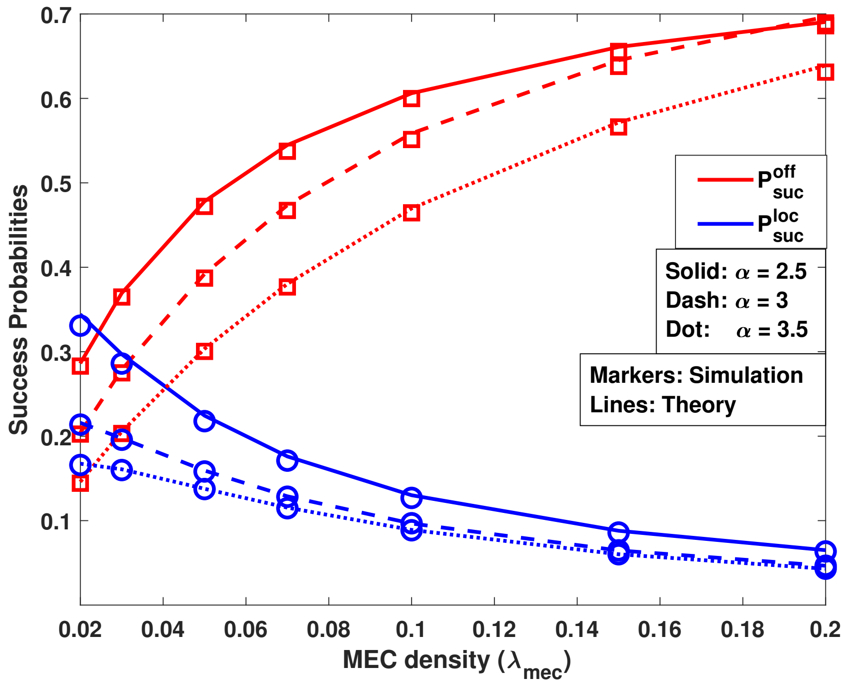


FIGURE 5.5: Success offloading and success local computation probabilities versus $\lambda_{\text{mec}}$.

system has been improved by using the energy minimization strategy. Moreover, increment on the density of the MEC servers has an detrimental effect on the success probability of local computation while it improves the success probability of offloading.

## 5.5 Summary

In this chapter, we make use of the SG framework to model and analyse the effect of blocking objects on the performance of a SWIPT-based MEC system. We have adopted the derived expressions of SINR coverages and success probabilities of offloading/local computation in the previous chapter to our model where the effect of the blockage objects are considered. In order to simplify the SG analyses, wall attenuation is approximated by its expectation and we have obtained a shadowing model that only depends on the distance between the source and the destination. The trade-off between the energy harvested and the energy needed to perform the computation task has also been investigated. Finally, the impact of an adaptive offloading technique on the global success probability has been evaluated.

# Chapter 6

# Conclusions

The objective of this dissertation is to provide a system level perspective on the performance of SWIPT-enabled MEC systems in the presence of spatially correlated shadowing. In order to achieve that, we first study the achievable rate-energy trade-offs of an indoor SWIPT system. Then, we focus on mobile edge computing and study the success probabilities of SWIPT-enabled MEC systems. Finally, we study the impact of the blocking objects on the trade-offs and complete the dissertation by providing a comprehensive understanding on the performance of SWIPT-enabled MEC systems in the presence of spatially correlated shadowing. This chapter sums up the conclusions drawn from each part of this research and also presents some possible future extensions.

In Chapter 3, we have considered an indoor MIMO SWIPT systems with power splitting receiver architecture. We have made use of SG in order to analyse the impact of the blocking obstacles on the system performance. To achieve this the locations of the power heads have been distributed by using PPP and the positions of obstacles have been modelled by utilizing MPLP. The rate-energy trade-offs defining the performance of SWIPT system have been quantified with the aid of J-CCDF. In order to obtain the expression of J-CCDF, we have first studied the stochastic behaviours of signal attenuation, multi-user interference and serving channel gain. We have shown that the obstacles can be beneficial in some cases where their effect in reducing the received power is compensated by the decrease of multi-user interference. Moreover, we have discovered that the power splitting ratio and the transmit power do not have any effect on the maximum achievable information rate. However, with their higher values, LPDs can harvest more energy. With the help of the studied rate-energy trade-offs, we have analysed the performance of a SWIPT-enabled real time mobile computing system. The operating points for this setup have been discovered and the performance of the system has been investigated as a function of task complexities.

In Chapter 4, we have extended our analyses to SWIPT-enabled MEC system. The locations of the network elements have been modelled by PPP. In this setup, SWIPT has been used to simultaneously send command message and transfer power. We have proposed a decision strategy for LPDs to choose performing either local computation or offloading. Moreover, we have introduced a random probability to deal with the interference issue in the offloading and uploading phases. Probabilities of offloading and local computation as well as their success probabilities have been obtained. To achieve this, we have used dominant-BS approach. Moreover, a triple trade-off between energy, communication and computation has been investigated.

Since SWIPT systems are more suitable for indoor scenario, in Chapter 5, we have taken the shadowing effect into account and have analysed the performance of SWIPT-enabled MEC systems in an indoor environment. In order to do that, we have considered a path loss model that is combination of distance dependent path loss, wall blockages and small scale fading. For simplifying the SG analyses, we have approximated the wall attenuation by its expectation. In this setup, a decision strategy based on energy minimization has been considered. Since interference is beneficial for energy harvesting, we have assumed that it can be exploited in the downlink, although we have power control in the uplink and the task offloading has been performed over orthogonal frequency bands. We have derived the coverage probabilities and then have obtained the total success probability.

Overall, in this dissertation, we first study the impact of the shadowing on SWIPT-enabled networks and by extending our model step by step, finally we provide a comprehensive overview for SWIPT-MEC systems in the presence of spatially correlated shadowing at network level.

# Appendix A

# Proof of Proposition 1

First, we note that the process collecting all the propagation losses $L = \left\{ l(r^{(\mathrm{n})}), \mathrm{n} \in \Psi \right\}$ can be characterised as a transformation of the points of $\Psi$. Hence, invoking the displacement theorem, [19, Theorem 1.3.9], and recalling that $\Psi$ can be expressed as the superposition of the PPPs $\Psi_N$, the processes $L_N = \left\{ l_N(r^{(\mathrm{n})}), \mathrm{n} \in \Psi_N \right\}$, $N \in \{0, N_{\max}\}$, are PPPs whose intensity is given by

$$\begin{aligned} \Lambda_N([0,\xi)) &= \Pr\left\{ \frac{\kappa (r^{(\mathrm{n})})^{\alpha}}{K^N} \in [0,\xi), \mathrm{n} \in \Psi_N \right\} \\ &= \lambda_{\mathrm{ph}} \int_0^{2\pi} \int_0^{\infty} \mathcal{H}\left( \xi - \frac{\kappa r^{\alpha}}{K^N} \right) P_N(r,\theta)\, r dr d\theta. \end{aligned} \tag{A.1}$$

Now, by substituting (3.3) in (A.1) and integrating it over $r$, we get $\Lambda_N([0,\xi))$ as

$$\begin{aligned} &\Lambda_N([0,\xi)) = \frac{\lambda_{\mathrm{ph}}}{N!} \int_0^{2\pi} \left( \lambda_{\mathrm{w}} |\cos(\theta)| + \lambda_{\mathrm{w}} |\sin(\theta)| \right)^{-2} \\ &\times \left[ \left( \Gamma(2+N) - \Gamma\left( 2+N, \left( \frac{\xi K^N}{\kappa} \right)^{1/\alpha} \left( \lambda_{\mathrm{w}} |\cos(\theta)| + \lambda_{\mathrm{w}} |\sin(\theta)| \right) \right) \right) \bar{\mathcal{H}}\left( \xi - \frac{R_{\mathrm{a}}^{\alpha} \kappa}{K^N} \right) \right. \\ &\left. + \left( \Gamma(2+N) - \Gamma\left( 2+N, R_{\mathrm{a}} \left( \lambda_{\mathrm{w}} |\cos(\theta)| + \lambda_{\mathrm{w}} |\sin(\theta)| \right) \right) \right) \mathcal{H}\left( \xi - \frac{R_{\mathrm{a}}^{\alpha} \kappa}{K^N} \right) \right] d\theta. \end{aligned} \tag{A.2}$$

In order to have an analytical expression for the integration over the variable $\theta$, we can express the the upper-incomplete Gamma functions of $\theta$ through their Taylor expansions, i.e.,

$$\begin{aligned} &\Gamma\left( 2+N, \left( \frac{\xi K^N}{\kappa} \right)^{1/\alpha} \left( \lambda_{\mathrm{w}} |\cos(\theta)| + \lambda_{\mathrm{w}} |\sin(\theta)| \right) \right) = \\ &\Gamma(2+N) - \sum_{\mathrm{i}=0}^{\infty} \frac{(-1)^{\mathrm{i}} \left( \frac{\xi K^N}{\kappa} \right)^{(N+2+\mathrm{i})/\alpha}}{\mathrm{i}!(\mathrm{i}+N+2)} \\ &\times \left( \lambda_{\mathrm{w}} |\cos(\theta)| + \lambda_{\mathrm{w}} |\sin(\theta)| \right)^{(N+2+\mathrm{i})}, \end{aligned} \tag{A.3}$$

and

$$\begin{aligned} &\Gamma\left( 2+N, R_{\mathrm{a}} \left( \lambda_{\mathrm{w}} |\cos(\theta)| + \lambda_{\mathrm{w}} |\sin(\theta)| \right) \right) = \Gamma(2+N) \\ &- \sum_{\mathrm{i}=0}^{\infty} \frac{(-1)^{\mathrm{i}} R_{\mathrm{a}}^{(N+2+\mathrm{i})}}{\mathrm{i}!(\mathrm{i}+N+2)} \left( \lambda_{\mathrm{w}} |\cos(\theta)| + \lambda_{\mathrm{w}} |\sin(\theta)| \right)^{(N+2+\mathrm{i})}, \end{aligned} \tag{A.4}$$

and, substituting (A.3) and (A.4) into (A.2), we get the final expression of $\Lambda_N([0,\xi))$ as

$$\begin{aligned}
&\Lambda_N([0,\xi)) = \\
&\frac{4\lambda_{\mathrm{ph}}}{N!}\sum_{\mathrm{i}=0}^{\infty}\frac{(-1)^{\mathrm{i}}\lambda_{\mathrm{w}}^{N+\mathrm{i}}}{\mathrm{i}!(N+\mathrm{i}+2)}\left[\frac{2^{\frac{N+\mathrm{i}}{2}}\sqrt{\pi}\,\Gamma(\frac{N+\mathrm{i}+1}{2})}{\Gamma(\frac{N+\mathrm{i}+2}{2})}-\frac{\sqrt{2}\,{}_2F_1\left(\frac{1}{2},\frac{N+\mathrm{i}+1}{2},\frac{N+\mathrm{i}+3}{2},\frac{1}{2}\right)}{N+\mathrm{i}+1}\right] \\
&\qquad\times\left[R_{\mathrm{a}}^{N+2+\mathrm{i}}\quad\mathcal{H}\left(\xi-\frac{R_{\mathrm{a}}^{\alpha}\kappa}{K^N}\right)+\left(\frac{\xi K^N}{\kappa}\right)^{\frac{N+\mathrm{i}+2}{\alpha}}\bar{\mathcal{H}}\left(\xi-\frac{R_{\mathrm{a}}^{\alpha}\kappa}{K^N}\right)\right].
\end{aligned} \tag{A.5}$$

Eventually, it worth recalling that the Heaviside function is defined as

$$\mathcal{H}(x)=\begin{cases}1 & \text{if } x\geq 0\\ 0 & \text{if } x<0\end{cases}$$

and that $\bar{\mathcal{H}}(x)=1-\mathcal{H}(x)$. Hence, by introducing the compound variable $\eta=N+\mathrm{i}$ in (A.5) and defining the function $\chi_\eta(\lambda_{\mathrm{w}})$ as in (3.5), the proof is complete.

# Appendix B

# Proof of Proposition 2

First, let note that the multi-user interference $\mathcal{I}_{\mathrm{MU}}$ can be expressed as the sum of the interferences produced by the PHs belonging to $\Psi_N$, $N \in \{0, N_{\max}\}$, where the processes $\Psi_N$ are assumed to be independent. Then, given the minimum propagation loss $L^{(0)}$, the characteristic function of $\mathcal{I}_{\mathrm{MU}}$ is given by

$$\begin{aligned}\Phi\left(\omega; L^{(0)}\right) &= \mathbb{E}\left(\exp\left\{j\omega\mathcal{I}_{MU}(L^{(0)})\right\}\right)\\ &= \prod_{N=0}^{N_{max}} \Phi_N\left(\omega; L^{(0)}\right)\end{aligned} \tag{B.1}$$

where $\Phi_N\left(\omega; L^{(0)}\right)$ is the characteristic function of the interference generating from the PHs associated with $\Psi_N$.

In order to compute $\Phi_N\left(\omega; L^{(0)}\right)$, we can invoke the Probability Generating Functional (PGFL) theorem for PPPs, thus getting

$$\begin{aligned}&\Phi_N\left(\omega; L^{(0)}\right) =\\ &\exp\left(\mathbb{E}_{h^{(\mathrm{n})}}\left\{\int_{L^{(0)}}^{\infty}\left(\exp\left(j\omega h^{(\mathrm{n})}/\xi\right) - 1\right)\widehat{\Lambda}_N([0,\xi))d\xi\right\}\right)\end{aligned} \tag{B.2}$$

where $\widehat{\Lambda}_N([0,\xi))$ is the first derivative of $\Lambda_N([0,\xi))$ with respect to $\xi$, given by

$$\begin{aligned}&\widehat{\Lambda}_N([0,\xi)) =\\ &\begin{cases}\frac{4\lambda_{\mathrm{ph}}}{N!}\frac{K^N}{\kappa\alpha}\sum\limits_{\eta=N}^{\infty}\frac{(-1)^{\eta-N}\chi_\eta(\lambda_{\mathrm{w}})}{(\eta-N)!}\left(\frac{\xi K^N}{\kappa}\right)^{\frac{\eta+2}{\alpha}-1} & \text{if } 1 \le \xi < \frac{R_{\mathrm{a}}^{\alpha}\kappa}{K^N}\\ 0 & \text{if } \xi \ge \frac{R_{\mathrm{a}}^{\alpha}\kappa}{K^N}\end{cases}\end{aligned} \tag{B.3}$$

with $\chi_\eta\left(\lambda_{\mathrm{w}}\right)$ defined as in (3.5).

Hence, similarly to what has been done in [63], we can use the notable result

$$\begin{aligned}&\int_{\mathcal{N}}^{+\infty}\left(\exp\left\{j\omega\mathcal{A}/x\right\} - 1\right)x^{v-1}dx =\\ &\qquad (1/v)\mathcal{N}^v\left(1 - {}_1F_1\left(-v, 1-v, j\omega\mathcal{A}/\mathcal{N}\right)\right)\end{aligned}$$

and compute the expectation with respect to $h^{(\mathrm{n})}$ by taking advantage of the identity in [78, Eq. 7.521]. After some manipulations, the expression of the characteristic function is given as

$$
\begin{aligned}
&\Phi_N\left(\omega; L^{(0)}\right) = \\
&\exp\left\{\frac{4\lambda_{\mathrm{ph}}}{N!}\sum_{\eta=N}^{\infty}\frac{(-1)^{\eta-N}\chi_\eta\left(\lambda_{\mathrm{w}}\right)}{(\eta-N)!(\eta+2)}\right. \\
&\times\left[\left(\frac{L^{(0)}K^N}{\kappa}\right)^{\frac{\eta+2}{\alpha}}\left(1-{}_2F_1\left(1,-\frac{\eta+2}{\alpha},1-\frac{(\eta+2)}{\alpha},\frac{j\omega}{L^{(0)}}\right)\right)\right. \\
&\left.\left.-R_{\mathrm{a}}^{\eta+2}\left(1-{}_2F_1\left(1,-\frac{\eta+2}{\alpha},1-\frac{(\eta+2)}{\alpha},\frac{j\omega K^N}{R_{\mathrm{a}}^{\alpha}\kappa}\right)\right)\right]\bar{\mathcal{H}}\left(L^{(0)}-\frac{R_{\mathrm{a}}^{\alpha}\kappa}{K^N}\right)\right\}
\end{aligned}
\tag{B.4}
$$

Then, invoking the Gil-Pelaez inversion theorem

$$
\begin{aligned}
&F_{\mathcal{I}_{\mathrm{MU}}}(z; L^{(0)}) = \\
&\qquad 1/2-\int_0^\infty\frac{1}{\pi\omega}\,\mathrm{Im}\left\{\mathrm{e}^{-j\omega z}\Phi\left(\omega; L^{(0)}\right)\right\}d\omega,
\end{aligned}
\tag{B.5}
$$

and recalling (3.9) and (B.1), Proposition 2 is finally proven.

# Appendix C

# Proof of Proposition 3

We obtain (3.15) by using (3.12) as follows:

$$
\begin{aligned}
F_{\mathrm{c}}(R^*, Q^*) = \Pr\{R \geq R^*, Q \geq Q^*\} &= \Pr\left\{\mathcal{I}_{\mathrm{MU}} \leq \frac{g^{(0)}\beta}{L^{(0)}} - \frac{\sigma_*^2}{P}, \mathcal{I}_{\mathrm{MU}} \geq \frac{-g^{(0)}}{L^{(0)}} + \frac{q*}{P}\right\} \\
&= \begin{cases} \frac{-g^{(0)}}{L^{(0)}} + \frac{q*}{P} \leq \mathcal{I}_{\mathrm{MU}} \leq \frac{g^{(0)}\beta}{L^{(0)}} - \frac{\sigma_*^2}{P} & \text{if} \quad g^{(0)} \geq (\mathcal{T}_*/P)L^{(0)} \\ 0 & \text{otherwise} \end{cases}
\end{aligned}
\tag{C.1}
$$

where it leads to (3.15). Substituting (3.14) and (B.5) into (3.15) and using the law of unconscious statistician, i.e. $\mathbb{E}\{g(L^{(0)})\} = \int_0^{+\infty} g(y) f_{L^{(0)}}(y) dy$ where $f_{L^{(0)}}$ is the PDF of $L^{(0)}$ and can be trivially obtained from (3.6), completes the proof.

# Appendix D

# Proof of Theorem 1

Using the approximation given in (4.13) the conditional probability $\mathbb{P}(E_{\text{off}} < E_{\text{h}} < E_{\text{loc}}|\Psi_{\text{ph}}, \Psi_{\text{mec}})$ can be computed as,

$$\begin{aligned}
&\mathbb{P}(E_{\text{off}} < E_{\text{h}} < E_{\text{loc}}|\Psi_{\text{ph}}, \Psi_{\text{mec}}) = \mathbb{P}(E_{\text{off}} < \tau_{\text{eh}}\eta P \left(g_1 r_1^{-\alpha} + g_2 r_2^{-\alpha} + \chi(r_2)\right) < E_{\text{loc}}|\Psi_{\text{ph}}, \Psi_{\text{mec}}) \\
&= \mathbb{P}\left(\frac{E_{\text{off}}}{\tau_{\text{eh}}\eta P} - \chi(r_2) < \left(g_1 r_1^{-\alpha} + g_2 r_2^{-\alpha}\right) < \frac{E_{\text{loc}}}{\tau_{\text{eh}}\eta P}|\Psi_{\text{ph}} - \chi(r_2), \Psi_{\text{mec}}\right) \\
&\overset{(a)}{=} \frac{r_1^{\alpha}\left[\exp\left(-r_2^{\alpha} Z_{\text{loc}}^{+}(r_2, R)\right) - \exp\left(-r_2^{\alpha} Z_{\text{off}}^{+}(r_2, R)\right)\right]}{r_2^{\alpha} - r_1^{\alpha}} \\
&\qquad - \frac{r_2^{\alpha}\left[\exp\left(-r_1^{\alpha} Z_{\text{loc}}^{+}(r_2, R)\right) - \exp\left(-r_1^{\alpha} Z_{\text{off}}^{+}(r_2, R)\right)\right]}{r_2^{\alpha} - r_1^{\alpha}}
\end{aligned} \tag{D.1}$$

where step $(a)$ is due to hypo-exponential distribution of $g_1 r_1^{-\alpha} + g_2 r_2^{-\alpha}$ (sum of two exponential random variables with rates $r_1$ and $r_2$ ) and $[x]^+ = max\{0, x\}$. Here, $Z_{\text{off}}^{+}(r_2, R)$ and $Z_{\text{loc}}^{+}(r_2, R)$ can be obtained by using function defined in (4.15) with substituting (4.14) into it. Following the same steps, conditional probabilities $\mathbb{P}(E_{\text{h}} \geq \max\{E_{\text{loc}}, E_{\text{off}}\}|\Psi_{\text{ph}}, \Psi_{\text{mec}})$ and $\mathbb{P}(E_{\text{loc}} < E_{\text{h}} < E_{\text{off}}|\Psi_{\text{ph}}, \Psi_{\text{mec}})$ can be easily derived as given in (4.16) and (4.18), respectively.

# Appendix E

# Derivation of Conditional SINR Coverages

Using the definition of $\text{SINR}_{\text{id}}$ in (4.3) and approximating the interference $\mathcal{I}_{\text{id}}$, the probability that the downlink $\text{SINR}_{\text{id}}$ is greater than $\beta_{\text{id}}$, conditioned on $r_1$ and $r_2$, can be found as follows:

$$\begin{aligned}
\mathbb{P}(\text{SINR}_{\text{id}} \geq \beta_{\text{id}} || r_1, r_2) &= \mathbb{P}\left(\frac{Ph_1\kappa^{-1}r_1^{-\alpha}}{\sigma_{\text{id}}^2 + \mathcal{I}_{\text{id}}} \geq \beta_{\text{id}} || r_1, r_2\right) \\
&= \mathbb{P}\left(\frac{Ph_1\kappa^{-1}r_1^{-\alpha}}{\sigma_{\text{id}}^2 + Ph_1\kappa^{-1}r_2^{-\alpha} + P\chi(r_2)} \geq \beta_{\text{id}} || r_1, r_2\right) \\
&= \mathbb{P}\left(h_1 r_1^{-\alpha} \geq \frac{\sigma_{\text{id}}^2\beta_{\text{id}}}{P\kappa^{-1}} + h_1 r_2^{-\alpha}\beta_{\text{id}} + \frac{\chi(r_2)\beta_{\text{id}}}{\kappa^{-1}}\right) \\
&\overset{(a)}{=} \mathbb{E}_{h_1}\left[\exp\left(-r_1^{\alpha}\left(\frac{\sigma_{\text{id}}^2\beta_{\text{id}}}{P\kappa^{-1}} + h_1 r_2^{-\alpha}\beta_{\text{id}} + \frac{\chi(r_2)\beta_{\text{id}}}{\kappa^{-1}}\right)\right)\right] \\
&\overset{(b)}{=} \exp\left\{-\frac{\beta_{\text{id}} r_1^{\alpha}}{\kappa^{-1}}\left(\frac{\sigma_{\text{id}}^2}{P} + \chi(r_2)\right)\right\}\left(\frac{1}{1 + \beta_{\text{id}}\frac{r_1^{\alpha}}{r_2^{\alpha}}}\right)
\end{aligned} \tag{E.1}$$

where steps (a) and (b) follow from the assumptions that $h_1 \sim$ exp(1) and $h_2 \sim$ exp(1).

As we explained before, in order to have the offloading/uploading SINR coverages dependent on $\Psi_{\text{mec}}$, the locations of active LPDs in uploading/offloading phase is approximated by independently thinning $\Psi_{\text{mec}}$ with probability $P_{\text{loc}}/P_{\text{off}}$ where we have new density $\lambda_{\text{mec}}P_{\text{s}}$, s $\in$ {off,loc}. With the SINR expression given in (4.6), $\mathbb{P}(\text{SINR}_{\text{i(s)}} \geq \beta_{\text{i(s)}}$ can be found as,

$$\begin{aligned}
\mathbb{P}(\mathrm{SINR}_{\mathrm{i(s)}} \geq \beta_{\mathrm{i(s)}}||R) &= \mathbb{P}\left(\frac{w_{\mathrm{i},1}}{\frac{\sigma_{\mathrm{i}}^2}{\eta} + \mathcal{I}_{\mathrm{i}}} \geq \beta_{\mathrm{i(s)}}||R\right) \\
&= \mathbb{E}_{\mathcal{I}_{\mathrm{i}}}\left[\mathbb{P}\left(w_{\mathrm{i},1} \geq \left(\frac{\sigma_{\mathrm{i}}^2}{\eta} + \mathcal{I}_{\mathrm{i}}\right)\beta_{\mathrm{i(s)}}\right)||R, \mathcal{I}_{\mathrm{i}}\right] \\
&\overset{(a)}{=} \mathbb{E}_{\mathcal{I}_{\mathrm{i}}}\left[\exp\left(-\left(\frac{\sigma_{\mathrm{i}}^2}{\eta} + \mathcal{I}_{\mathrm{i}}\right)\beta_{\mathrm{i(s)}}\right)\right] \\
&\overset{(b)}{=} \exp\left(\frac{\sigma_{\mathrm{i}}^2\beta_{\mathrm{i(s)}}}{\eta}\right)\mathcal{L}_{\mathcal{I}_{\mathrm{i}}}\left(\beta_{\mathrm{i(s)}}\right)
\end{aligned} \tag{E.2}$$

where step (a) is due to the assumption that $w_{\mathrm{i},1} \sim \exp(1)$, and step (b) results from using the Laplace transform of $\mathcal{I}_{\mathrm{i}}$.

By using the expression of Laplace transform of the interference given in [58] and substituting $\lambda_{\mathrm{mec}}P_{\mathrm{s}}$, we obtain $\mathcal{L}_{\mathcal{I}_{\mathrm{i}}}\left(\beta_{\mathrm{i(s)}}\right)$ as,

$$\mathcal{L}_{\mathcal{I}_{\mathrm{i}}}\left(\beta_{\mathrm{i(s)}}\right) = \exp\left(-2\pi\lambda_{\mathrm{mec}}P_{\mathrm{s}}\int_0^{R_{\mathrm{a}}}\int_0^{x^2}\frac{\pi\lambda_{\mathrm{mec}}P_{\mathrm{s}}\exp(-\pi\lambda_{\mathrm{mec}}P_{\mathrm{s}}u)}{1+\left(\frac{1}{\beta_s}\right)u^{\frac{-\alpha}{2}}x^{\alpha}}du\,x\,dx\right). \tag{E.3}$$

# Appendix F

# Derivation of Conditional Probability of Local Computation

Following the same steps as in [66], it can be found as,

$$\begin{aligned}
&\mathbb{P}(E_{\text{loc}} < E_{\text{off}} | R, h_{\text{mec}}) \\
&= \mathbb{P}\Bigg( c_{\text{e}} \frac{(kL_{\text{task}})^3}{(\tau_{\text{loc}})^2} + c_{\text{dec}}\tau_{\text{id}} \log(1+\beta_{\text{id}}) + \tau_{\text{up}} \frac{\beta_{\text{mec}}\sigma_{\text{mec}}^2 R^{\alpha}\kappa}{h_{\text{mec}}\mathrm{J}(R)} \\
&\qquad\qquad < c_{\text{dec}}\tau_{\text{id}} \log(1+\beta_{\text{id}}) + (\tau_{\text{loc}} + \tau_{\text{up}}) \frac{\beta_{\text{mec}}\sigma_{\text{mec}}^2 R^{\alpha}\kappa}{h_{\text{mec}}\mathrm{J}(R)} \Bigg) \\
&= \mathbb{P}\left( c_{\text{e}} \frac{(kL_{\text{task}})^3}{(\tau_{\text{loc}})^2} < \frac{\tau_{\text{loc}}\beta_{\text{mec}}\sigma_{\text{mec}}^2 R^{\alpha}\kappa}{h_{\text{mec}}\mathrm{J}(R)} \right) \\
&= \mathbb{P}\left( \frac{R^{\alpha}}{\mathrm{J}(R)} > c_{\text{e}} \frac{(kL_{\text{task}}}{(\tau_{\text{loc}})})^3 \frac{h_{\text{mec}}}{\beta_{\text{mec}}\sigma_{\text{mec}}^2 \kappa} \right) \\
&\overset{(a)}{=} \mathcal{H}\left[ \frac{R^{\alpha}}{\mathrm{J}(R)} - c_{\text{e}} \left( \frac{kL_{\text{task}}}{\tau_{\text{loc}}} \right)^3 \frac{h_{\text{mec}}}{\beta_{\text{mec}}\sigma_{\text{mec}}^2 \kappa} \right].
\end{aligned} \tag{F.1}$$

where (a) comes from the definiton of Heaviside function [78].

# Bibliography

[1] A. Ahmed and E. Ahmed, "A survey on mobile edge computing," in *2016 10th International Conference on Intelligent Systems and Control (ISCO)*, 2016, pp. 1–8.

[2] P. Mach and Z. Becvar, "Mobile edge computing: A survey on architecture and computation offloading," *IEEE Communications Surveys & Tutorials*, vol. 19, no. 3, pp. 1628–1656, 2017.

[3] P. Porambage, J. Okwuibe, M. Liyanage, M. Ylianttila, and T. Taleb, "Survey on multi-access edge computing for internet of things realization," *IEEE Communications Surveys & Tutorials*, vol. 20, no. 4, pp. 2961–2991, 2018.

[4] J. A. Paradiso and T. Starner, "Energy scavenging for mobile and wireless electronics," *IEEE Pervasive computing*, vol. 4, no. 1, pp. 18–27, 2005.

[5] S. Sudevalayam and P. Kulkarni, "Energy harvesting sensor nodes: Survey and implications," *IEEE Communications Surveys & Tutorials*, vol. 13, no. 3, pp. 443–461, 2010.

[6] S. J. Roundy, "Energy scavenging for wireless sensor nodes with a focus on vibration to electricity conversion," Ph.D. dissertation, University of California, Berkeley Berkeley, CA, 2003.

[7] S. K. Divakaran and D. D. Krishna, "RF energy harvesting systems: An overview and design issues," *International Journal of RF and Microwave Computer-Aided Engineering*, vol. 29, no. 1, p. e21633, 2019.

[8] H.-V. Tran and G. Kaddoum, "RF wireless power transfer: Regreening future networks," *IEEE Potentials*, vol. 37, no. 2, pp. 35–41, 2018.

[9] L. R. Varshney, "Transporting information and energy simultaneously," in *2008 IEEE international symposium on information theory*. IEEE, 2008, pp. 1612–1616.

[10] L. Mohjazi, "Analysis and optimisation of SWIPT networks." Ph.D. dissertation, University of Surrey, 2020.

[11] I. Krikidis, "Simultaneous information and energy transfer in large-scale networks with/without relaying," *IEEE Transactions on Communications*, vol. 62, no. 3, pp. 900–912, 2014.

[12] Z. Ding, C. Zhong, D. W. K. Ng, M. Peng, H. A. Suraweera, R. Schober, and H. V. Poor, "Application of smart antenna technologies in simultaneous wireless information and power transfer," *IEEE Communications Magazine*, vol. 53, no. 4, pp. 86–93, 2015.

[13] X. Chen, D. W. K. Ng, and H.-H. Chen, "Secrecy wireless information and power transfer: Challenges and opportunities," *IEEE Wireless Communications*, vol. 23, no. 2, pp. 54–61, 2016.

[14] T. D. P. Perera, D. N. K. Jayakody, S. K. Sharma, S. Chatzinotas, and J. Li, "Simultaneous wireless information and power transfer (SWIPT): Recent advances and future challenges," *IEEE Communications Surveys & Tutorials*, vol. 20, no. 1, pp. 264–302, 2017.

[15] J. G. Andrews, F. Baccelli, and R. K. Ganti, "A tractable approach to coverage and rate in cellular networks," *IEEE Transactions on communications*, vol. 59, no. 11, pp. 3122–3134, 2011.

[16] M. Di Renzo, A. Guidotti, and G. E. Corazza, "Average rate of downlink heterogeneous cellular networks over generalized fading channels: A stochastic geometry approach," *IEEE Transactions on Communications*, vol. 61, no. 7, pp. 3050–3071, 2013.

[17] G. Zheng, I. Krikidis, C. Masouros, S. Timotheou, D.-A. Toumpakaris, and Z. Ding, "Rethinking the role of interference in wireless networks," *IEEE Communications Magazine*, vol. 52, no. 11, pp. 152–158, 2014.

[18] L. Liu, R. Zhang, and K.-C. Chua, "Wireless information transfer with opportunistic energy harvesting," *IEEE Transactions on Wireless Communications*, vol. 12, no. 1, pp. 288–300, 2012.

[19] F. Baccelli and B. Błaszczyszyn, *Stochastic geometry and wireless networks*. Now Publishers Inc, 2009, vol. 1.

[20] Y. C. Hu, M. Patel, D. Sabella, N. Sprecher, and V. Young, "Mobile edge computing—A key technology towards 5G," *ETSI white paper*, vol. 11, no. 11, pp. 1–16, 2015.

[21] X. Zhou, J. Guo, S. Durrani, and I. Krikidis, "Performance of maximum ratio transmission in ad hoc networks with SWIPT," *IEEE Wireless Communications Letters*, vol. 4, no. 5, pp. 529–532, 2015.

[22] L.-T. Tu, A. Bradai, and Y. Pousset, "Performance evaluation of SWIPT-enabled cellular networks with adaptive modulation-A stochastic geometry approach," in *Réseaux du futur: 5G et au-delà*, 2020.

[23] S. Kusaladharma, W.-P. Zhu, W. Ajib, and G. A. A. Baduge, "Stochastic geometry based performance characterization of SWIPT in cell-free massive MIMO," *IEEE Transactions on Vehicular Technology*, vol. 69, no. 11, pp. 13 357–13 370, 2020.

[24] N. Janatian, I. Stupia, and L. Vandendorpe, "Optimal offloading strategy and resource allocation in swipt-based mobile-edge computing networks," in *2018 15th International Symposium on Wireless Communication Systems (ISWCS)*. IEEE, 2018, pp. 1–6.

[25] E. Xuefei, Z. Ma, and K. Yu, "Energy-efficient computation offloading and resource allocation in SWIPT-based MEC networks," *IEEE Access*, 2020.

[26] J. Fu, J. Hua, J. Wen, H. Chen, W. Lu, and J. Li, "Optimization of energy consumption in the MEC-assisted multi-user FD-SWIPT system," *IEEE Access*, vol. 8, pp. 21 345–21 354, 2020.

[27] D. Bol, G. de Streel, and D. Flandre, "Can we connect trillions of iot sensors in a sustainable way? a technology/circuit perspective (invited)," in *2015 IEEE SOI-3D-Subthreshold Microelectronics Technology Unified Conference (S3S)*, 2015, pp. 1–3.

[28] S. Barbarossa, S. Sardellitti, and P. Di Lorenzo, "Communicating while computing: Distributed mobile cloud computing over 5g heterogeneous networks," *IEEE Signal Processing Magazine*, vol. 31, no. 6, pp. 45–55, 2014.

[29] H. T. Dinh, C. Lee, D. Niyato, and P. Wang, "A survey of mobile cloud computing: architecture, applications, and approaches," *Wireless Communications and Mobile Computing*, vol. 13, no. 18, pp. 1587–1611, 2013.

[30] L. Guan, X. Ke, M. Song, and J. Song, "A survey of research on mobile cloud computing," in *2011 10th IEEE/ACIS International Conference on Computer and Information Science*, 2011, pp. 387–392.

[31] Y. Mao, C. You, J. Zhang, K. Huang, and K. B. Letaief, "A survey on mobile edge computing: The communication perspective," *IEEE Communications Surveys & Tutorials*, vol. 19, no. 4, pp. 2322–2358, 2017.

[32] S. Wang, X. Zhang, Y. Zhang, L. Wang, J. Yang, and W. Wang, "A survey on mobile edge networks: Convergence of computing, caching and communications," *IEEE Access*, vol. 5, pp. 6757–6779, 2017.

[33] W. Shi, J. Cao, Q. Zhang, Y. Li, and L. Xu, "Edge computing: Vision and challenges," *IEEE Internet of Things Journal*, vol. 3, no. 5, pp. 637–646, 2016.

[34] J. G. Andrews, R. K. Ganti, M. Haenggi, N. Jindal, and S. Weber, "A primer on spatial modeling and analysis in wireless networks," *IEEE Communications Magazine*, vol. 48, no. 11, pp. 156–163, 2010.

[35] M. Patel, B. Naughton, C. Chan, N. Sprecher, S. Abeta, A. Neal *et al.*, "Mobile-edge computing introductory technical white paper," *White paper, mobile-edge computing (MEC) industry initiative*, vol. 29, pp. 854–864, 2014.

[36] K. Zhang, Y. Mao, S. Leng, Q. Zhao, L. Li, X. Peng, L. Pan, S. Maharjan, and Y. Zhang, "Energy-efficient offloading for mobile edge computing in 5G heterogeneous networks," *IEEE access*, vol. 4, pp. 5896–5907, 2016.

[37] C. Park and J. Lee, "Successful edge computing probability analysis in heterogeneous networks," in *2018 IEEE International Conference on Communications (ICC)*. IEEE, 2018, pp. 1–6.

[38] Y. Wang, M. Tang, S. Zhou, G. Tan, Z. Zhang, and J. Zhan, "Performance analysis of heterogeneous mobile edge computing networks with multi-core server," in *2020 IEEE 20th International Conference on Communication Technology (ICCT)*. IEEE, 2020, pp. 1540–1545.

[39] P. Grover and A. Sahai, "Shannon meets tesla: Wireless information and power transfer," in *2010 IEEE international symposium on information theory*. IEEE, 2010, pp. 2363–2367.

[40] A. S. Boaventura and N. B. Carvalho, "Maximizing DC power in energy harvesting circuits using multisine excitation," in *2011 IEEE MTT-S International Microwave Symposium*. IEEE, 2011, pp. 1–4.

[41] B. Clerckx and E. Bayguzina, "Waveform design for wireless power transfer," *IEEE Transactions on Signal Processing*, vol. 64, no. 23, pp. 6313–6328, 2016.

[42] B. Clerckx, R. Zhang, R. Schober, D. W. K. Ng, D. I. Kim, and H. V. Poor, "Fundamentals of wireless information and power transfer: From RF energy harvester models to signal and system designs," *IEEE Journal on Selected Areas in Communications*, vol. 37, no. 1, pp. 4–33, 2018.

[43] D. I. Kim, J. H. Moon, and J. J. Park, "New swipt using papr: How it works," *IEEE Wireless Communications Letters*, vol. 5, no. 6, pp. 672–675, 2016.

[44] T. M. Hoang, X. N. Tran, N. Thanh *et al.*, "Performance analysis of MIMO SWIPT relay network with imperfect CSI," *Mobile Networks and Applications*, vol. 24, no. 2, pp. 630–642, 2019.

[45] P. Mukherjee, S. Lajnef, and I. Krikidis, "MIMO SWIPT systems with power amplifier nonlinearities and memory effects," *IEEE Wireless Communications Letters*, vol. 9, no. 12, pp. 2187–2191, 2020.

[46] L.-T. Tu and M. Di Renzo, "Analysis of millimeter wave cellular networks with simultaneous wireless information and power transfer," in *2017 International Conference on Recent Advances in Signal Processing, Telecommunications & Computing (SigTelCom)*. IEEE, 2017, pp. 39–43.

[47] L. Dai, B. Wang, M. Peng, and S. Chen, "Hybrid precoding-based millimeter-wave massive MIMO-NOMA with simultaneous wireless information and power transfer," *IEEE Journal on Selected Areas in Communications*, vol. 37, no. 1, pp. 131–141, 2018.

[48] J. Tang, J. Luo, M. Liu, D. K. So, E. Alsusa, G. Chen, K.-K. Wong, and J. A. Chambers, "Energy efficiency optimization for NOMA with SWIPT," *IEEE Journal of Selected Topics in Signal Processing*, vol. 13, no. 3, pp. 452–466, 2019.

[49] S. Bayat, A. Khalili, and Z. Han, "Resource allocation for MC MISO-NOMA SWIPT-enabled hetnets with non-linear energy harvesting," *IEEE Access*, vol. 8, pp. 192 270–192 281, 2020.

[50] R. Zhang and C. K. Ho, "MIMO broadcasting for simultaneous wireless information and power transfer," *IEEE Transactions on Wireless Communications*, vol. 12, no. 5, pp. 1989–2001, 2013.

[51] X. Zhou, R. Zhang, and C. K. Ho, "Wireless information and power transfer: Architecture design and rate-energy tradeoff," *IEEE Transactions on communications*, vol. 61, no. 11, pp. 4754–4767, 2013.

[52] A. M. Fouladgar and O. Simeone, "On the transfer of information and energy in multi-user systems," *IEEE Communications Letters*, vol. 16, no. 11, pp. 1733–1736, 2012.

[53] C. You, K. Huang, and H. Chae, "Energy efficient mobile cloud computing powered by wireless energy transfer," *IEEE Journal on Selected Areas in Communications*, vol. 34, no. 5, pp. 1757–1771, 2016.

[54] X. Hu, K.-K. Wong, and K. Yang, "Wireless powered cooperation-assisted mobile edge computing," *IEEE Transactions on Wireless Communications*, vol. 17, no. 4, pp. 2375–2388, 2018.

[55] C. Li, J. Tang, and Y. Luo, "Dynamic multi-user computation offloading for wireless powered mobile edge computing," *Journal of Network and Computer Applications*, vol. 131, pp. 1–15, 2019.

[56] F. Wang, J. Xu, X. Wang, and S. Cui, "Joint offloading and computing optimization in wireless powered mobile-edge computing systems," *IEEE Transactions on Wireless Communications*, vol. 17, no. 3, pp. 1784–1797, 2017.

[57] Z. Wen, K. Yang, X. Liu, S. Li, and J. Zou, "Joint offloading and computing design in wireless powered mobile-edge computing systems with full-duplex relaying," *IEEE Access*, vol. 6, pp. 72 786–72 795, 2018.

[58] J. G. Andrews, A. K. Gupta, and H. S. Dhillon, "A primer on cellular network analysis using stochastic geometry," *arXiv preprint arXiv:1604.03183*, 2016.

[59] H. P. Keeler, "Campbell's theorem," 2015.

[60] A. D. Wyner, "Shannon-theoretic approach to a Gaussian cellular multiple-access channel," *IEEE Transactions on Information Theory*, vol. 40, no. 6, pp. 1713–1727, 1994.

[61] V. H. Mac Donald, "Advanced mobile phone service: The cellular concept," *The bell system technical Journal*, vol. 58, no. 1, pp. 15–41, 1979.

[62] X. Lu, I. Flint, D. Niyato, N. Privault, and P. Wang, "Performance analysis of simultaneous wireless information and power transfer with ambient RF energy harvesting," in *2015 IEEE Wireless Communications and Networking Conference (WCNC)*. IEEE, 2015, pp. 1303–1308.

[63] W. Lu, M. Di Renzo, and T. Q. Duong, "On stochastic geometry analysis and optimization of wireless-powered cellular networks," in *2015 IEEE Global Communications Conference (GLOBECOM)*. IEEE, 2015, pp. 1–7.

[64] T. L. Thanh, M. Di Renzo, and J. P. Coon, "MIMO cellular networks with simultaneous wireless information and power transfer," in *2016 IEEE 17th International Workshop on Signal Processing Advances in Wireless Communications (SPAWC)*. IEEE, 2016, pp. 1–5.

[65] A. H. Sakr and E. Hossain, "Analysis of $K$-tier uplink cellular networks with ambient rf energy harvesting," *IEEE Journal on Selected Areas in Communications*, vol. 33, no. 10, pp. 2226–2238, 2015.

[66] M. A. Kishk and H. S. Dhillon, "Joint uplink and downlink coverage analysis of cellular-based RF-powered IoT network," *IEEE Transactions on Green Communications and Networking*, vol. 2, no. 2, pp. 446–459, 2017.

[67] N. Kouzayha, Z. Dawy, J. G. Andrews, and H. ElSawy, "Joint downlink/uplink RF wake-up solution for IoT over cellular networks," *IEEE Transactions on Wireless Communications*, vol. 17, no. 3, pp. 1574–1588, 2017.

[68] F. Baccelli and X. Zhang, "A correlated shadowing model for urban wireless networks," in *2015 IEEE Conference on Computer Communications (INFOCOM)*. IEEE, 2015, pp. 801–809.

[69] K. Rizk, J.-F. Wagen, and F. Gardiol, "Two-dimensional ray-tracing modeling for propagation prediction in microcellular environments," *IEEE Transactions on Vehicular Technology*, vol. 46, no. 2, pp. 508–518, 1997.

[70] K. R. Schaubach, N. J. Davis, and T. S. Rappaport, “A ray tracing method for predicting path loss and delay spread in microcellular environments,” in *[1992 Proceedings] Vehicular Technology Society 42nd VTS Conference-Frontiers of Technology*. IEEE, 1992, pp. 932–935.

[71] T. Bai, R. Vaze, and R. W. Heath, “Analysis of blockage effects on urban cellular networks,” *IEEE Transactions on Wireless Communications*, vol. 13, no. 9, pp. 5070–5083, 2014.

[72] S. N. Chiu, D. Stoyan, W. S. Kendall, and J. Mecke, *Stochastic geometry and its applications*. John Wiley & Sons, 2013.

[73] X. Zhang, F. Baccelli, and R. W. Heath, “An indoor correlated shadowing model,” in *2015 IEEE Global Communications Conference (GLOBECOM)*. IEEE, 2015, pp. 1–7.

[74] J. Lee, X. Zhang, and F. Baccelli, “A 3-D spatial model for in-building wireless networks with correlated shadowing,” *IEEE Transactions on Wireless Communications*, vol. 15, no. 11, pp. 7778–7793, 2016.

[75] M. K. Muller, M. Taranetz, and M. Rupp, “Analyzing wireless indoor communications by blockage models,” *IEEE Access*, vol. 5, pp. 2172–2186, 2016.

[76] M. Haenggi, *Stochastic geometry for wireless networks*. Cambridge University Press, 2012.

[77] R. Dekimpe, P. Xu, M. Schramme, P. Gérard, D. Flandre, and D. Bol, “A batteryless ble smart sensor for room occupancy tracking supplied by 2.45-ghz wireless power transfer,” *Integration*, vol. 67, pp. 8–18, 2019.

[78] I. S. Gradshteyn and I. M. Ryzhik, *Table of integrals, series, and products*. Academic press, 2014.

[79] J. Gil-Pelaez, “Note on the inversion theorem,” *Biometrika*, vol. 38, no. 3-4, pp. 481–482, 1951.

[80] A. Maaref and S. Aissa, “Closed-form expressions for the outage and ergodic Shannon capacity of MIMO MRC systems,” *IEEE Transactions on Communications*, vol. 53, no. 7, pp. 1092–1095, 2005.

[81] P. Series, “Propagation data and prediction methods for the planning of indoor radiocommunication systems and radio local area networks in the frequency range 900 MHz to 100 GHz,” *Recommendation ITU-R*, pp. 1238–7, 2012.

[82] T. D. Burd and R. W. Brodersen, “Processor design for portable systems,” *Journal of VLSI signal processing systems for signal, image and video technology*, vol. 13, no. 2, pp. 203–221, 1996.

[83] K. Huang and V. K. Lau, “Enabling wireless power transfer in cellular networks: Architecture, modeling and deployment,” *IEEE Transactions on Wireless Communications*, vol. 13, no. 2, pp. 902–912, 2014.

[84] I. Flint, X. Lu, N. Privault, D. Niyato, and P. Wang, “Performance analysis of ambient RF energy harvesting with repulsive point process modeling,” *IEEE Transactions on Wireless Communications*, vol. 14, no. 10, pp. 5402–5416, 2015.

[85] T. L. Thanh, M. Di Renzo, and J. P. Coon, "Stochastic geometry analysis of receiver diversity in cellular networks with SWIPT," in *2018 IEEE 19th International Workshop on Signal Processing Advances in Wireless Communications (SPAWC)*. IEEE, 2018, pp. 1–5.

[86] K. Chen, X. Wen, W. Jing, Z. Lu, H. Shao, and H. Xu, "Simultaneous information and energy transfer in large-scale cellular networks with sleep mode," in *2016 IEEE International Conference on Communications (ICC)*. IEEE, 2016, pp. 1–6.

[87] M. K. Müller, S. Schwarz, and M. Rupp, "Investigation of area spectral efficiency in indoor wireless communications by blockage models," in *2018 16th International Symposium on Modeling and Optimization in Mobile, Ad Hoc, and Wireless Networks (WiOpt)*. IEEE, 2018, pp. 1–6.

[88] J. Liao and A. Berg, "Sharpening jensen's inequality," *The American Statistician*, 2018.